The mechanisms to regulate arsenic behaviors in redox transition zones in paddy soils

UNIVERSITY OF LIVERPOOL

Zhao-Feng Yuan

Faculty of Science and Engineering

This dissertation is submitted for the degree of

Doctor of Philosophy

I would like to dedicate this thesis to my loving wife,

李妞妞

for your steady support and endless love.

Declaration

I, **Zhao-Feng Yuan**, hereby declare that except where specific reference is made to the work of others, the contents of this dissertation are original and have not been submitted in whole or in part for consideration for any other degree or qualification in this, or any other university. This dissertation is my own work and contains nothing which is the outcome of work done in collaboration with others, except as specified in the text and acknowledgements.

Signed: 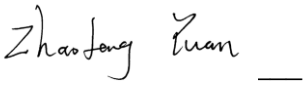

Zhao-Feng Yuan (Candidate)

13th January 2020

Acknowledgement

First and foremost I would like to thank Dr. Zheng Chen, for his constant guidance and constructive input throughout the course of this project. I would also like to thank my co-supervisors, Dr. Sekar Raju, John Boyle, Jonathan Bridge and Prof. H. Ouyang for their constant support and guidance during my research.

I would like to thank Yi Liang for providing the excellent hollow fiber membrane tube. Without that, I would not develop the indispensable technique and complete my PhD. I also want to thank two great designers, Yang Zou and Fuyuan Liu. Without their help, the technique developed would not become a robust tool for peers interested in biogeochemistry of porewaters.

I would like to thank all the team members from eBiogeochemistry for their valuable suggestion and constant support, especially Williamson Gustave, Yuxiang Ren, Tongyao Pu, Chenyu Jin, Jiayue Wang, Weijia Feng. I also want to acknowledge the kind help of Yili Cheng, Xiao Zhou, Xiaoyan Zhang and Liangping Long for their support in laboratory analysis.

I wish to express my immense gratitude to my order brother Lefeng Yuan and my parents Qiuzheng Yuan and Runmiao Zhang. Without their strong encouragement and selfless support, I would not start an academic career.

Finally, I really appreciate the funds that supported my living and research, including PhD scholarship from XJTLU, the XJTLU Research Development Fund (RDF-15-01-39), Key Programme Special Fund of XJTLU (KSF-A-20), the National Science Foundation of China (41571305, 41977320) and Jiangsu Science and Technology Program (BK20161251).

Abstract

Rice (*Oryza sativa* L.) is the staple food for people especially in Asia, but rice production is threatened by arsenic (As) contamination in paddy soil. Contamination of As in paddy soil is mainly caused by anthropogenic activities, such as mining and irrigation of high As groundwater. External As firstly enters overlying water, and then accumulates in paddy soil. Soil-water interface (SWI) is the gate controlling As exchange between soil and overlying water, and rhizosphere is the inlet of As from soils into rice root. Under natural conditions, a redox transition occurs along both micro interfaces due to atmospheric O_2 diffusion or radial O_2 loss from root. Arsenic is sensitive to redox conditions and tends to change over space and time across those micro interfaces. However, a deep understanding of As cycling in paddy water-soil-rice system has been hindered to date by techniques available to sample micro interfaces repeatedly in high-resolution. In order to fill this gap, a novel high-resolution porewater sampler was developed in this study. Using the technique, the spatiotemporal control of As was studied at paddy SWI and rhizosphere.

A hollow fiber membrane tube (~ 2 mm diameter) was evaluated to sample dissolved elements with passive diffusion mechanism. The results showed quantification of solutes surrounding the tube can be achieved in every $\geq$ 24 h regardless of pH, ionic strength, and dissolved organic matter conditions. This technique, called *In-situ* Porewater Iterative (IPI) sampler, was further validated in soils under an anoxic-oxic transition by bubbling N_2 and air into overlying water. The results showed that the IPI sampler is a powerful and robust technique in monitoring dynamics of element profile in soil porewater in high-resolution (mm).

Moreover, measurement methods in ICP-MS and IC-ICP-MS were optimized to promote the measurement throughput of multi-element in limited samples (μL level) collected by high-resolution porewater samplers (e.g. IPI samplers). Major elements (e.g. iron (Fe) and manganese (Mn), mg·L^{-1} level) were measured by ICP-MS in extended dynamic range mode to avoid signal overflow, while trace elements (e.g. As, μg·L^{-1} level) in dynamic reaction cell (O_2) mode to alleviate potential polyatomic interferences. Ammonium bicarbonate mobile phase was further demonstrated to simultaneously measure common species of As, phosphorus (P) and sulfur (S) with IC-ICP-MS analysis. With the optimized analytical methods and IPI samplers, the measurement throughput of multi-element and their species were improved up to 10 times compared to traditional methods.

Furthermore, the cycling of As across SWI and rhizosphere was studied with the updated IPI sampler and state-of-art analytical techniques. In SWI, profiles of As, Fe and other associated elements in five paddy soils were mapped. The results showed a close coupling of Fe, Mn, As and P in 4 out of 5 paddy soils. However, decoupling of Fe, Mn and As was observed in the oxic-anoxic transition zone of one paddy soil. The study provided *in situ* evidence showing decoupling of As with Fe and Mn may happen in the oxic-anoxic transition zone of SWI.

For rhizosphere, dynamic profiles of Fe and As were mapped by IPI samplers from days after transplanting 0 to 40. The results showed Fe and As change spatiotemporally in rhizosphere. Interestingly, Fe oxides formed in rhizospheric soil, rather than on rice root (Fe plaque), play the key role for immobilizing mobile As from bulk soil. A model of As transport from soil to rice, linking the temporal and spatial regulation of As in paddy soils, was provided to help better understand As cycling in paddy soils.

Keywords: arsenic, iron, micro interface, paddy soil, rice, element profile

Table of content

List of figures

List of tables

List of abbreviations

AAS	Atomic absorption spectroscopy
ANOSIM	Analysis of similarity
ANOVA	One-way analysis of variance
ArsM	As(III) S-adenosylmethionine methyltransferase
As	Arsenic
As(III)	Arsenite
As(V)	Arsenate
BI	Bijie paddy soil
bp	Base pair
Cd	Cadmium
cm	Centimeter
℃	Degree celsius
d	Day
DAT	Days after rice transplanting
DET	Diffusive equilibration in thin films
DGT	Diffusive gradient in thin-films
DMA	Dimethylarsinic acid
DRC	Dynamic reaction cell
EDR	Extended dynamic range
EDTA	Ethylenediamine-N,N'-disuccinic acid
Eh	Redox potential
Fe	Iron
g	Gram
GZ	Ganzhou soil
h	Hour
H_2O_2	Hydrogen peroxide

HA	Humic acid
HCl	Chloride acid
HNO_3	Nitric acid
HPLC	High performance liquid chromatography
IC	Ion chromatography
ICP-MS	Inductively coupled plasma mass spectrometry
OES	Optical emission spectrometry
IPI	*In-situ* Porewater Iterative
Kg	Kilogram
Km	Kilometer
LA	Laser ablation
LEfse	Linear discriminant analysis (LDA) effect size
LOD	Limit of detection
λ	Wavelength
mg Ł$^{-1}$	Milligram per liter
min	Minute
mL	Milliliter
mm	Millimeter
mM Ł$^{-1}$	Millimolar per liter
MMA	Monomethylarsonic acid
Mn	Manganese
µg Ł$^{-1}$	Microgram per liter
µL	Microliter
mV	Millivolt
µM Ł$^{-1}$	Micromolar per liter
N_2	Nitrogen
NaCl	Sodium chloride
$NaNO_3$	Sodium nitrate
NaOH	Sodium hydroxide
ng	Nanogram

NH_4HCO_3	Ammonium bicarbonate
Ni	Nickel
nm	Nanometer
O.	Oryza
O_2	Oxygen
OUT	Operational taxonomic units
P	Phosphorus
P(V)	Phosphate
Pb	Lead
PCoA	Principal coordinates analysis
PTFE	Polytetrafluoroethylene
QY	Qingyuan paddy soil
R^2	Coefficient of determination
ROL	Radial O_2 loss
RSD	Relative standard deviation
S	Sulfur
s	Second
S(-II)	Sulfide
S(VI)	Sulfate
Sb	Antimony
SD	Standard deviation
SG	Shaoguan soil
SWI	Soil-water interface
TMAO	Trimethylarsine oxide
WS	Wenshan paddy soil
WX	Wuxue paddy soil
XAFS	X-ray absorption fine structure
YLY-1	Yliangyou-1 rice hybrid

1. Introduction and overview

Rice (*Oryza sativa* L.) consumption represents an important arsenic (As) exposure pathway to human in addition to drinking water. Background As is not high for most paddy soils in the world. Contamination of As in paddy soil is mainly caused by anthropogenic activities, such as mining, irrigation, application of pesticides, herbicides and fertilizers (Abedin et al. 2002, Awasthi et al. 2017, Kumarathilaka et al. 2018a). External As firstly enters overlying water, and then accumulates in paddy soil through multiple pathways, such as diffusion, seepage and ploughing. Therefore, studies of As transformation and migration in paddy soils should take paddy water, soil and rice plant as a whole system.

Micro interfaces are key zones controlling As transformation and migration in paddy water-soil-rice system. There are two typical micro interfaces in paddy, namely soil-water interface (SWI) between soil and overlying water, and rhizosphere between bulk soil and root surface. SWI is the key zone controlling As exchange between soil and overlying water, while rhizosphere is the inlet of As from soils into rice root (Arsic et al. 2018, Chen et al. 2005). Both micro interfaces are the key zone linking microorganism-mineral interface (nm to μm scale) and paddy field environment (mm to km scale). However, the micro-interactive mechanism of microorganism-minerals associated with As demonstrated in the simulation study is usually not consistent with its transformation and migration observed in mesocosm and paddy fields. One of the most possible reasons is that the heterogeneous environment is not taken into consideration, especially the influence of heterogeneous micro interface on As behaviors (Arsic et al. 2018, Bennett et al. 2012a, Fang et al. 2018).

1.1 The influence of micro interfaces on transformation and migration of As in paddy soil

Micro interfaces, including SWI and rhizosphere, are not only the gate controlling As migration in paddy water-soil-rice system, but also the key zone mediating As transformation. A sharp redox transition occurs along SWI and rhizosphere as a result of a large amount of organic matters in soils and radial oxygen loss from roots. The redox change simultaneously causes transformation of As species. This is particularly true for rhizosphere, since arsenite [As(III)] substrate is rich in reducing soils, while release of oxygen (O_2) and organic matter from root could provide the potential micro-aerobic condition to activate microbial-mediated oxidation or methylation of As(III).

Most studies in SWI and rhizosphere were performed under a steady or transient status. A typical distribution of elemental profiles across SWI was summarized in Fig. 1.1a. SWI normally covered a thin zone from several mm to cm scale, but redox potential (Eh) decreased rapidly from +400 mV to -200 mV from overlying water to subsoil (*vs.* Ag/AgCl reference electrode) (Wang et al. 2019b, Xu et al. 2017). When flooded, overlying water is aerobic due to atmospheric O_2 diffusion. The rapid change of Eh in subsoil is mediated by microorganisms (Borch et al. 2010). With organic matter as the electron donor, microorganisms successively utilize energetically favorable electron acceptors, such as O_2, nitrate, sulfate and iron-manganese (Fe-Mn) oxides. After flooding, O_2 is rapidly depleted in top soil. At the same time, reductive products, including ferrous Fe, sulfide and methane, increase along soil depth (Arsic et al. 2018, Damgaard et al. 2014, Pi et al. 2018). It is generally believed that distribution of As along SWI is coupled with reductive dissolution of Fe-oxides and shares the same behavior as ferrous Fe.

Rhizosphere is more complex than SWI. Along root development, rhizosphere changes, hence it's hard to define the zone of rhizosphere. A typical transient distribution of elements in rhizosphere was given in Fig. 1.1b. A high concentration of O_2 was observed around root tip, and

rhizosphere is also a hotspot of trace metal(loid)s, such as As and lead (Pb). The formation of rhizosphere is mainly ascribed to O_2 and organic matter release from root. Generally, release of O_2 from root is the dominant factor, and an O_2 gradient is formed around root (Williams et al. 2014, Zhao et al. 2013). The Fe plaque formed on rice root is an important sink for As, and could serve as a barrier for uptake of As from soils into rice root.

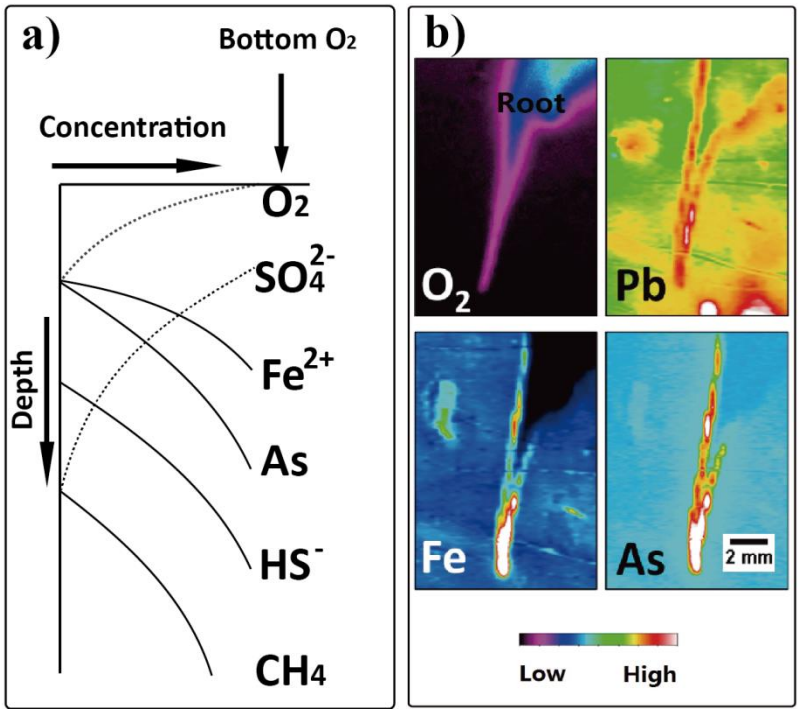

Figure 1.1 Typical distribution of arsenic across micro interfaces in flooded paddy soils. a) typical distribution of arsenic and associated elements across soil-water interface under steady status; b) distribution of arsenic and associated elements captured in a transient rhizosphere (Williams et al. 2014).

Arsenic behaviors in SWI and rhizosphere have been intensively studied, mainly focusing on the changes of total dissolved As. The transformation mechanism of As species at micro interfaces is not clear. For example, it has been well recognized that behavior of As and Fe is coupling (Arsic et al. 2018, Di et al. 2012, Ma et al. 2017, Wu et al. 2016a), but whether decoupling of As with Fe occurring in soils remains unclear. In addition, whether transformation of different As species along a stable redox gradient at micro interfaces is regulated by different

mechanisms is unknown. Further research focusing on investigating As behaviors in fine-scale is essential to answer those scientific questions. Studies of As behavior at micro interfaces would provide a novel perspective to understand the migration of As in paddy water-soil-rice system.

Arsenic and associated elements vary at the mm scale across mirco interfaces (spatially), and are easily shifted when the external environment changes (temporally) (e.g., pH, Eh, seasonal wet-dry cycle, exogenous pollutants introduction, microbial degradation, and wetland plant roots activity) (Kalbitz and Wennrich 1998a, Leermakers et al. 2005). To date, illustration of the associated mechanisms responsible for regulating As behavior at micro interfaces is hindered by techniques available to capture the spatiotemporal changes of As and associated elements.

1.2 Current techniques for sampling soil/porewater at micro interfaces

The number of porewater studies to investigate the chemical composition of interstitial fluids and biogeochemical processes along micro interface has increased considerably in recent years. In order to measure parameters at micro interfaces spatially, dynamically, *in situ* or in multi-element, many techniques were developed. Those techniques include soil slicing, Rhizon sampler, *in situ* equilibrium dialysis samplers (Peeper), diffusive equilibration in thin films (DET), diffusive gradient in thin films (DGT), X-ray absorption fine structure (XAFS) spectroscopy, micro-electrode, and optode sensor (Arsic et al. 2018, Muehe et al. 2019, Rathnayake et al. 2017, Seeberg-Elverfeldt et al. 2005). A comprehensive summary of their work mechanism, phase of sample, and study areas was presented in Table 1.1.

1.2.1 Slicing

Initially, *ex situ* slicing of frozen soil cores under anaerobic conditions was used to study the behavior of elements along SWI (Klinkhammer 1980a, Ratering and Schnell 2000, 2001). When

using, the soil is subcored with (or directly incubated in) an appropriate plastic core, and the cored soil is frozen immediately under O_2-free conditions. The frozen soil core is fixed onto a holding device, and sliced into thin layers. To obtain stratified soil porewaters, squeezing of sliced soil is required via inert gas pressure or centrifugation (Seeberg-Elverfeldt et al. 2005). The sample volume depends on the size of soil core as well as the sliced interval. Generally > 2 mL porewater were extracted (Garnier et al. 2015, Ratering and Schnell 2000). This technique could be used to reflect the spatial distribution of elements and their interactions in solid or liquid phase. However, the soil slicing method is destructive, complex and easily contaminated (De Lange et al. 1992). More recent work has focused on nondestructive sampling methods.

1.2.2 Rhizon sampler

Rhizon sampler is a classic nondestructive method that is widely used to sample porewater from soils (Muehe et al. 2019, Seeberg-Elverfeldt et al. 2005, Xu et al. 2017). When using, soil porewater can be *in situ* extracted from soils via a filter part of Rhizon sampler, which is powered by a syringe or vacuum vial. The sample volume depends on the vacuum pressure and sampling time. Generally ≥ 2 mL liquid sample were extracted in every sampling event (Beesley et al. 2010, Seeberg-Elverfeldt et al. 2005, Shotbolt 2010). After dissolved elements in extracted porewaters are measured, their correlation (e.g. coupling or decoupling) can be investigated (Xu et al. 2017). Moreover, when Rhizon samplers are placed horizontally along SWI, they can measure the vertical distribution of elements. However, the sampling zone of the sampler is poorly defined and generally > 1 cm, hence its application in high-resolution mapping at micro interface is limited (Seeberg-Elverfeldt et al. 2005).

1.2.3 *In situ* equilibrium dialysis samplers (Peeper)

In situ equilibrium dialysis samplers (Peeper) is a commonly used dialysis technique consisted

with multi-chamber (Franz et al. 2013, Hesslein 1976, Mayer 1976). The principle of this technique is to use a dialysis membrane to separate multi-chambered receiver solutions (e.g. ultrapure water) from surrounding liquids. When deployed in saturated soils, dissolved chemicals diffuse across the membrane into the chamber. After the passive diffusion reaches equilibrium, the peeper is retrieved from soils, and solutions in chambers are removed for downstream chemical analysis. Generally, there is a conflict between sample volume achievable and spatial resolution measured (Di et al. 2012, Teasdale et al. 1995). For instance, through narrowing sampling chamber, the spatial resolution of peeper can be improved to mm level, yet only 0.5 mL sample can be collected from a typical 5 cm soil depth (Di et al. 2012). In addition, peeper can only be used once after deployment, which limits the application of this technique in tracking temporal element change.

1.2.4 Diffusive equilibration in thin films (DET)

Diffusive equilibration in thin films (DET) shares a similar sampling mechanism as peeper, but rather than confining the solution to compartments, it uses a thin film of hydrogel and membrane for equilibration with solutes in porewaters (Davison and Zhang 1994, Zhang and Davison 1999). Prior to deployment, the DET probe filled with hydrogel and covered with membrane is needed to be treated with an electrolyte (e.g. $NaNO_3$ or NaCl) to alleviate potential electrostatic interactions during sampling. When deployed in saturated soils, dissolved chemicals diffuse across the membrane and at equilibrium DET probes are retrieved from soils. Then the hydrogels are removed and sliced for downstream chemical analysis (Arsic et al. 2018, Bennett et al. 2012a, Garnier et al. 2015). Generally, DET probe can sample the same volume of porewater as high-resolution peeper (< 0.5 mL) (Dočekalová et al. 2002, Su et al. 2018). This technique has been widely used to measure element profiles with high spatial resolution (μm to cm level) (Arsic et al.

2018, Davison and Zhang 1994, Gao et al. 2006). However, similarly to peeper, DET probe can only be used once after deployment, which limits the application of this technique in tracking temporal element change.

1.2.5 Diffusive gradient in thin films (DGT)

Compared to DET, DGT employs a resin sink beneath the hydrogel to enrich target analyte (Davison and Zhang 1994, Zhang and Davison 1999). When using, solutes diffuse across the hydrogel, and are adsorbed by the functional resin sink. This process continues until the resin sink is saturated. Thus, DGT probe can not only measure target analyte in soil porewater but also its resupply from solid phase. Various types of DGT devices have been developed for the purpose of measuring different contaminants (Guan 2019, Li et al. 2019), however, it is still a challenge to apply DGT probe to study the coupling behavior of various anions and cations along SWI at a certain place (Arsic et al. 2018, Gao et al. 2006, Garnier et al. 2015). This is because DGT probe can only be used once after deployment, and few parameters are measured by each type of DGT.

1.2.6 X-ray absorption fine structure (XAFS) spectroscopy

X-ray absorption fine structure (XAFS) spectroscopy provides a solution to extract chemical information from soil matrix (Koningsberger and Prins 1988, Weber et al. 2010, Welter et al. 1999). The XAFS spectroscopy uses high energy X-ray beam (4.5 to 23.5 keV) to scan sample and references, and record their absorption spectrum immediately. According to the unique fine structure spectrum of references (“fingerprints”), chemical information in samples, including nature, distance and number of the 2 - 3 next neighbor atoms of the absorbing element, can be extracted from the XAFS spectra. Combined with soil slicing method, XAFS is able to reflect spatial distribution of elements in solid phase.

1.2.7 Micro-electrode

Micro-electrode is an electrochemical method, which is very powerful for repeatedly measuring target parameter in high-resolution (μm level) (Malkin et al. 2014, Nielsen et al. 2010, Ratering and Schnell 2001). When working, voltammetric signal produced between a sharp working electrode (e.g. 10 - 100 μm diameter) and a reference electrode (*vs.* Ag/AgCl electrode) is able to *in situ* reflect the change of target parameters (Meijer and Avnimelech 1999). However, only few parameters can be measured by this method, like O_2, H_2S, Eh, and pH (Malkin et al. 2014, Nielsen et al. 2010, Ratering and Schnell 2001). Although attempts were tried to develop micro-electrodes to measure inorganic elements like As, Fe and Mn (Brendel and Luther 1995, Liu and Huang 2014), their application in real soils is limited due to the complex matrices.

1.2.8 Optode sensor

Optode sensor is an optimal method, which is very powerful for repeatedly measuring target parameter in high-resolution (μm level) (Maisch et al. 2019a). Core part of this tool is a specific luminophore, which is fixed on a foil before using. When using, the luminophore is excited with a short pulse of light of the correct wavelength. The existing of target substrate can react or collide with the excited luminophore, resulting in transfer of excited luminophore to its ground state. Then excess energy is emitted as a light (i.e. quenching), which is recorded by a camera for downstream parameter analysis (Bittig et al. 2018). Similarly to micro-electrode, only few parameters can be measured by this method, like O_2 and Eh (Bittig et al. 2018, Maisch et al. 2019a). In addition, optode sensor is very sensitive to temperature and light, thus requiring a constant temperature, dark room to enable take quantified pictures. Hence, its application in real

Table 1.1 Techniques to study micro interfaces

Technique	Working mechanism	Sample phase	Porewater removed †	Spatial mapping	Dynamic Test	*In situ* Test	Element coupling	References
Slicing	Mechanical cutting	Solid/liquid	>2000 μL	Yes	No	No	Yes	(Klinkhammer 1980a, Ratering and Schnell 2000, 2001)
Rhizon sampler	Suction	Liquid	≥2000 μL	No	Yes but limited	Yes	Yes	(Muehe et al. 2019, Seeberg‐Elverfeldt et al. 2005, Xu et al. 2017).
Peeper	Passive diffusion	Liquid	≥500 μL	Yes	No	Yes	Yes	(Chen et al. 2015a, Di et al. 2012, Teasdale et al. 1995)
DET	Passive diffusion	Gel	≥500 μL	Yes	No	Yes	Yes	(Arsic et al. 2018, Gao et al. 2006, Garnier et al. 2015)
DGT	Passive diffusion & adsorption	Resin	NA.	Yes	No	Yes	Yes	(Arsic et al. 2018, Gao et al. 2006, Garnier et al. 2015)
XAFS spectroscopy	Scanning	Solid	NA.	Yes	Yes	No	Yes	(Koningsberger and Prins 1988, Weber et al. 2010, Welter et al. 1999).
Micro-electrode	Electrochemical sensing	Liquid	NA.	Yes	Yes	Yes	No	(Malkin et al. 2014, Nielsen et al. 2010, Ratering and Schnell 2001)
Optode sensor	Luminophore sensing & scanning	Liquid	NA.	Yes	Yes	No	No	(Bittig et al. 2018, Maisch et al. 2019a)

Note: DET, diffusive equilibration in thin films; DGT, diffusive gradient in thin-films; XAFS, X-ray absorption fine structure.
† The length of DET probe and peeper is normalized to 5 cm.
NA. means not applicable.

soils is limited.

To study biogeochemical process along micro interface, numerous techniques were developed to measure the associated elements in soil solid/liquid phase in high-resolution. Due to dissolved elements represent their mobile forms in soils, hence high-resolution soil porewater samplers (e.g. peeper, DET and DGT) are most widely used. However, those samplers are disposable, and unable to track temporal element change. Thus, development of appropriate techniques able to fill this gap would greatly facilitate studies of biogeochemical processes at micro interfaces.

1.3 Analysis of dissolved elements

In addition to lacking of an appropriate method (hardware) to *in situ* repeatedly measure elements in high-resolution, associated research is also hindered by lacking of a high-throughput method (software) to take the most use of the limited porewater collected by high-resolution porewater samplers, such as DET and peeper.

There is a conflict when measuring multi-element profiles in high-resolution across the micro interface. The sharp and sensitive redox gradient along SWI or rhizosphere requires that the porewater volume sampled should be as small as possible to minimize the disturbance to the sampling environment (Seeberg‐Elverfeldt et al. 2005), yet as large as possible to meet the need to detect all the parameters interested (Arsic et al. 2018, Bennett et al. 2012a, Ding et al. 2016, Motelica-Heino et al. 2003). The samplers designed for element profile mapping generally can only take < 0.5 mL solution, which is just enough for one sample injection. An alternative to collect more samples is to collect porewater repeatedly at different place or time, assuming the soil or sediment matrix is homogenous and stable over time. However, this assumption is generally not true since the elements and their species are always changing with locations and

environmental conditions (Arsic et al. 2018, Yuan et al. 2019a). Thus, it would be better to solve the issue by optimizing the analytical techniques used in extracting data from the samples.

1.3.1 Total elements analysis

Common methods used to analyze aqueous elements were summarized in Table 1.2, including colorimetric, atomic absorption spectroscopy (AAS), inductively coupled plasma-optical emission spectrometry (ICP-OES), -mass spectrometry (ICP-MS). Colorimetric and AAS are element-specific, indicating each measurement can only measure one element composition. For colorimetric method, specific reagent for the element is essential needed for the measurement, such as ferrozine (Yamamoto et al. 2010) or phenanthroline (Tesfaldet et al. 2004) for Fe, and molybdenum for P (Ganesh et al. 2012). Accordingly, Fe and P need to be measured independently under a single source of monochromatic light (e.g. 248.3 and 214.9 nm for Fe and P respectively) with AAS (Duan et al. 1993, Jajda et al. 2015, Ng and Garner 1993). By contrast, ICP-OES and ICP-MS provide a solution to simultaneously measure multi-element (Gao et al. 2006, Jajda et al. 2015, Pyle et al. 1995), which have greatly facilitated studies of element behavior by improving the measurement throughput.

For limit of detection (LOD) (Table 1.2), colorimetric method has a high LOD (sub-mg L^{-1}), while AAS and ICP-OES have a moderate LOD (μg to sub-mg L^{-1}). In contrast, ICP-MS has a very low LOD (ng to μg L^{-1}). Among these methods, ICP-MS is the best fitted method for multi-element analysis because of its extremely low LOD (Cotta and Enzweiler 2009, Jajda et al. 2015). Although measurement of major element is easily got saturation in ICP-MS, many techniques are provided to avoid the saturation of majors. For an example, dynamic collision/reaction cells (KED/DRC) in ICP-MS are able to attenuate the sensitivity of selected elements via adjusting the velocity of reaction gas used (Cotta and Enzweiler 2009, Persson et al.

2009). More recently, a new technique, called extended dynamic range (EDR), was introduced to measure major elements through reducing their sensitivity during the measurement (Hilbig et al. 2017). The EDR technique can attenuate the counts of selected elements through the spectrometer by tuning the Rpa value, thus it enables the detection of major and minor elements in a single run. Therefore, with proper optimization, ICP-MS technique will become very powerful for multi-element analysis.

Table 1.2 Analysis of total aqueous elements

Method	Element specific	Multi-element	LOD	References
Colorimetric	Yes	No	sub-mg L^{-1}	(Ganesh et al. 2012, Tesfaldet et al. 2004)
AAS	Yes	No	µg to sub-mg L^{-1}	(Duan et al. 1993, Jajda et al. 2015, Ng and Garner 1993)
ICP-OES	No	Yes	µg to sub-mg L^{-1}	(Gao et al. 2006, Olesik 1991, Pyle et al. 1995)
ICP-MS	No	Yes	ng to µg·L^{-1}	(Cotta and Enzweiler 2009, Gao et al. 2006, Jajda et al. 2015, Persson et al. 2009)

Note: atomic absorption spectroscopy (AAS), inductively coupled plasma-optical emission spectrometry (ICP-OES), -mass spectrometry (ICP-MS); limit of detection (LOD).

1.3.2 Arsenic species analysis

Arsenic species, including arsenite [As(III)], arsenate [As(V)], monomethylarsonic (MMA) and dimethylarsinic (DMA) acid, were frequently investigated in environmental samples. Initially attempts were tried to use pH, reaction matrix, chelating agents and redox agents to selectively reduce As species for their sequential determination with colorimetric or spectrometric method, but this method is easily interfered by existence of metal ions (Anderson et al. 1986). Hence its application is limited in environmental samples like soil porewater, which usually contains Fe and Mn over 10 mg L^{-1} (Xu et al. 2017). With the development of chromatographic technique, like ion chromatography (IC) and high-performance liquid chromatography (HPLC), the coupling of HPLC/IC and ICP-MS has become the most powerful method for determining As species. Table 1.3 summarized the most widely used HPLC/IC-ICP-MS methods to analyze

Table 1.3 Analysis of arsenic species with HPLC/IC-ICP-MS under different conditions

Column	Eluent	As species	Throughput (min/sample)	References
AS4A-SC	Na_2CO_3-NaOH	As(III), As(V)	6	(Mattusch and Wennrich 1998)
AS7	$(NH_4)_2HPO_4/NH_4H_2PO_4$	As(III), As(V), MMA and DMA	10	(Pongratz 1998)
AS7	HNO_3	As(III), As(V), MMA and DMA	5	
AS14	NaH_2PO_4	As(III), As(V)	6	(Jackson and Bertsch 2001)
AS16	NaOH	As(III), As(V), MMA and DMA	7	
AS22	NH_4HCO_3	As(III), As(V), MMA and DMA	9	(Suzuki et al. 2009)
PRP-X100	$(NH_4)_2CO_3$ $(NH_4)_2HPO_4$	As(III), As(V), MMA and DMA	13 12	(da Rosa et al. 2019)
PRP-X100	$NH_4H_2PO_4$, NH_4NO_3	As(III), As(V), MMA and DMA	10	(Heitkemper et al. 2001)
IC-Pak	$(NH_4)_2CO_3$	As(III), As(V), MMA and DMA	17	
AS11	HNO_3	As(III), As(V), MMA and DMA	8	(Xie et al. 2006)
PCX-500	HNO_3	MMA, DMA	7	
Pak C18	Butanesulfonic acid sodium	As(III), As(V), MMA and DMA	5	(Hirata and Toshimitsu 2005)
CEC	$(NH_4)_2HPO_4$	As(V), MMA and DMA	11	(Li et al. 2017)
AS23			11	
RP-18	TBAH	As(III), As(V), MMA and DMA	11	(Beauchemin et al. 1989)
C18 μBondapak			16	
PRP-1			13	
Radial-Pak SAX	Na_2HPO_4/NaH_2PO_4		9	
PRP-X100			7	
PRP-1	Sodium dodecylsulphate	DMA	6	
C18-Pierce			2	

Note: common As species include arsenite [As(III)], arsenate [As(V)], monomethylarsonic (MMA) and dimethylarsinic (DMA) acid; TBAH: tetrabutylammonium hydroxid.

As species under different conditions.

The fundamental requirement in As speciation is the need to quantitatively determine each of As species independently and without interference from the other forms. The coupling of HPLC/IC and ICP-MS provides an ideal solution to achieve this. HPLC/IC is able to separate As species via ion exchange columns (Jain and Ali 2000). Then, ICP-MS can act as a high sensitive detector to determine the separated As form. Many columns are commercially available (Table 1.3). Among those columns, the most widely used are PRP-X100 and AS series (4A-SC/7/11/14/16/22/23). By employing proper eluent, the common four As species can be separated and measured in ~ 10 min. However, performance of Na_2CO_3, NaOH, HNO_3, Na_2HPO_4, NaH_2PO_4 and sodium dodecylsulphate was not stable (Beauchemin et al. 1989, Jackson and Bertsch 2001, Mattusch and Wennrich 1998), leading to unsuccessful separation and quantification of common As species. The widely used eluent for As species detection always contains PO_4^{3-}, CO_3^{2-} and NO_3^{-1}. These compounds have been identified to be strong exchanger for elution of As species (Jackson and Bertsch 2001). To avoid clogging of the cone orifices when passing the eluent through the high temperature region of the plasma, it's better to use a mobile phase consisted with volatile compounds (Divjak and Goessler 1999). This is the reason why Na^+ in eluent was replaced by NH_4^+ in recent studies (Muehe et al. 2019, Xu et al. 2017). Although high throughput measurement (e.g. 5 min) was obtained under certain eluent conditions (Hirata and Toshimitsu 2005, Jackson and Bertsch 2001), the measurement of each As specie is easily interfered by the other form with a similar retention time. Hence measurement throughput should be optimized to assure the measurement of As speciation at good-separation, good-efficiency as well as at good-

precision.

1.4 Research aims

Micro interfaces, including SWI and rhizosphere, are key zones controlling As transformation and migration in paddy water-soil-rice system. Porewater As represents its mobile form in the system. Although the study of porewaters at micro interfaces has provided the key information for understanding biogeochemical process of As, investigation of temporal As in high-resolution has been hindered by available porewater sampling techniques (Arsic et al. 2018, Muehe et al. 2019, Rathnayake et al. 2017, Seeberg-Elverfeldt et al. 2005). It is speculated that spatiotemporally tracking of As and associated element across SWI and rhizosphere could provide novel insights for understanding its cycling in paddy water-soil-rice system. Therefore, in this PhD work, I aim to resolve the cycling of As at micro interfaces with a novel soil porewater sampling technique. To achieve this aim the following topics were addressed.

1.4.1 Chapter 2 Development of techniques to sample porewater repeatedly in high-resolution

A novel soil porewater sampling technique, called *In-situ* Porewater Iterative (IPI) sampler, was developed to facilitate *in situ* monitor dynamics of dissolved elements across SWI in high spatial resolution (mm). The technique was validated in solutions and soils. The results showed IPI sampler is a powerful and robust technique for monitoring spatiotemporal dynamics of multi-element across SWI in high-resolution. The technique is patent pending (201811025505.8). The associated work has been published in *Environmental Science & Technology* (DOI: 10.1021/acs.est.8b05390).

1.4.2 Chapter 3 Optimization of analyses to measure multi-element in limited

porewaters

Analytical methods were optimized and validated in solutions and soils to measure multi-element in limited samples (μL level). With the optimized method, information of multi-element and their species can be extracted from μL level porewaters collected by high-resolution porewater samplers. The associated manuscript is under review.

1.4.3 Chapter 4 The cycling of As at paddy soil-water interface

With the novel technique developed and the high-throughput method optimized, the behavior of As in SWI was investigated. The results supported As mobilization along SWI was mainly controlled by coupling of As with Fe. Moreover, this study provided direct evidence showing decoupling processes of As and Fe could happen in the oxic-anoxic transition zone of SWI. The associated manuscript is under review.

1.4.4 Chapter 5 The cycling of As at paddy rhizosphere

With the novel technique developed and the high-throughput method optimized, the behavior of As in rhizosphere was investigated. The results showed As mobile pool in paddy soil was temporally dynamic upon flooding. Moreover, a spatially dynamic trend of As was induced by radial O_2 loss from rice root. Interestingly, most of mobile As (40 - 80%) was immobilized in 0 - 5 mm distance from root surface by the newly formed Fe oxides in rhizospheric soils. I presented a model of As transport from soil to rice, linking the temporal and spatial regulation of As in paddy soils. The associated manuscript is under preparation.

2. Development of techniques to sample porewater repeatedly in high-resolution

In flooded soils, soil-water interface is the key zone controlling biogeochemical dynamics. Chemical species and concentrations vary greatly at mm- to cm-scales. Techniques able to track these changing element profiles both in space and over time with appropriate resolution are rare. Here, I report a patent-pending technique, the *In-situ* Porewater Iterative (IPI) sampler, which is designed for soil porewater sampling with minimum disturbance to saturated soil environment. IPI sampler employs a single hollow fiber membrane tube to passively sample porewater surrounding the tube. When working, it can be integrated into the sample introduction system, thus the sample preparation procedure is dramatically simplified. In this study, IPI samplers were coupled to ICP-MS at data-only mode. The limits of detection of IPI-ICP-MS for Ni, As, Cd, Sb and Pb were 0.12, 0.67, 0.027, 0.029 and 0.074 $\mu g \cdot L^{-1}$, respectively. Furthermore, 25 IPI samplers were assembled into an SWI profiler using 3D printing in a one-dimensional array. The SWI profiler is able to analyze element profiles at high spatial resolution (~ 2 mm) every $\geq$ 24 h. When deployed in As-contaminated paddy soils, it depicted the distributions and dynamics of multiple elements at anoxic-oxic transition. The results show that the IPI sampler is a powerful and robust technique in monitoring dynamics of element profile in soil porewater at high spatial resolution. The method will greatly facilitate studies of elements behaviors in sediments of wetland, rivers, lakes and oceans.

2.1 Introduction

Aquatic sediments play an important role as sinks for metals and metalloids (Jacob and

Otte 2003). The chemical speciation and mobility of elements are mainly controlled by the redox condition, pH and organic matter content of the sediments (Arsic et al. 2018, Gaillardet et al. 2003, Violante et al. 2010). Under natural conditions, a redox transition occurs along the soil-water interface (SWI), and the biogeochemical characters vary at the mm scale in sediment (Ratering and Schnell 2001). The element profile along SWI varies when the external environment changes (e.g. pH, seasonal wet-dry cycle, exogenous pollutants introduction, microbial degradation, wetland plant roots activity) (Chen et al. 2005, Kalbitz and Wennrich 1998b, Leermakers et al. 2005, Zhang et al. 2017a). For example, arsenic (As) in soils is immobilized by mineral oxides adsorption under oxidizing conditions, but mobilized by the desorption of As from mineral oxides under reducing conditions (Arsic et al. 2018, Smedley and Kinniburgh 2002). The redox changes along the SWI result in a distinct change of As concentration in a saturated soil profile. As a gate controlling the mass exchange between the sediment and waterbody, it has always been of great interest to study the spatial as well as the temporal distribution of elements along the SWI in high-resolution. However, a deep understanding of the elemental behavior in the environment has been hindered to date by the techniques available to sample this zone.

Many techniques have been developed to study the behavior of elements along the SWI. Initially, slicing of frozen soil cores under anaerobic conditions was used (Klinkhammer 1980b, Ratering and Schnell 2000, 2001). However, the soil slicing method is destructive, complex and easily contaminated (De Lange et al. 1992). More recent work has focused on non-destructive sampling methods. The Rhizon sampler is a typical non-destructive method that is at low cost and easy to operate (Beesley et al.

2010, Gustave et al. 2018a, Gustave et al. 2018b, Meijboom and van Noordwijk 1991, Seeberg‐Elverfeldt et al. 2005). When the samplers are placed horizontally along a profile, they can measure the vertical distribution of elements (Seeberg‐Elverfeldt et al. 2005). However, the sampling zone of Rhizon samplers is poorly defined and generally greater than 1 cm, its application in high-resolution SWI studies is limited.

Compared to Rhizon samplers, peeper, diffusive equilibration in thin films (DET) and diffusive gradient in thin-films (DGT) are much powerful (Arsic et al. 2018, Chen et al. 2015a, Davlson and Zhang 1994, Di et al. 2012, Gao et al. 2006, Luo et al. 2010, Santner et al. 2010, Teasdale et al. 1995). Peeper and DET/DGT probes passively sample the solutes in porewater through diffusion/adsorption. When equilibrated, the liquid or gel is removed for element mapping analysis. The techniques have been used to map elements with high spatial resolution (μm to cm level). Although peeper and DET/DGT are powerful in mapping element profile, they can only be used once after deployment, which limits the application of the technique in tracking temporal element change (Arsic et al. 2018).

In this study, a novel technique, called *In-situ* Porewater Iterative (IPI) sampler, was developed to map spatial and temporal distribution of elements along the SWI. The IPI sampler uses a single hollow fiber membrane tube for passive sampling and active sample injection, thus the workload for sample preparation is minimized. We investigated the limit of detection (LOD), influences of carrier solution and humic acid (HA), and the characteristics of time-dependent diffusion across the sampling tube. We also reported the integration of an array of IPI samplers (IPI profiler) into a device that enables one-dimensional element profiling. The performance of IPI profiler was evaluated in field-

collected paddy soils under a changing anoxic-oxic environment by pumping N_2 or air.

2.2 Materials and methods

2.2.1 Reagents and materials

The chemicals used in this study were of analytical or electronic grade and supplied by Aladdin Chemical Reagent Co., Ltd. (Shanghai, China), unless stated elsewise. Calibration standards, including nickel (Ni), arsenic (As), cadmium (Cd), antimony (Sb) and lead (Pb), were purchased from Guobiao (Beijing) Testing & Certification Co., Ltd (Beijing, China). Humic acid (HA) was provided by Alfa Aesar (catalog # 41747). All solutions were prepared with ultrapure water (18.2 MΩ cm, Millipore Corp., Bedford, USA) deoxygenated by purging with pure N_2 for more than 4 h. The sampling tube is made of a hollow fiber membrane tube (inner*outer diameter = 1.0*2.0 mm^2, polyvinylidene fluoride, Motimo Membrane Technology Co., Ltd, Tianjin, China). The membrane has a pore size of 0.05 μm, and pore rate of 70 - 80%. All the materials were ultrasonic washed with 2% HNO_3 and 1% Decon solution for 15 min respectively, and rinsed five times with ultrapure water. All the narrow tubes were oven-dried at 40 ℃ before use.

The soil samples used in the study were collected from paddy fields in Gan Zhou (GZ, 25 °30 'N, 114 °36'E) and Qing Yuan (QY, 23 °35'N, 113 °20'E), China. The top 20 cm of soil was sampled. Soil samples were wet sieved through a 1 mm diameter sieve. The soil characteristics are shown in Table S1.1.

2.2.2 IPI sampler design and SWI profiler assembly

The structure of a typical IPI sampler is shown in Fig. 2.1A (Tidu Environment Inc.

Suzhou, China). The IPI sampler contains four components: 1. the hollow fiber membrane tube (20 mm in length), with a volume of 16 μL; 2. the diffusion depressor (0.3*0.8*5 mm^3, inner*outer diameter*length, PTFE); 3. pipe (silica tube, 0.5*1.5*180 mm^3, inner*outer diameter*length), with a volume of 35 μL; 4. cap (carbon fiber, 0.8*20 mm^2, diameter*length). The hollow fiber membrane serves as a passive sampling tube during the sample collection (loading) stage. The diffusion depressor is designed to suppress the side diffusion of solutes from the hollow fiber membrane tube to the conduits through narrowing their connection. When connected to ICP-MS, the porewater sample in hollow fiber membrane tube is pumped out through the conduits (Fig. 2.1 B). In order to avoid the negative influence of O_2 and dust in atmosphere, a carbon fiber cap is used to seal IPI sampler during sample loading stage. In order to extract soil porewater at different depth along SWI, SWI profiler was used. A SWI profiler is consisted of 25 IPI samplers, which are assembled side by side in a 3D printed holder (Fig. 2.1C). The IPI sampler and SWI profiler were stored in carrier solution before use.

2.2.3 The working procedure of IPI sampler

Once the IPI sampler is deployed into solution or saturated soil, the small molecules and ions diffuse into the hollow fiber membrane tube through the membrane (passive sampling stage, Fig. 2.1A). When equilibrium state is reached, the solution inside the tubes is introduced into ICP-MS (NexION 350X, PerkinElmer, Inc., Shelton, CT USA) (active sample introduction stage, Fig. 2.1B). When introducing the samples into ICP-MS, the caps were removed; the IPI sampler was integrated into the sampling system by replacing the sample loop in a six-way valve. The sample solution in an IPI sampler is pumped by ICP-MS peristaltic pump at the speed of 24 rpm. Twenty $\mu g \cdot L^{-1}$ rhodium in

4% HNO_3 was used as the internal standard. The ICP-MS conditions were as follows: STD mode; data only analysis; RF power 1600W; plasma gas flow rate 15 L min^{-1}; auxiliary gas flow 1.2 L min^{-1}; nebulized gas flow 0.94 L min^{-1}; the uptake flow rate is 0.5 mL min^{-1}; nickel sampling and skimmer cones were used.

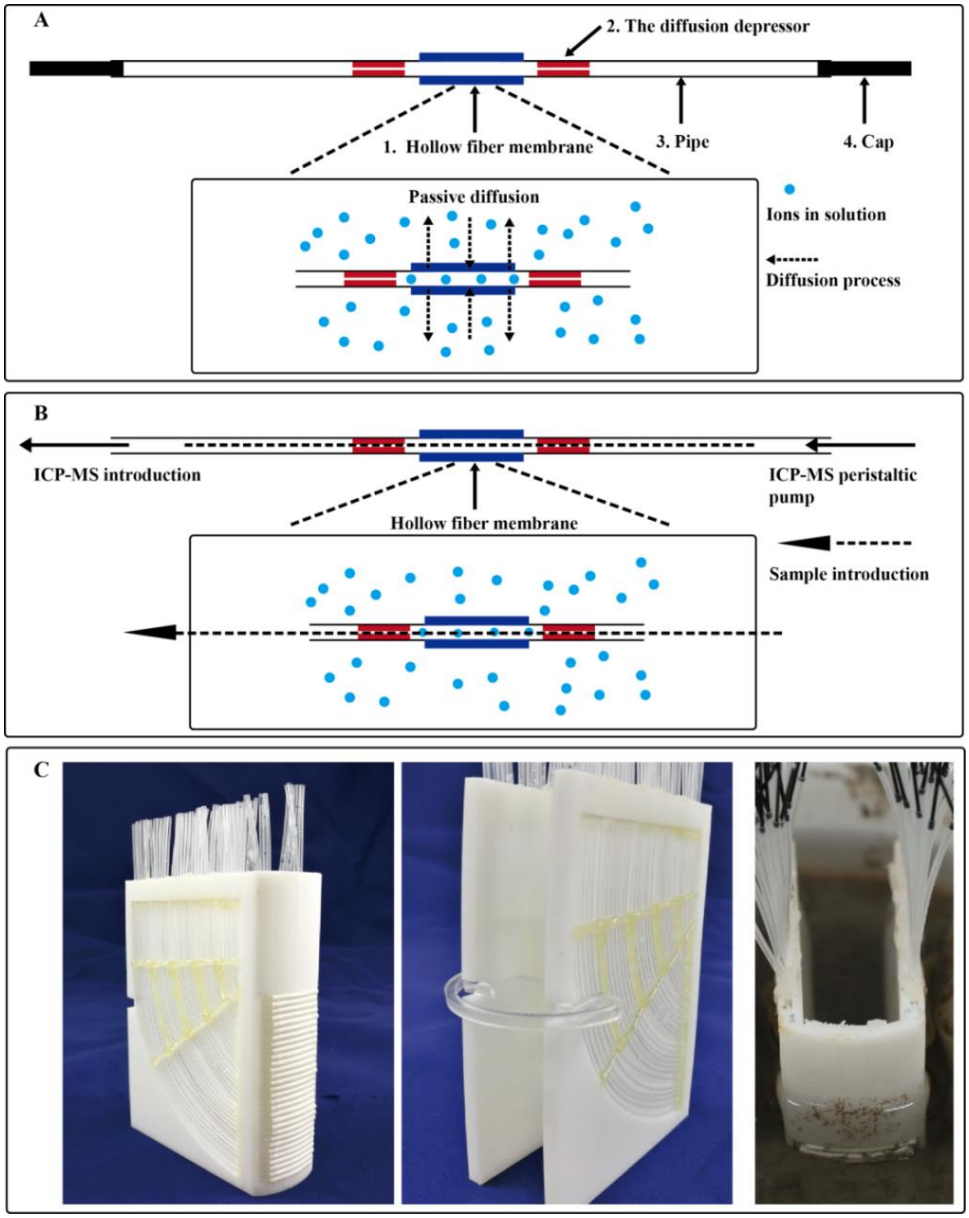

Figure 2.1 Schematic diagram of IPI sampler. (A) the loading stage of IPI sampler, element ions diffuse through the hollow fiber membrane; (B) the sample injection stage of IPI sampler, the solution inside the hollow fiber membrane is pumped into ICP-MS; (C) photos of SWI profiler (from left to right, front, back and working in soil). Notes (A): 1. hollow fiber membrane; 2. the diffusion depressor; 3. pipe; 4. cap.

2.2.4 Carrier solution test

The IPI samplers were deployed in the test solution of 10 μg·L^{-1} Ni, As, Cd, Sb and Pb before test. Six kinds of matrix condition were tested: i) ultrapure water in acidic condition (pH 1); ii) ultrapure water in near-neutral condition (pH 6); iii) 10 mM $NaNO_3$ in pH 1; iv) 10 mM $NaNO_3$ in pH 6; v) 10 mM NaCl in pH 1; vi) 10 mM NaCl in pH 6. The solution pH was adjusted by using NaOH or HNO_3.

The carrier effect of ultrapure water and 10 mM NaCl carrier solutions in pH 6 were also tested in flooded soils. The IPI samplers were deployed at a depth of 2 cm in two flooded paddy soils (GZ and QY) respectively. After 24 h incubation, the sample was analyzed by directly introducing to ICP-MS.

2.2.5 Humic acid test

The humic acid (HA) was prepared according to the previous study (Dočekalová et al. 2002). The influence of HA on Ni, As, Cd, Sb and Pb was investigated in pH 6 and 10 mM NaCl solutions (20 and 100 μg·L^{-1}) during a period of 0 - 48 h. Three levels of HA were tested: 1) 0 mg Ł$^{-1}$ HA; 2) 5 mg Ł$^{-1}$ HA; 3) 20 mg Ł$^{-1}$ HA.

2.2.6 The time-dependent response and calibration curve

The time-dependent response of IPI samplers was conducted in acidic and near-neutral conditions (pH 1 and 6; 10 μg·L^{-1} Ni, As, Cd, Sb and Pb; 10 mM NaCl). The carrier solution was 10 mM NaCl. The solutions inside the samplers were measured after 0.5, 1, 3 and 6 h equilibrium time.

When developing the calibration curve a series of standard solutions, containing 1.0, 2.0, 5.0, 10, 20 μg·L^{-1} Ni, As, Cd, Sb and Pb at pH 1 and 10 mM NaCl, were measured.

The carrier solution was 10 mM NaCl. The ICP-MS measurements were conducted after 24 h of equilibrium time.

2.2.7 Comparison of IPI sampler and Rhizon sampler

Rhizon sampler and IPI sampler with the same hollow fiber membrane tube were compared in flooded soils. The samplers were fixed alternately on a clean acrylic plate with an interval of 1 cm in triplicate, and deployed horizontally at a depth of 2 cm in GZ and QY soils. After 24 h equilibration, the sample in IPI sampler was analyzed by ICP-MS. Then, 2 mL porewater was extracted by Rhizon sampler and analyzed by ICP-MS.

2.2.8 Non-destructive measurement of the temporal element profile change in SWI

An SWI profiler is made of 25 individual samplers with the assistance of a 3D printer. The SWI profiler is able to measure the elements distribution over a distance of 6 cm, with a resolution of ~ 2 mm. To detect the element profile, the SWI profilers were inserted into paddy soils which have been flooded for half a year, with 1 cm above SWI and 5 cm buried in paddy soils (Fig. 2.1C). The porewater element concentrations were measured every day under different environmental disturbance: Day 0, SWI profiler installation; Day 1, no disturbance; Day 2-3, continuously N_2 bubbling in surface water; Day 4-6, continuously air bubbling in surface water; Day 7-8, continuously N_2 bubbling in surface water. Nitrogen gas was provided by a high pressure tank, air by an air pump. Three pipettes were deployed evenly at 1 cm above the SWI in the container, and the bubbling in surface water was via these pipettes.

2.2.9 Statistical analysis

We used the statistical program R version 3.5.0 to analyze and plot the data. Standard

deviation (SD) was used to show the variance. All raw data and the R scripts used to process and analyze the data can be found in Supporting Information. A one-way analysis of variance (ANOVA, $p < 0.05$, IBM SPSS statistics 22) was carried out to analyze the difference of IPI sampler and Rhizon sampler for measuring elements.

2.3 Results and discussion

2.3.1 Effects of carrier solution

Carrier solution was used to expel the solution in the sampling tube. The composition of carrier solution may affect the diffusion processes of target ions across the membrane during passive sampling stage, and interfere the measurement during active sample injection stage. It is supposed that carrier solution may modify the characteristics of the membrane. Similarly, a certain ionic strength carrier solution is efficient in reducing the electrostatic interactions in DET/DGT (Arsic et al. 2018, Garnier et al. 2015, Zhang and Davison 1999). As for polyvinylidene fluoride membrane, complexation effect may occur between metals, like Pb, and fluoride on the membrane (Urbansky and Schock 2000). If there is no significant interaction between target elements and membrane then O_2-free ultrapure water is the preferred carrier solution which has minimal interference to the sampling environment. In this study, three kinds of solutions, including ultrapure water, 10 mM $NaNO_3$ and 10 mM NaCl, were used to drive the sample solution inside the IPI samplers to ICP-MS.

The influences of carrier solution are summarized in Table S1.2. The results indicated that the pH condition did not significantly alter the response of the elements tested. Nickel, As, Cd and Sb ions showed high permeability through the sampler membrane. High sensitivities of those elements were founded when water, $NaNO_3$ and

NaCl solution were used as carrier solution in acidic and near-neutral conditions (Table S1.2). However, no Pb signal was observed under near-neutral conditions when using ultrapure water and 10 mM $NaNO_3$. High sensitivities for Pb ions were observed under acidic conditions, or 10 mM NaCl as the carrier solution under near-neutral conditions. It is speculated that the Pb ions were trapped by the fluorine on polyvinylidene fluoride membrane by forming fluoride-complexes (Urbansky and Schock 2000). Moreover, the blocking effect disappeared when there was Cl, which forms Pb complexes which are more stable in solution (Seward 1984). Considering the negative influence of fluorine on the measurement of Pb as well as the possible influence on other metals, fluorine-free membrane, like modified polyethersulfone membrane, maybe a better choice than polyvinylidene fluoride membrane for the quantitatively sampling of metals by IPI samplers.

The carrier solution effects were further tested in soil conditions. When ultrapure water and 10 mM NaCl in pH 6 were used as the carrier solution for soil porewater measurement, a similar phenomenon as in solution experiment was observed. No Pb was detected in samples from either soils with ultrapure water as the carrier solution (Fig. S1.1A&B); however, significant Pb was observed in both soils with 10 mM NaCl as the carrier solution (Fig. S1.1C&D). In order to test the samplers' performance on Pb measurement, NaCl solution was chosen as the carrier solution in this study.

The Cl in matrix is known to interfere the detection of As by forming $^{40}Ar^{35}Cl^{+}$, which is of the same mass-to-charge ratio of $^{75}As^{+}$ (Hirata et al. 2006). In this study, we also noticed an increase of As counting from 800 to 2500 (Fig. S1. 2A&B), when the carrier solution switched from ultrapure water to 10 mM NaCl. The detection limit gets

worse when NaCl solution is used but still acceptable because As concentrations are generally high in As-contaminated soils. Thus, the NaCl solution was used as carrier solution to measure As in solution and soil porewater samples (Fig. S1.2C&D).

2.3.2 Effects of humic acid

Humic acids are ubiquitous in soil environment, and they may act as natural chelates to complex metals (Leermakers et al. 2005, Violante et al. 2010, Zhai et al. 2018). The large HA-metal complex may be rejected by the porewater samplers as a result of their large size (Dočekalová et al. 2002, Reynolds et al. 2004, Zhai et al. 2018). The influences of HA on Ni, As, Cd, Sb and Pb are shown in Fig. S1.3.

The results indicated HA treatment had no significant influence on As and Sb at all levels. Unlike As and Sb, Pb measured by the IPI sampler was significantly reduced by the HA with a concentration of 5 - 20 mg L^{-1}. Similar phenomena were found on other metals (Ni, Cd). Moreover, HA also extended the equilibration time of Pb, Ni and Cd from 3 h to 12 - 24 h with increasing HA. The longer equilibration time for metals after adding HA is because HA-metal complex has much smaller diffusion coefficient than the free metal (Dočekalová et al. 2002). Due to the small pores (50 nm) on the IPI sampler, large HA-metal complexes maybe rejected during the sampling (Davison 2016, Reynolds et al. 2004, Zhai et al. 2018). Therefore, 24 h equilibration time is recommended for the using of IPI sampler in soils, especially for the environments containing large metal complexes.

2.3.3 Time-dependent sample loading into hollow fiber membrane tubes

The working procedure of IPI sampler consisted of a passive sampling stage followed by

an active sample injection stage. At the passive sampling stage, the ion concentrations across the tube membrane were equilibrated. The equilibration time determines the time resolution of the IPI sampler. The time can be calculated by Fick's second law. *Eq. 1* yields the time required for a solute to reach a distance x (Harper et al. 1997, Kärger and Ruthven 2016).

$$t = \frac{x^2}{2D} \quad (1)$$

where t is the time (s) that the concentration of solute at distance x (cm) can reach equilibration, D ($cm^2\ s^{-1}$) is the diffusion coefficient of solute.

In the IPI sampler, x equals to the radius of the tube (1 mm), and D is ~ 5×10^{-6} $cm^2\ s^{-1}$ for most metal ions at room temperature (Zhang and Davison 1999). Thus we estimated the equilibration time is approximately 17 min (*Eq. 1*). However, the calculated duration may be an underestimate, because the extended ion diffusive pathway through the membrane and other factors are not counted in the calculation (Chou et al. 2005).

The time-dependent sample loading process was tested in solution condition. As showed in Fig. 2A, all the 5 elements share a similar time-dependent loading process pattern regardless of pH conditions. The elements' concentrations in IPI samplers increased sharply within the first hour, and then increased slowly to a plateau after 3 h. The equilibrium time (hour level) in IPI sampler is consistent with the time (hour level) yielded in a partial resupply mode of analytes when leaving one side of DET gel to the medium (Harper et al. 1998, Zhang and Davison 1999). Therefore, it is concluded that the minimum time required to reach equilibrium of the solute across the IPI membrane is 3 hours with HA free medium, but ≥ 24 hours equilibrium time is recommended for the

sampling of porewaters.

2.3.4 Comparison of sample introduction and IPI sampler based introduction in ICP-MS

IPI sampler provides an alternative way to bridge the environmental samples and analytical machines. Compared to direct sample introduction mode for general ICP-MS analysis, IPI samplers contain a hollow fiber membrane tube. The tube serves as a passive sampling tube during the sample loading stage and a conduit in active sample injection stage, as described in Fig. 2.1. Based on the working mechanism, we consider the quantitative measurement of the solutes may be influenced by 1) the diffusion of solute from the sampling tube to the silica tube (side diffusion); 2) solution leakage/exchange during active sample injection stage.

Side diffusion might lead the total amount of solute inside the sampler increasing with deployment time. In the IPI samplers, diffusion suppressors were placed on each side of the sampling tube to reduce the side diffusion (Fig. 2.1A). According to Fig. 2.2A, the increasement of sample loading into the tube was insignificant after 3 hours, which implies the movement of solutes from sampling tube to silica tube was negligible. However, the influence of side diffusion is inevitable, in order to measure elements in environmental samples accurately, it is recommended that the IPI samplers for calibration and testing should be deployed in the standard solutions and environmental samples for a same period to reduce the influence of deployment time on elements' signals.

During the active sample injection stage, the pump may induce a pressure difference across the membrane, therefore an exchange of solution may occur. The positive pressure inside the tube may cause solution leakage and undercount the signal, *viz.* negative

pressure may cause solution suck-in and overcount the signal. Thus we analyzed the ele-

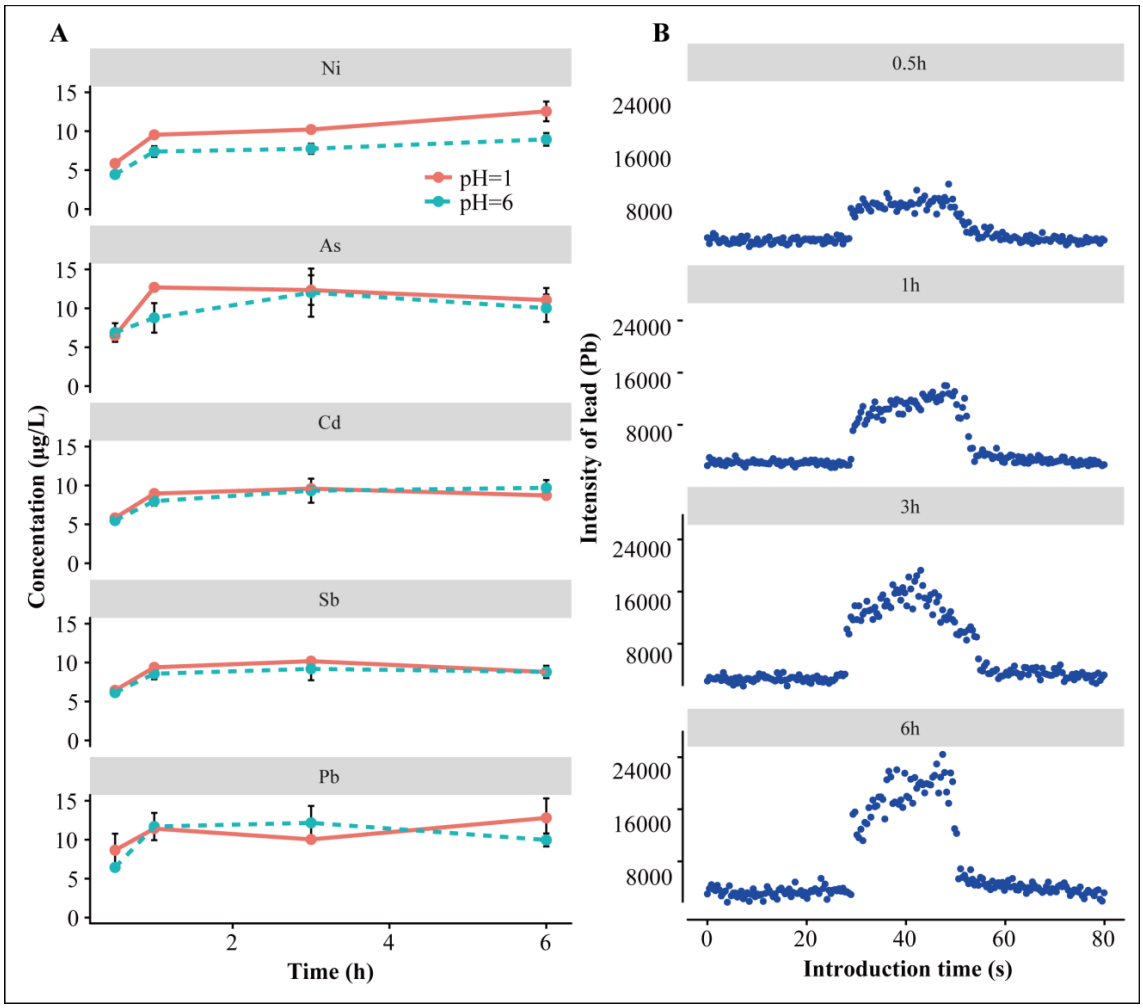

Figure 2.2 The dynamic equilibration process and peak area based calibration curve of different elements. (A) the dynamic equilibration process of 10 μg·L^{-1} nickel (Ni), arsenic (As), cadmium (Cd), antimony (Sb) and lead (Pb) under acidic (pH 1, 10 mM NaCl) and near-neutral (pH 6, 10 mM NaCl) conditions; (B) the peaks of Pb in different equilibration time under near-neutral conditions.

-ment signals generated from IPI sampling mode and direct sampling mode. Broad peaks of ~ 20 s of every element (e.g. Pb, Fig. 2.2B) were detected in IPI sampling mode. Considering the flow rate of carrier solution was 0.5 mL min^{-1}, the sample volume for the peak was ~ 170 μL (0.5 mL/60 s*20 s), which equals to the whole volume inside the sampler (~ 86 μL) plus another 86 μL of the internal standard solution. This result

indicates the sample in hollow fiber membrane tube (16 μL) is mixed with the carrier solution in two pipes (35 μL*2) during sample introduction. This indicates IPI sampler always has a dilution coefficient of ~ 5 times of the outer solution, which can be used as a parameter to determine whether an IPI sampler works appropriately. No obvious mass exchange across the hollow membrane was observed during the sample injection.

2.3.5 Calibration curve and LOD

The calibration curve was generated by deploying the IPI samplers in a series of standard solutions for 24 hours. The response of each element was calculated by the peak areas. The data processing method is shown in Fig. S1.4. The points higher than baseline + 5SD are selected for peak area integration. The coefficients of determination for all the five elements are > 0.995. According to IUPAC definition (Long and Winefordner 1983, Yola and Özaltin 2011), the LODs are 0.12, 0.67, 0.027, 0.029 and 0.074 $\mu g \cdot L^{-1}$ for Ni, As, Cd, Sb and Pb, respectively.

2.3.6 Comparison of IPI sampler and Rhizon sampler

The comparison of IPI sampler and Rhizon sampler for measuring Ni, As, Cd, Sb and Pb was carried out in GZ and QY paddies (Table S1.3). Cadmium was below the LOD in both samples. The two methods showed no difference in measuring As and Sb. However, lower Ni and Pb were obtained by IPI sampler than Rhizon sampler for both soils, which can be explained by the different sampling mechanisms for Rhizon samplers and IPI samplers. Tension-free samplers, like IPI sampler, measure the metal species with the molecular size enabling them to pass through the diffusion pores on the sampler freely. In principle, free metals and colloidal metals with the size < 50 nm are able to be measured by the IPI sampler. However, larger size particles may be squeezed into Rhizon samplers

by the tension generated by syringes, which lead to an over-estimation of metal concentrations (Reynolds et al. 2004). The experiment on HA addition showed some Ni, Cd and Pb form complexation with HA and cannot diffuse into IPI samplers, the complexation effect is insignificant for As and Sb (Fig. S1.3). Thus, in soil condition, IPI samplers have comparable performance with Rhizon samplers for elements in ions or small moleculars, like As and Sb, but give smaller counts if huge colloidal metals exist.

2.3.7 Nondestructive spatial and temporal metal measurement by SWI profiler

With developed calibration curves, the SWI profiler is able to measure the dynamic changes of element profile in two As-contaminated paddy soils. The soils were exposed to different redox conditions by bubbling air or N_2 gases. The vertical changes of As in GZ soil porewater are depicted in Fig. 2.3. At Day 1, the As concentrations were generally lower than 40 $\mu g \cdot L^{-1}$ with small variation. The As levels increased slightly with the depth. The deployment of SWI profiler at Day 0 was probably responsible for the low As concentration observed at Day 1 as it may introduce O_2 to soils. Similar As gradients along SWI were clearly observed in other days. The results represented a typical redox controlled element profile, which have been widely reported in other studies (Arsic et al. 2018, Gaillardet et al. 2003, Leermakers et al. 2005).

The temporal changes of As profile in SWI were rarely reported. In this study, we are able to track the daily changes of As profile by using SWI profiler. In GZ soil, the As profile below 10 mm of SWI was not influenced by the surface water redox condition, but porewater As near SWI was sensitive to anoxic-oxic transition (Fig. 2.4A&S1.4A). It increased under anoxic conditions (Day 2-3, Day 7-8) and decreased under oxic conditions (Day 4-6). The increase of As after pumping N_2 (Day 2-3, Day 7-8) around

SWI could be attributed to the release of As during metal mineral reduction and dissolution when the redox conditions at SWI shifted from oxic to anoxic, and from day 4 to 6, the air pumped into surface water facilitated Fe oxides formation and As(III) oxidation at SWI, thus As was adsorbed by the oxides and decreased in porewater (Arsic et al. 2018, Fawcett et al. 2015, Zhang et al. 2017b). However, no obvious As fluctuation was observed in QY soil (Fig. S1.5A). The result reflects a quick matter movement in sandy GZ soil and a relative slow change in loamy QY soil (Shaheen et al. 2013). This finding strongly supports the SWI profiler is a powerful and robust tool to trace the temporal change of elements. However, more tests are essentially needed before applying SWI profiler in other environments, like salty or acidic soils and sediments.

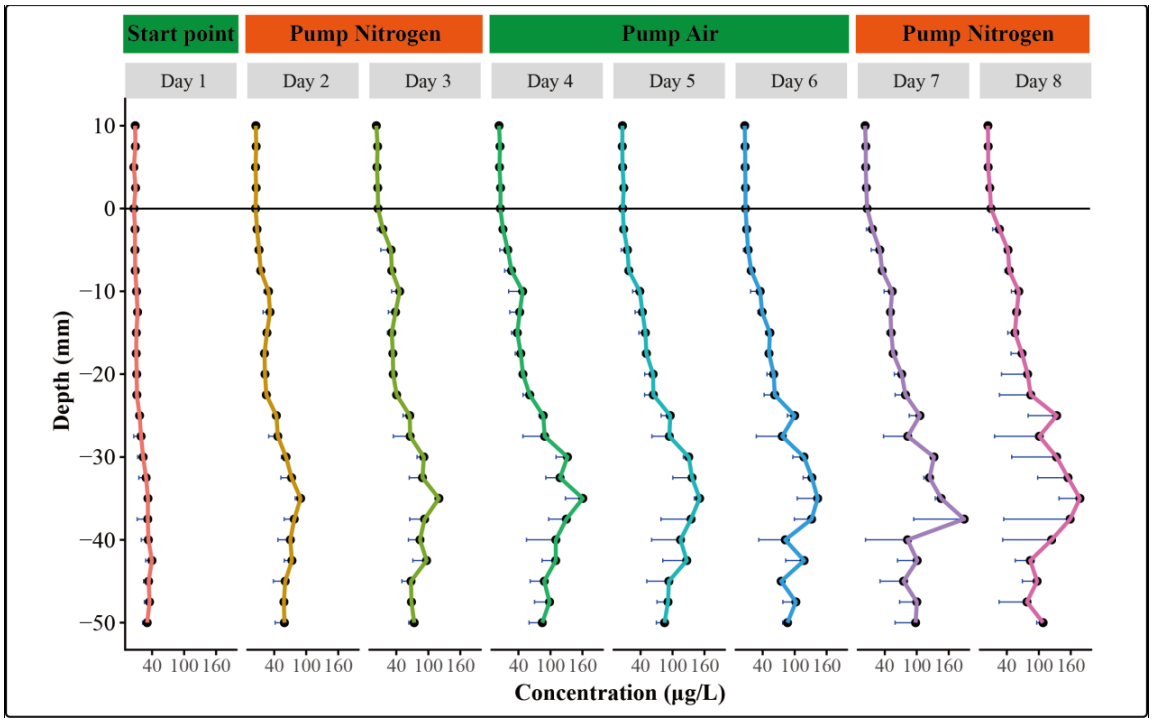

Figure 2.3 The vertical profile changes of soil porewater arsenic (As) along the 60 mm SWI in 8 days under different conditions. The error bars are standard deviations (SD, n = 3).

The dynamic changes of other elements, including Ni, Cd, Sb and Pb, were also tracked and presented in Fig. 2.4&Fig. S1.5. The concentrations of those elements were

much lower than As. Nickle profile was constant with time in both soils (Fig. 2.4B&Fig. S1.5/6/7B). Spatially, porewater Ni concentrations were higher than Ni in surface water in QY soil. The concentrations of Cd in both soils were as low as < 1 $\mu g \cdot L^{-1}$ (Fig. 2.4C&Fig. S1.5/6/7C). Antimony was found to be mobile in SWI (Fig. 2.4D&Fig. S1.5/6/7D), which is consistent with the previous results using DGT probe (Arsic et al. 2018, Guan et al. 2015). Lead showed a fluctuation along with the anoxic-oxic transition in both soils (Fig. 2.4E&Fig. S1.5/6/7E), and it tends to be immobilized under anoxic conditions (Day2-3, Day7-8) (Bryan and Langston 1992, Liu et al. 2018).

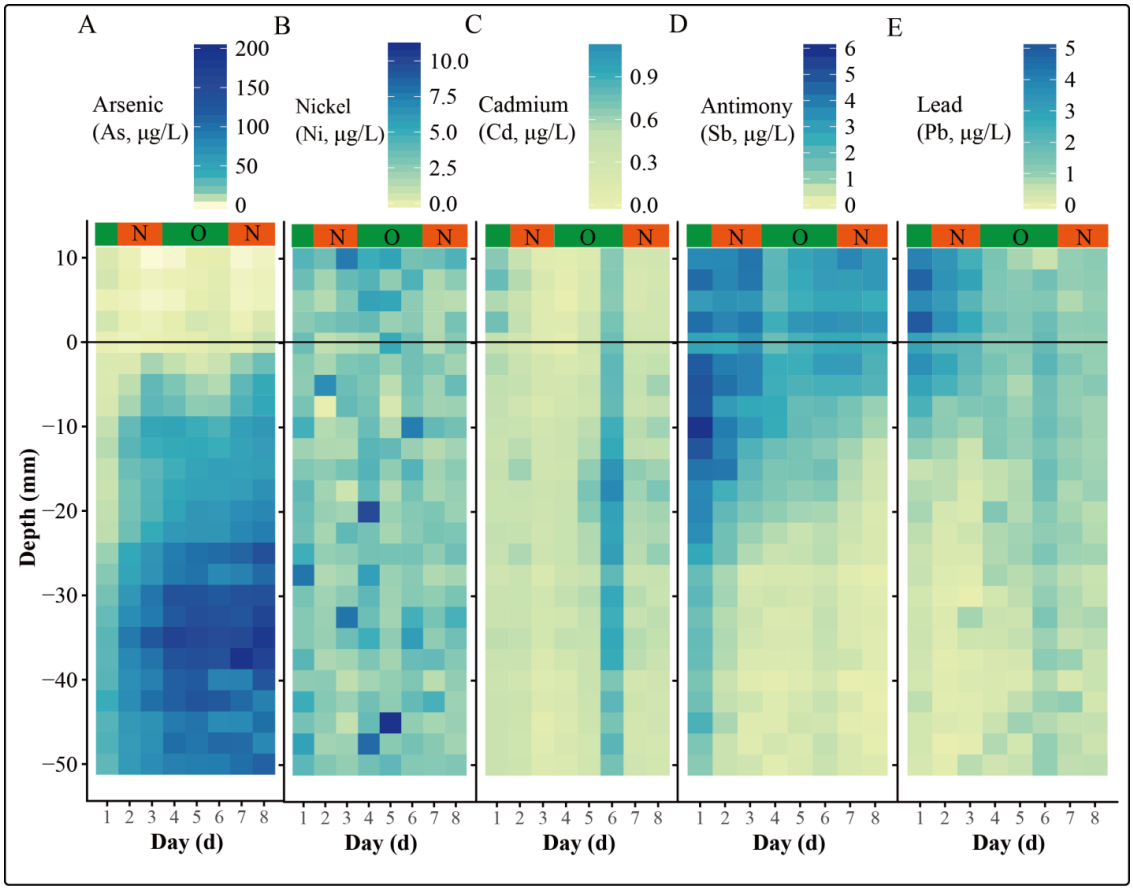

Figure 2.4 The dynamic vertical profile changes of As (A), Ni (B), Cd (C), Sb (D), and Pb (E) in GZ soils showed in heatmaps. "N" and "O" represent pumping N_2 and air respectively.

2.3.8 Comparison with other commercial techniques

Rhizon samplers, peepers and DET probes are most widely used and commercially available devices for the studies on soil/sediment porewater. Rhizon sampler can extract porewater within minutes to hours (Meijboom and van Noordwijk 1991, Shotbolt 2010). Peeper and DET probe are able to passively collect the solutes in porewater after several hours/days deployment (Di et al. 2012, Garnier et al. 2015). A comparison of these three methods with SWI profiler is given in Table 2.1.

The sediment porewater sampling techniques mentioned above have been used to reveal the element gradient along SWI (Fawcett et al. 2015, Leermakers et al. 2005). Horizontal insertion of Rhizon samplers can give a good spatial resolution (~ cm) of elements along SWI (Seeberg‐Elverfeldt et al. 2005). However, the sampling zone of Rhizon sampler strongly depends on the volume of the retrieved fluids (Seeberg‐Elverfeldt et al. 2005), which may cause bias to the element profile. Peeper has a typical resolution of 1 cm, but higher resolution (mm) can be achieved by using small volume chamber (Chen et al. 2015a, Di et al. 2012, Teasdale et al. 1995). The spatial resolution of DET probe is around 2 mm if the gel was cut before ICP-MS measurement (Dočekalová et al. 2002, Gao et al. 2007). The spatial resolution of SWI profiler is determined by the size of the hollow fiber membrane tube, which has a comparable spatial resolution with high-resolution peeper (HR-peeper) and DET probe (mm scale) in this study (Table 2.1).

SWI profiler has big advantages when being applied to the time-dependent element change in soil porewater. The volume of porewater extracted or equivalent porewater was used to compare the disturbance to soil/sediment environment among different sampling techniques in one sampling event (Table 2.1). The measurement zone of high-resolution

porewater samplers was calibrated to 5 cm. Rhizon sampler extracts porewater directly from the soil via a syringe or vacuum vial, the sample volume is depended on the vacuum pressure and sampling time, generally ≥ 2 mL liquid sample were taken in every sampling event (Beesley et al. 2010, Meijboom and van Noordwijk 1991, Seeberg‐Elverfeldt et al. 2005, Shotbolt 2010, Su et al. 2018). Other samplers work passively, i.e. only the dissolved components were extracted, thus the disturbance of passive samplers is evaluated by the equivalent porewater volume. The removed solute in porewater by peeper is determined by the designed chamber volume. Low spatial resolution peeper (1 cm) could extract a large equivalent porewater volume (~ 10 mL) (Teasdale et al. 1995), but HR-peeper only consumes a small volume of porewater (~ 450 μL) (Chen et al. 2015a, Di et al. 2012). By contrast, the least solute in porewater was consumed by DET (440 μL) and SWI profiler (400 μL) (Dočekalová et al. 2002). The low disturbance of SWI profiler to porewater makes it an ideal tool to repeatedly sample porewater at a certain place. Although HR-peeper and DET probe can be used to study the time series of element change by continuously deploying and taking out of HR-peeper or DET probes, the deployment and take-out cycles may pose disturbances to the sediment, and the coarse sediment may in turn tear the membrane or gel layer on DET probes (Davison 2016, Martin et al. 2003, Seeberg‐Elverfeldt et al. 2005). These influencing factors may cause high variability to the element profile. Low mechanical disturbance of the sediment can be achieved with Rhizon sampler method (Seeberg‐Elverfeldt et al. 2005). However, Rhizon sampler would be blocked by the suspended soil particles under repeated usage (Beesley et al. 2010, Seeberg‐Elverfeldt et al. 2005). By contrast, SWI profiler has much longer service life, and no blocking event was noticed after 10 times

use in soils.

With SWI profiler, it is easy to monitor the high spatial (mm level) distribution of metals at a certain place repeatedly. However, great care should be taken to sample porewater from SWI profiler in high frequency (e.g. daily), since the buffer capacity to porewater is varying among different soils and sediments (Harper et al. 1997). This indicates, when sampling in high frequency, underestimation of the components in porewater may happen, especially for the soils or sediments with limited buffer capacity. Therefore, in order to yield the reliable element profiles, low sampling frequency is recommended for applying SWI profiler in long-term monitoring.

Although all the samplers' quality was checked before application, failed samplers were occasionally found in SWI profiler. A diagnostic graph is shown in Fig. S1.8 to help users to preview the data and remove invalid data. In this test, no peaks were observed in sample11&32, and part of sample83 peak was missing. A post-experiment check found the blocking problem was caused by the dropping debris from carbon fiber caps.

The complexity of sample preparation before measurement is a key parameter when selecting analytical methods. There is almost no cost for sample preparation for SWI profiler method, since the samples were directly introduced to ICP-MS. For Rhizon sampler and peeper methods, it is common to use a small amount of acid to stabilize the element before instrument analysis (Di et al. 2012, Su et al. 2018). The sample preparation of DET technique is manually intensive (Davison 2016). In addition, a 24 hours elution with NaOH or HNO_3 is needed for the instrument analysis (Gao et al. 2007, Garnier et al. 2015). In comparison with DET, an advantage for peeper, SWI sampler and Rhizon sampler is to obtain clean liquid porewater sample directly, which is almost ready

for instrument analysis (Table 2.1). Many alternative solutions were proposed to reduce the sample preparation steps for DET probes, e.g. replacing manually gel slicing with guillotine devices (Shuttleworth et al. 1999), and coupling DET probe with colorimetric analysis (Davison 2016). As for SWI profiler, the sample collection and introduction into ICP-MS share the same single hollow fiber membrane tube, which would greatly simplify the sample preparation and analysis. Typically, it takes only 50 min for the multi-element sampling and measurement of the whole samples from one SWI profiler when directly connecting to ICP-MS (2 min/sample*25 samples/SWI profiler). The high sample measurement throughput is only achievable in "on-line" mode by connecting IPI samplers with ICP-MS. If dirt samples are not allowed in clean lab for ICP-MS operation, the IPI samplers can work in "off-line" mode. The "off-line" mode is time-consuming because soil pore water must be extracted first and sent for ICP-MS lab with proper preparation.

2.4 Conclusion

I presented the feasibility of coupling IPI sampler with ICP-MS. When the IPI sampler is applied in field, the solution can be pumped out and stored in tubes for lab-based analysis by the instruments able to measure small volume of sample (~ 100 μL), for examples, ion chromatography (IC), microplate reader, flow cytometer and dynamic light scattering (Chen et al. 2011, Das 2012, Jackson and Bertsch 2001). More application based on IPI samplers can be foreseen in the future and assist the studies on soil and sediment sciences.

Table 2.1 The comparison between commercial methods for soil porewater study and SWI profiler

Method	Time Resolution	Spatial Resolution	Porewater removed (μL)†	Repeated usage	Liquid sample	Sample process & analysis time	References
Rhizon sampler	Minutes to Hours	~cm	≥2000	Yes but limited	Yes	Hour to day	(Beesley et al. 2010, Meijboom and van Noordwijk 1991, Seeberg-Elverfeldt et al. 2005, Shotbolt 2010, Su et al. 2018)
DET probe	Hours to days	mm to cm	440	No	No	Day to week	(Davison 2016, Dočekalová et al. 2002, Gao et al. 2007, Garnier et al. 2015)
Peeper	Hours to days	mm to cm	450-10000	No	Yes	Hour to day	(Chen et al. 2015a, Di et al. 2012, Teasdale et al. 1995)
SWI profiler	Hours to days	Mm	400	Yes	Yes	Min to hour	This work

†: The porewater volume extracted or equivalent porewater volume calculated by the solute diffused into the samplers was used to evaluate the disturbance of sampling techniques to soil/sediment environments. The lengths of DET probes, peeper, and SWI profiler are normalized to 5 cm.

3. Optimization of analyses to measure multi-element in limited porewaters

The soil-water interface (SWI) is a zone of complex aqueous chemistry which controls element cycling in flooded lands. However, detailed investigation of chemical reaction dynamics within SWI is limited by the sampling and analytical methods available. Here with an optimized ICP-MS method and an updated porewater sampler, I demonstrate mapping of chemical profile in high-resolution (1.7 mm) across SWI, for priority elements including arsenic (As), iron (Fe), manganese (Mn), phosphorus (P), and sulfur (S) as well as speciation of As, P and S. Dissolved Fe and Mn in high concentrations (> 10 mg L^{-1}) were measured by ICP-MS in an extended dynamic range (EDR) mode to avoid signal overflow. The dissolved Fe profile along SWI generated by ICP-MS was slightly lower than that measured by colorimetric method, but of the same trend. Furthermore, four As, one P and two S species were separated in 10 minutes by IC-ICP-MS with NH_4HCO_3 mobile phase. I verified the technique in paddy soils collected from the field. The technique developed in this study will greatly facilitate the study of biogeochemical cycling of redox sensitive elements in flooded soils.

3.1 Introduction

In flooded soils, the chemical environments of the surface water and saturated sediment pores are very different. The surface water is oxidizing due to the high dissolved O_2, however, the sediments are generally in a reducing state owing to the lack of O_2 and the abundance of organic matters (Frenzel et al. 1992). The narrow zone between the surface

water and sediments, i.e. soil-water interface (SWI), displays a sharp redox change (Ratering and Schnell 2001). Iron (Fe), manganese (Mn) and sulfur (S) are important elements in SWI, existing in both solid and liquid phase through complex redox processes (Peng et al. 2019). The redox processes of Fe, Mn and S significantly impact the fate of many elements of environmental concern, such as arsenic (As) and phosphorus (P) (Gao et al. 2016, Gao et al. 2006, Mcadams et al. 2016, Pi et al. 2018). Although it is of great importance to study the behavior of these elements in SWI, the high-resolution (mm) mapping of those elements and their species has been severely limited to date by the lack of suitable available methods.

Many efforts have been made to measure the high-resolution element profile in porewater along SWI. The most commonly used methods are the diffusive equilibrium/gradient in thin films (DET/DGT) technique and *in situ* equilibrium dialysis samplers (peepers) (Arsic et al. 2018, Bottrell et al. 2007, Di et al. 2012, Dočekalová et al. 2002, Guan et al. 2015, Monbet et al. 2008). Thus far, DGT probe is the most powerful tool, which can provide a μm-resolution map of elements when coupled with laser ablation inductively coupled plasma mass spectrometry (LA-ICP-MS) (Williams et al. 2014). Various types of DGT devices have been developed for measurement of different contaminants (Guan 2019, Li et al. 2019). However, it is still a challenge to apply DGT probe to study the coupling behavior of various anions and cations along SWI at the same location. This is because DGT probe can only be used once after deployment, and multiple parameter require more than one DGT probe. Peepers can sample porewater at a resolution as high as 2 mm (Di et al. 2012). However, they require several days' deployment before reaching equilibrium across membrane. Recently, a novel porewater

sampler, called *In-situ* Porewater Iterative (IPI) sampler, was developed to monitor the fine-scale (mm) heterogeneity of heavy metals in saturated soils (Yuan et al. 2019a). The IPI sampler, unlike DGT and Peeper, is able to be used repeatedly at a single place. Once the porewater samples are collected, the range of analyses possible is broad and limited only by the sample volume and the analytical instruments available.

There is a conflict when mapping multi-element profiles in high-resolution across SWI. The sharp and sensitive redox gradient along SWI requires that the porewater volume sampled should be as small as possible to minimize the disturbance to the sampling environment (Seeberg‐Elverfeldt et al. 2005), and yet as large as possible to meet the need to detect all the parameters interested (Arsic et al. 2018, Bennett et al. 2012a, Ding et al. 2016, Motelica-Heino et al. 2003). The samplers designed for element profile mapping generally can only take less than 0.5 mL solution, which is just enough for one sample injection. An alternative to collect more samples is to collect porewater repeatedly at different place or time, assuming the soil or sediment matrix is homogenous and stable over time. However, this assumption is generally not true since the elements and their species are always changing with locations and environmental conditions (Arsic et al. 2018, Yuan et al. 2019a). Thus, it would be better to solve the issue by optimizing the analytical techniques used in extracting data from the samples.

As the most powerful analytical machine for elements, the development of ICP-MS has greatly enhanced the understanding of elements behaviors in environments. For examples, the combination of LA-ICP-MS and DGT probes allows to map μm-scale elements profiles, and provided key information for understanding As behaviors on root apexes (Williams et al. 2014). The measurement of As speciation was very difficult until

the method based on HPLC-ICP-MS was developed (Islam et al. 2004). The discovery of thio-arsenic benefited from dynamic range cell (DRC) technique, which enables the simultaneous measurement of As and S (Wallschläger and Stadey 2007). More recently, a new technique, called extended dynamic range (EDR), was introduced to simultaneously measure major and trace metals by ICP-MS (Hilbig et al. 2017). The EDR technique can attenuate the counts of selected elements through the spectrometer by tuning the Rpa value, thus it enables the detection of major and minor elements in a single run. The technique could be applied to measure all the elements in porewater, which always contains Fe and Mn over 10 mg L^{-1}, and other elements in several μg L^{-1}. To date, however, it has not been tested.

In this study I aimed to simultaneously measure profiles of multiple elements and element species in porewater with newly developed IPI samplers and optimized ICP-MS methods. The typical redox active elements, including Fe, Mn, As, P and S, were investigated. The application condition of the method was validated both in laboratory solutions and flooded paddy soils.

3.2 Materials and methods

3.2.1 Reagents and materials

All reagents used in this study were of analytical grade or higher, and purchased from Aladdin Chemical Reagent Co., Ltd. (Shanghai, China), unless noted elsewhere. Element standards for calibration, including As, Fe, Mn, P, S as well as P, S and As species, were supplied by Guobiao (Beijing) Testing & Certification Co., Ltd (Beijing, China). All solutions were prepared with ultrapure water (18.2 MΩ cm, Millipore Corp., Bedford, USA) deoxygenated by bubbling pure N_2 overnight.

The soil sample used in the study was collected from paddy fields in Shaoguan (SG, 25 °6'N, 113 °38'E), China. The top layer soil (0 - 20 cm) was sampled and soils were wet sieved through a 1.0 mm diameter sieve to remove stones and plant debris. The soil characteristics are shown in Table S2.1.

3.2.2 Porewater sampler preparation

The IPI sampler used in this study has the same design as reported in the previous study with some modifications (Yuan et al. 2019a). Novel hollow fiber membrane tubes (modified polyethersulfone) and pipe (PTFE) are used to construct the IPI sampler. Silicon caps are applied to seal the IPI sampler during the sampling events. The IPI sampler employs hollow fiber membrane tube (1.7 mm in diameter) to passively sample porewater in its surroundings (Fig. S2.1A). When the equilibrium state is reached, the solution inside the tube is sampled, which is immediately ready for downstream instrumental analysis.

Thirty-four IPI samplers were assembled side by side in a 3D printed holder to collect the porewater samples every 1.7 mm along SWI (Fig. S2.1B). The IPI sampler array is also known as the SWI profiler (Tidu Environment Inc. Suzhou, China). The SWI profiler has a sampling depth of 60 mm. In order to eliminate the introduction of O_2, the SWI profiler was stored in O_2-free ultrapure water for at least one day before deploying into flooded, saturated soils (Fig. S2.1C).

3.2.3 Analytical method and quality control

Element concentrations were quantified by ICP-MS (NexION 350X, PerkinElmer, Inc., Shelton, CT USA). The conditions were as follows: DRC mode (O_2, gas flow, 1.0

mL min^{-1}); data only analysis; RF power 1600W; plasma gas flow rate 15 L min^{-1}; auxiliary gas flow 1.2 L min^{-1}; nebulized gas flow 0.94 L min^{-1}; nickel sampling and skimmer cones. The porewater sample collected by the IPI sampler was self-aspirated into ICP-MS by a PFA-200 Microflow Nebulizer (0.2 mL min^{-1} uptake rate). Iron and Mn were measured by ICP-MS in EDR mode, and As, P and S were analyzed by ICP-MS in DRC mode with O_2 as reaction gas. Counts of $^{91}AsO^+$, $^{57}Fe^+$, $^{47}PO^+$, $^{48}SO^+$ and $^{55}Mn^+$ were recorded.

Element species were measured by ion chromotography (IC)-ICP-MS. The IC (Dionex ICS-1100, Thermo Scientific, USA) consisted of a standard 25 µL sample loop and an anion-exchange column (IonPac AS23, 250mm×4mm, Dionex). Mobile phases used for the separations were 20 mM NH_4HCO_3 at pH 10 (Suzuki et al. 2009), with a flow rate of 1.0 mL min^{-1}. The end of the analytical column was connected to a Type C0.5 Glass Nebulizer (0.5 mL min^{-1} uptake rate) inlet to the ICP-MS. Before the measurement, solution was manually injected in the 25 µL standard sample loop of IC. Element species were separated by IC, and quantified by ICP-MS. Separation of common four As, one P and two S species were tested in IC, and measured by ICP-MS. The standard samples were prepared in neutral conditions (pH 7; 100 $\mu g \cdot L^{-1}$ phosphate [P(V)], arsenite [As(III)], arsenate [As(V)], monomethylarsonic (MMA) and dimethylarsinic (DMA) acid; 1 mg L^{-1} sulfide [S(-II)] and sulfate [S(VI)]). Peak area was used to fit the standard curve, and three times standard deviation was used to calculate limit of detection (LOD). Data quality was assured by testing a spiked standard after every 30 samples.

3.2.4 Time-dependent response of total elements and element species

Total elements were prepared in acidic conditions (pH 2; 10 $\mu g \cdot L^{-1}$ As and Mn; 10 $mg \cdot L^{-1}$ Fe, P and S), and As species were prepared in neutral conditions (pH 7; 100 $\mu g \cdot L^{-1}$ As(V), As(III), MMA and DMA). The time-dependent response of IPI samplers to As, Fe, Mn, P, S as well as As species was measured by ICP-MS and IC-ICP-MS respectively. The solutions inside the samplers were measured after 0, 0.5, 1, 3, 6 and 12 h equilibrium time (n = 3).

3.2.5 Multi-element profile mapping

Each SWI profiler is made up of 34 IPI samplers. The SWI profiler is able to measure the elements distribution over a distance of 60 mm, with a resolution of 1.7 mm. To detect the element profile, two SWI profilers were inserted into two pots containing ~ 12 cm depth SG paddy soils, with 10 mm above SWI and 50 mm buried in paddy soils (Fig. S2.1C).

The paddy soils were flooded for three months prior to the deployment of SWI profilers. Before sampling, the solution inside IPI samplers was replaced by O_2-free ultrapure water driven by an injection pump (TYD01, Lei Fu, China). To avoid the negative influence of O_2 and dust from the atmosphere, silicon caps are used to seal IPI sampler during sampling.

The solution in the IPI samplers was sampled every 24 hours and preserved in O_2-free EDTA solution (Gallagher et al. 2001). The EDTA solution (2 $g \cdot L^{-1}$) was online mixed with the porewater in 1:3 volume ratio driven by two injection pumps (Fig. S2.2). In total, 100 µL porewater was collected with an EDTA concentration of 500 $mg \cdot L^{-1}$. Each sample was equally divided into two parts (2*50 µL) and measured by ICP-MS and IC-ICP-MS respectively. A microplate reader with 96-well plate (200 µL) was also used

to measure the profile of Fe in SG paddy soil with 1, 10-phenanthroline method (λ = 510 nm). Finally, mm-scale profiles of multi-element and their species were mapped and evaluated.

3.2.6 Data analysis

Statistical program R version 3.5.0 was used to analyze and plot the data in this study. Standard deviation (SD) was used to show the variance of the data.

3.3 Results and discussion

3.3.1 Evaluation of IPI sampler

I first evaluated the applicability of IPI samplers in collecting porewater with As, Fe, Mn, P and S. The results showed the concentrations of those elements increased rapidly in the first three hours, and then reached a plateau representing their concentration in solutions (Fig. S2.3). The time-dependent diffusion curves are consistent with the previous report for As, antimony, cadmium, lead and nickel (Yuan et al. 2019a). Therefore, I consider the IPI sampler can be applied for the measurement of As, Fe, Mn, P and S.

3.3.2 Detection of Fe and Mn with ICP-MS in EDR mode

The impact of attenuation via the Rpa value on Fe and Mn signals was investigated (Fig. S2.4). The response of Fe and Mn signals to Rpa from 0 to 0.2 is shown in Fig. S2.5. The results indicate that Fe and Mn counts are very sensitive to Rpa value in a range from 0.0035 to 0.0084, in which Fe counts decreased linearly from 300000 to 25000, and Mn from 85000000 to 1000000.

The detection range of Fe and Mn is controllable by adjusting Rpa. The LODs of Fe and Mn are 21.2, 30.9, 210 and 0.504, 1.53, 1.56 $\mu g \cdot L^{-1}$ under Rpa 0, 0.005, and 0.01

respectively. Although LOD values increased about 9 and 2 times, respectively, for Fe and Mn when adjusting the Rpa from 0 to 0.01, they are still much lower than the Fe and Mn concentrations found in real porewater, which are always above 1 mg L^{-1} (Gustave et al. 2018b, Wang et al. 2019b, Xu et al. 2017). At the same time, the upper detection limits of Fe and Mn extend to a high value by tuning Rpa value from 0 to 0.01. The influence of Rpa value of Fe and Mn measurement were further investigated in real samples. With EDR and DRC mode, simultaneous measurement of Fe, Mn, As, P and S were achieved. Under DRC mode with O_2 as reaction gas, the LODs for As, P and S were 0.490, 7.76, and 60.2 $\mu g \cdot L^{-1}$, respectively, which agrees well with previous reports of measuring As, P and S with ICP-MS (Persson et al. 2009, Yuan et al. 2019a).

3.3.3 Comparison of colorimetric and ICP-MS for Fe profiles in field samples

Most studies on porewater Fe used colorimetric analysis for Fe measurement (Arsic et al. 2018, Bennett et al. 2012b). The results showed ICP-MS in EDR mode could act as an alternative to measure Fe. In this study, the ICP-MS using three Rpa values (0, 0.005, and 0.01) was compared with colorimetric method using phenanthroline with real porewater samples.

The profiling of Fe measured by the ICP-MS method is shown in Fig. 3.1. The three curves of Fe profiles generated by ICP-MS in EDR mode with different Rpa values are identical in top soils (0 - 25 mm) as shown in Fig. 3.1, which indicates that the method works well for low Fe condition. However, Rpa 0 was unable to measure Fe in soil depth > 25 mm when Fe > 17 mg L^{-1} in soil porewater (Fig. 3.1A). Increase of Rpa from 0 to 0.005 extended the measurement of Fe along soil depth from ~ 25 mm to ~36 mm (Fig. 3.1A&B), yet Rpa 0.005 was still unable to avoid the detector saturation of Fe > 42

mg L^{-1} in deep soil porewaters (Fig. 3.1B). Fig. 3.1C shows Fe profile could only be measured after the Rpa value was adjusted to 0.01 with Fe ≤ 70 mg L^{-1}. Similarly to Fe, Rpa 0.005 or 0.01 allowed measurement of Mn when Mn ≤ 3.8 mg L^{-1} in soil porewater (Fig. S2.6).

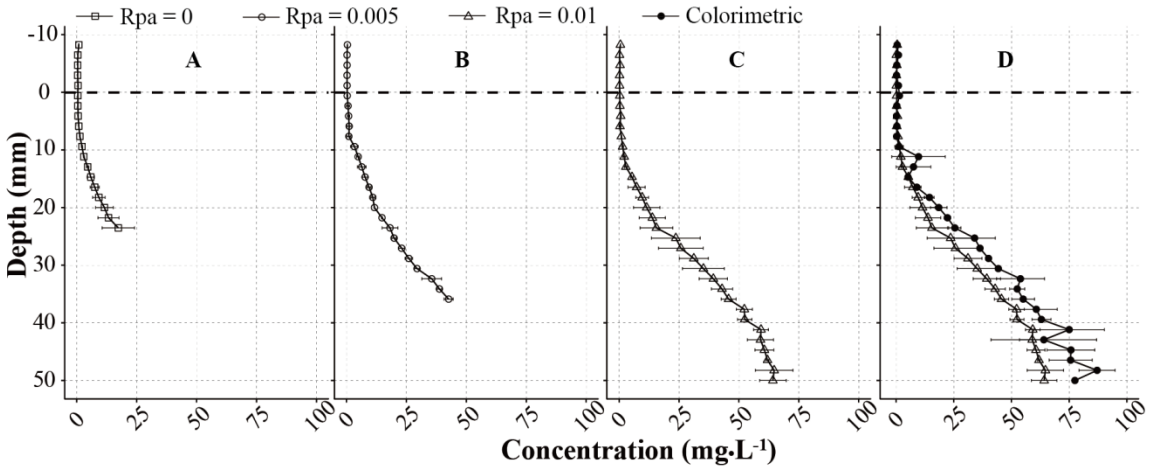

Figure 3.1 Iron (Fe) profile measured by ICP-MS or colorimetric method (phenanthroline) in Shaoguan (SG) paddy. (A-C): Fe profile measurement with ICP-MS method in extended dynamic range (EDR) mode when Rpa = 0, 0.005 and 0.01 respectively; (D) Fe profile measured by colorimetric and ICP-MS method (Rpa = 0.01). The error bar is standard deviation (SD, n = 2). The dashed line represents soil-water interface.

Iron profile was also measured by a colorimetric method with the same samples (Fig. 3.1D). Both colorimetric and ICP-MS methods gave similar results of Fe profiles, which suggested both methods are reliable. However, Fe concentration measured by colorimetric method was slightly higher than that obtained by ICP-MS method. The higher Fe values obtained by colorimetric method could be attributed to the interference from other cations (e.g. Mn, calcium, zinc etc.) in the porewater (Hatat-Fraile and Barbeau 2019, Miranda et al. 2016). Therefore, Fe concentrations might be overestimated by using colorimetric method.

3.3.4 Profiling of total As, Fe, Mn, P and S across SWI

The mm-scale co-distributions of As, Fe, Mn, P and S are shown in Fig. 3.2. The Fe remained a low concentration in surface water and top-soil porewater, but increased sharply from 9 mm below SWI and reached up to 70 mg L^{-1} in 50 mm deep soils. Similar trends were also observed in the distribution of Mn, P and As, which agrees well with the tightly coupling between Mn, P, As with Fe in soils (Arsic et al. 2018, Ma et al. 2017, Xu et al. 2017). Conversely, S was found to decrease with depth (Fig. 3.2). The subsurface decrease of S is presumably caused by S(VI) reducing bacteria in anoxic soils (Pester et al. 2012), during which mobile S(VI) is transformed to S(-II) minerals (e.g. FeS, FeS_2) (Wu et al. 2016b).

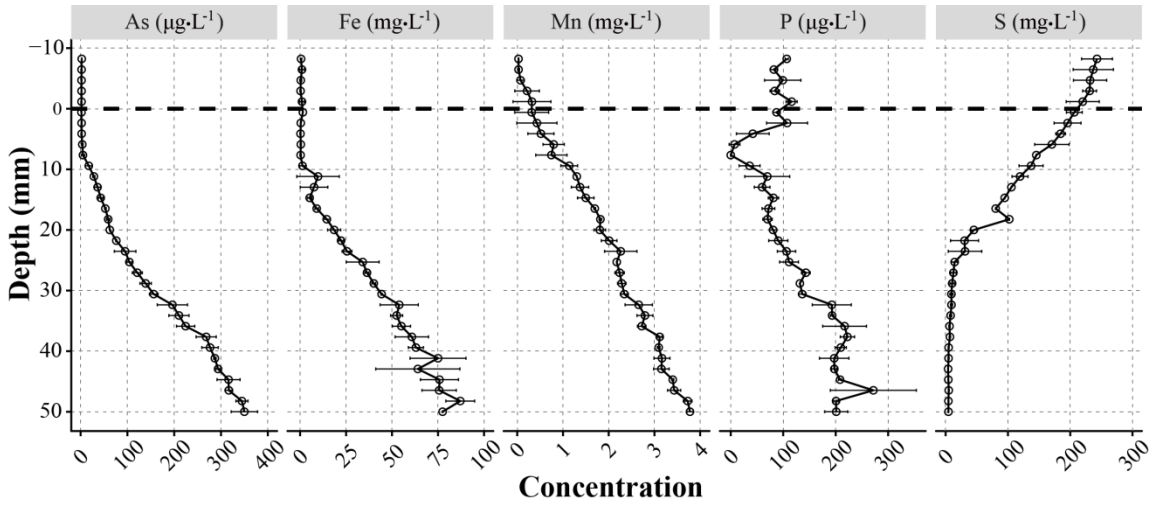

Figure 3.2 Mapping of As, Fe, Mn, P and S profiles in Shaoguan (SG) paddy with ICP-MS in EDR mode.

To date, there is no customized method to simultaneously measure major (e.g. Fe, Mn, P and S) and trace (i.e. As) elements in the redox gradient zone across SWI, which significantly hindered the researches on element biogeochemical behaviors in flooded environment. Traditionally, subsamples are required to measure Fe, Mn and P by colorimetric methods or inductively coupled plasma-optical emission spectrometry (ICP-OES) (Arsic et al. 2018, Rietra et al. 2001, Serrat 1998, Wang et al. 2019b, Yi et al.

2019), S by IC (Keller-Lehmann et al. 2006), and most trace elements (e.g. As and antimony etc.) by ICP-MS (Gustave et al. 2018a, Gustave et al. 2019b). With this strategy, it will take at least 10 min for Rhizon sampler to collect enough porewater to meet the request by different analyses, and additional 10 min are required for parameters analyses (Seeberg‐Elverfeldt et al. 2005). By contrast, it only takes two min when using SWI profiler and the optimized ICP-MS method. Thus, the measurement throughput of major and trace elements in limited samples could be significantly improved by the method.

3.3.5 Arsenic, P and S species measurement with IC-ICP-MS

Simultaneous detection of four As, one P and two S species in solution and anoxic soil porewater was achieved with NH_4HCO_3 mobile phase (Fig. 3.3). The retention times were 6.6, 3.2, 3.9, 6.0, 10, 3.2, and 8.8 min for P(V), DMA, As(III), MMA, As(V), S(-II) and S(VI) respectively. The separation of four As species agrees well with previous work using the same chromatographic conditions (Suzuki et al. 2009). The results also demonstrated NH_4HCO_3 mobile phase can be extended to measure P and S species.

Two As [As(III) and As(V)], one P [P(V)] and two S [S(-II) and S(VI)] species were detected in the anoxic soil porewater (Fig. 3.3). Arsenite, P(V) and S(-II) (> 70%) represent the dominant As, P and S in soil porewater, which agrees well with previous reports in multiple soils by using HPLC-ICP-MS, IC or colorimetric methods (Chen et al. 2019, Han et al. 2018, Xu et al. 2017). In addition, an unknown P was detected in both solution and porewater with a shorter retention time than P(V) (Fig. 3.3), which putatively was the peak of phosphite. The unknown P occurred in low concentrations in deep soil (Fig. 3.4), which is consistent with previous detection of phosphite using IC

method (Han et al. 2018).

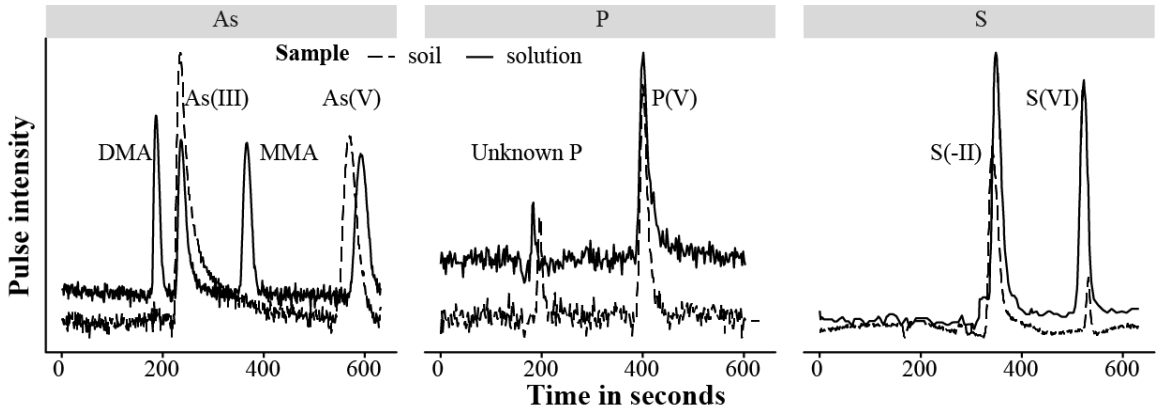

Figure 3.3 Arsenic (As), phosphorus (P) and sulfur (S) species detected by IC-ICP-MS. The samples include soil porewater and solution. The solution was prepared in neutral conditions (pH 7; 100 $\mu g \cdot L^{-1}$ phosphate [P(V)], arsenite [As(III)], arsenate [As(V)], monomethylarsonic (MMA) and dimethylarsinic (DMA) acid; 1 $mg \cdot L^{-1}$ sulfide [S(-II)] and sulfate [S(VI)]).

The measurement of As, P and S speciation in soil porewater receives attention because the elements are of great significance in environmental studies (Buschmann and Berg 2009, Chen et al. 2015b, Giles et al. 2015, Kumarathilaka et al. 2018a, Mucci et al. 2000). Previous speciation studies were generally analyzed by HPLC-ICP-MS, which is the most powerful technique to detect As, P and S species (da Rosa et al. 2019, Ritsema et al. 1998, Stürup et al. 2006). However, methods able to simultaneously measure As, P and S species are rare. The widely used mobile phase for As species detection always contains phosphate or butanesulfonate (Hu et al. 2019), which limits its application on P and S species measurement. In this study, we extended the application field of the mobile phase proposed by Suzuki and co-workers for As species measurement (Suzuki et al. 2009), and found it could sufficiently separate the species of P and S. By using the carbonate-based mobile phase (NH_4HCO_3), the common species of As, P and S can be separated and detected in 10 min in a single run, thereby analytical throughput is significantly improved.

Carbonate-based mobile phase is alkali (pH = 10), and may cause the precipitation of transition metal ions, especially for Fe and Mn. The precipitation of metal oxides may interfere with testing of anion species via co-precipitation or adsorption, and cause clogging in the analytical column. The potential interference could be mitigated by adding EDTA into samples, which shows a big advantage in eliminating precipitation of metal ions within a wide range of pH (Almkvist et al. 2013, Gallagher et al. 2001, Samanta and Clifford 2006). No precipitation of metal oxides was observed when porewater samples with immediate EDTA addition were mixed with NH_4HCO_3 mobile phase, thus we concluded the As, P and S species could be preserved with EDTA addition before and during IC-ICP-MS measurement.

3.3.6 Profiling of P, S and As species across SWI

With the optimized IC-ICP-MS method, we measured species of P, S and As in soil porewater collected by SWI profiler. Their vertical changes are depicted in Fig. 3.4. The concentration of As(III) was very low in top soils, but increased sharply from 3.3 $\mu g \cdot L^{-1}$ at ~ 10 mm below SWI to over 200 $\mu g \cdot L^{-1}$ in deep soils. Similarly, As(V), P(V) and S(-II) also showed a subsurface increase trend. An opposite trend was observed for S(VI). These results are consistent with previous reports of common As, P and S species distributions in saturated soils or sediments by using ICP-MS, IC, colorimetric or micro-electrode methods (Arsic et al. 2018, Han et al. 2018, Mcadams et al. 2016, Robertson et al. 2008).

Although the speciation of elements was known to couple with each other, most methods were developed for one element's species only (Divjak and Goessler 1999, Jackson and Bertsch 2001). Using single specie method, it would take around 30 min to

yield the concentration information of As, S and P species. In comparison with those methods, the major benefit of the optimized method presented here is its high throughput, which simultaneously measures As, P and S species within 10 min in a single run. The method is well suited for high-resolution mapping of elements and their species across SWI.

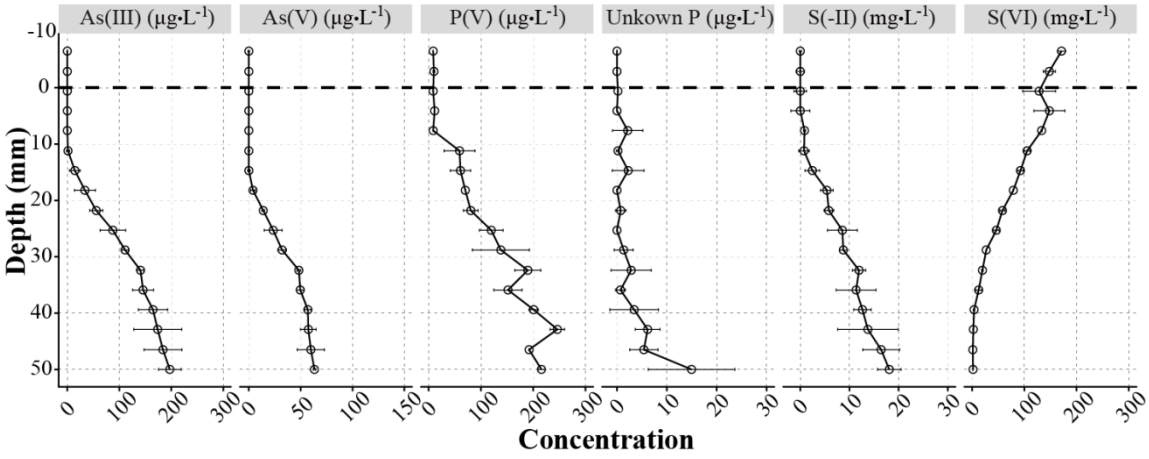

Figure 3.4 Profiles of P, S and As species in SG paddy measured by SWI profiler and NH_4HCO_3 eluent.

3.4 Conclusion

This study evaluated a novel IPI sampler for simultaneously measuring As, Fe, Mn, P, S as well as P, S and As species with optimized ICP-MS and IC-ICP-MS analysis both in solutions and soils. The method demonstrated both high sensitivity (μg·L^{-1} level for As, Mn, P, and sub-μg·L^{-1} level for Fe and S) and high throughput. I successfully measured the fine-scale (mm) co-distributions of multi-element (As, Fe, Mn, P and S) and their species [As(III), As(V), P(V), S(-II) and S(VI)] along SWI. With rapid measurement of multiple parameters from a limited sample, the optimized method could serve as a powerful tool for studying element distribution and dynamics in soils, sediments and other aqueous environments.

4. The cycling of As at paddy soil-water interface

Iron (Fe) oxides are sensitive to redox conditions and control the mobility of many other elements, especially for arsenic (As), in paddy soils. However, the coupling or decoupling processes among those element species are still unlocked due to the lack of *in situ* evidence. In this study, we depicted the mm-scale mapping of Fe, As and other associated elements along the redox gradient in soil-water interface (SWI) of five paddy soils. The results showed excellent positive linear relationship of aqueous Fe, manganese (Mn), As, and phosphate (P) in 4 of 5 paddy soils, indicating the close coupling of these elements. However, decoupling of Fe, Mn and As was observed in one paddy soil. Along the SWI, the releasing order was Mn, As and Fe, which follows the redox ladder of those elements. Further investigation of As species showed the ratio of arsenite to total As varied from 100% to 75.5% along depth. The study provided *in situ* evidences showing decoupling processes of multi-element could be revealed by using high-resolution porewater samplers and state-of-art analytical techniques.

4.1 Introduction

Paddy field is the biggest artificial wetland and provides food for more than half of world population (Chen et al. 2018, Fitzgerald et al. 2009). It is intermittent flooded to favor the growth of rice. During the flooding stage, the redox sensitive elements, such as iron (Fe), manganese (Mn), sulfur (S), arsenic (As) and phosphorus (P) shift their species in solid and liquid phase (Gao et al. 2016, Gao et al. 2006, Mcadams et al. 2016, Pi et al. 2018). Among them, the As is mobilized and efficiently uptaken by rice root and accumulated in

rice grain, threatening human health through food chain (Meharg 2004, Roberts et al. 2010). Therefore, it is a burning issue to understand the biogeochemical cycle of As in paddy soils.

The behavior of As in saturated soils is closely coupled to Fe. The Fe oxides provide the main adsorption sites for As (Chen et al. 2006, Tufano et al. 2008, Zobrist et al. 2000). When paddy soils are flooded, Fe oxides tend to be reduced and dissolved by dissimilatory Fe reducing bacteria, leading to simultaneous release of adsorbed As into porewater. "The coupling of Fe and As" was used to describe a process during soil flooding, in which dissolved Fe and As show a close positive correlation in porewaters (Weber et al. 2010). In contrast, "the decoupling of Fe and As" was defined to refer to the lack of a linear correlation between dissolved Fe and As concentrations.

Coupling of Fe and As has been well documented in soils, yet the decoupling process remains cryptic (Bennett et al. 2012a, Weber et al. 2010). To clarify the mechanisms regulating the potential decoupling of As and Fe, simplified water-Fe minerals-bacteria systems were employed (Tufano et al. 2008, Tufano and Scott 2008, Weber et al. 2010). These studies, combined with thermodynamic calculation, provided key evidence that decoupling process can occur under certain thermodynamic conditions. For example, Zobrist et al., identified *sulfurospirillum barnesii* was able to reduce adsorbed arsenate [As(V)] to arsenite [As(III)] without requiring dissolution of the host Fe oxides (Zobrist et al. 2000), which could be caused by an energy trade-off between reduction of adsorbed As(V) and host Fe minerals by microorganisms (Campbell et al. 2006). However, this has not been confirmed in soils.

In saturated soils, it has been a challenge to distinguish the potential decoupling

between Fe and As. Well-mixed soils were frequently used to investigate the time-dependent behaviors of Fe and As (Honma et al. 2016, Masscheleyn et al. 1991, Weber et al. 2010, Xu et al. 2017), but few direct evidence was acquired to support the happening of decoupling between Fe and As. The unsuccessful identification of the decoupling process is not surprising, because the Fe reduction and As releasing usually happen in sequence with tiny difference (Zhang et al. 2018). The dynamic change of Fe and As makes it almost impossible to catch the "sweat time points", in which Fe and As were decoupled, if it is happened.

When flooding, bulk soil becomes reducing owing to the abundant organic matters (Frenzel et al. 1992). At the same time, a redox gradient is formed between the O_2-rich surface water and beneath soil, which could significantly influence the behavior of elements spatially through complex redox processes (Arsic et al. 2018, Mucci et al. 2000, Widerlund and Davison 2007). Hence, the narrow but stable SWI is an ideal place to study the coupling/decoupling processes of Fe and As along depth (Bennett et al. 2012a, Gorny et al. 2015). Although As(V) reduction theoretically happened at higher redox potential compared to Fe(III) (Borch et al. 2010), few studies have detected the spatial separation of Fe(II) and As species in SWI of real soils. This could be attributed to the lack of a suitable method to simultaneously measure fine-scale Fe, As and other associated elements across SWI (Gorny et al. 2015).

I recently developed a high-throughput method to simultaneously measure multi-element [e.g. Fe, Mn, As, phosphorus (P) and sulfur (S)] and their species across SWI (Yuan et al. 2019b). In this study, the method was applied to reveal the coupling/decoupling process of Fe and As, as well as other redox-sensitive elements,

including Mn, S and P. Their profiles across the SWI in five paddy soils were mapped to 1) illustrate multi-element and redox potential (Eh) profiles in five typical flooded paddy soils; 2) study the coupling/decoupling behaviors among the redox-sensitive elements; 3) reveal the As speciation process across the SWI.

4.2 Materials and methods

4.2.1 Reagents, materials and solutions

Analytical grade or higher reagents were used in this study, and purchased from Aladdin Chemical Reagent Co., Ltd. (Shanghai, China), unless stated elsewhere. Calibration standards, including As, Fe, Mn, P, S as well as As species, were supplied by Guobiao (Beijing) Testing & Certification Co., Ltd (Beijing, China). All solutions were prepared with ultrapure water (18.2 MΩ cm, Millipore Corp., Bedford, USA) deoxygenated by bubbling pure N_2 overnight.

Five soils were collected from paddy fields in Wenshan (WS, 23°45'N, 105°26'E), Bijie (BI, 26°39'N, 105°47'E), Wuxue (WX, 29°59'N, 115°38'E), Shaoguan (SG, 25°6'N, 113°38'E) and Ganzhou (GZ, 25°30'N, 114°36'E), China. The plow layer soil (0 - 20 cm) was sampled and directly transported to laboratory. Soils were wet mixed and sieved through a 1.0 mm diameter sieve. The wet sieved soils were mixed evenly and added to three black plastic pots (inner diameter × height = 13 × 21 cm^2), with a soil depth of ~ 15 cm. Table S3.1 shows the selected soil properties. The soils were flooded and allowed to stabilize for 30 d in dark conditions, with a constant room temperature (22 ℃) controlled by an air-conditioner.

4.2.2 Deployment and *in situ* sampling of SWI profiler

SWI profiler is a recent developed high-resolution porewater sampler, which is modified based on previous reports (Yuan et al. 2019a, Yuan et al. 2019b). The updated SWI profiler is provided by Tidu Environment Inc. (Suzhou, China). Fifteen SWI profilers were inserted into 15 pots containing WS, BI, WX, SG, and GZ paddy soils, with 10 mm in overlying water and 50 mm buried in paddy soils. After 30 d incubation, porewater was sampled by SWI profiler. Eh profiles were simultaneously measured by a home-made platinum micro-electrode with Ag/AgCl electrode as a reference electrode.

Before sampling, O_2-free ultrapure water was pumped into SWI profiler with an injection pump (TYD01, Lei Fu, China). Based on preliminary measurement, the carrier solution volume and velocity was set at 0.4 mL and 1.0 mL $\cdot$min^{-1} respectively. After loading of the carrier solution, SWI profiler was sealed by silicon caps to avoid the potential influence of O_2 and dust in the atmosphere.

The sample in the SWI profilers was sampled every 24 hours and preserved in O_2-free HCl or EDTA solution (Gallagher et al. 2001, Yasui et al. 2016, Yuan et al. 2019b). The HCl (20 mM $\cdot$L^{-1}) or EDTA (2 g $\cdot$L^{-1}) was on-line mixed with porewater sample in SWI profiler at a ratio of 1:1 or 1:3 volume ratio driven by two injection pumps (Fig. S4.1). The sample was collected in a clean 0.6 mL centrifuge tube, and preserved at 4 ℃ fridge before instrumental analysis.

4.2.3 Total aqueous elements analysis

Total aqueous Fe, Mn, P, S and As were measured by inductively coupled plasma-mass spectrometry (ICP-MS, NexION 350X, PerkinElmer, Inc., Shelton, CT USA). The sample in 0.6 mL centrifuge tube (~ 0.2 mL) was self-aspirated into ICP-MS by a PFA-200 Microflow Nebulizer for elemental analysis. The counts of $^{57}Fe^{+}$, $^{55}Mn^{+}$, $^{47}PO^{+}$,

$^{48}SO^{+}$ and $^{91}AsO^{+}$ were recorded in dynamic reaction cell (DRC) or extended dynamic range (EDR) mode (Yuan et al. 2019b). Spiked standards were measured every 30 samples to enable appropriate correction of signal shift.

The ICP-MS were optimized to the following conditions: DRC (O_2, gas flow, 1.0 mL min^{-1}); data only analysis; RF power 1600W; plasma gas flow rate 15 L min^{-1}; auxiliary gas flow 1.2 L min^{-1}; nebulized gas flow 0.90 L min^{-1}; the uptake flow rate is 0.2 mL min^{-1}; nickel sampling and skimmer cones were used. A voltage parameter in EDR mode, called Rpa, was optimized to 0.01 for Fe and S to enable simultaneous measurement of major (e.g. Fe, S) and trace (e.g. As) elements by ICP-MS.

4.2.4 Speciation of arsenic in soil porewater

For As speciation analysis, the sample was manually injected into the sample loop of ion chromatography (IC, Dionex ICS-1100, Thermo Scientific, USA) (Yuan et al. 2019b). The IC system consisted of a 25 μL sample loop and an anion-exchange column (IonPac AS23, 250mm×4mm, Dionex). Twenty mM NH_4HCO_3 (pH = 10) were used as the mobile phase (Suzuki et al. 2009, Yuan et al. 2019b). We expanded the comparison to digitized As specie profile published by Arsic et al., (Arsic et al. 2018) with the Engauge Digitizing software used in paddy soil study (Yuan et al. 2016).

4.2.5 Statistical analysis

The data were analyzed and plotted by statistical program R (version 3.5.0). Standard deviation (SD) were used to show the variance, and linear regression analysis was used to identify the coupling and decoupling process of different elements.

4.3 Results and discussion

4.3.1 Vertical changes of Eh and elements across SWI

Redox potential (Eh) plays a key factor for regulating element behaviors in saturated soils. We measured Eh (*vs.* Ag/AgCl reference) across the SWI in five long-flooded paddy soils (WS, BI, WX, SG and GZ) by using platinum micro-electrode. The vertical changes of Eh were depicted in Fig. 4.1.

The Eh changed rapidly from highly oxidizing (~ 300 mV) to reducing along SWI. However, the reducing state varied in different soils. Highly reducing (~ -150 mV) was observed in WS/WX/SG, yet a relatively moderate one (~ -10 mV) in BI/GZ. This difference might be caused by different physico-chemical properties of soils. Manganese and Fe are important factors for regulating soil redox (Brannon et al. 1984, Xu et al. 2017). Here, we found high Mn (6.32 g Kg^{-1}, WS) or Fe (> 70 g Kg^{-1}, WX/SG) alone was unable to retard decrease of soil redox (Table S3.1). Retardation of soil redox was only achieved with both high Fe and Mn (> 70 and 1.10 g Kg^{-1}) in BI/SZ. Although Mn is believed to be the key for retarding soil redox (Xu et al. 2017), the formation of Fe oxides coating with the nucleating agent is essential for nucleation and growth of Mn oxides (Burns and Burns 1975). Hence, Fe may also get involved in retarding soil redox through affecting the reactivity of Mn.

Followed Eh measurement, vertical changes of Fe, Mn, As, P and S were mapped by SWI profiler (Fig. 4.1). Similarly to Eh, S decreased rapidly from as high as 1000 μM L^{-1} in oxidizing to a concentrations of ~ 300 μM L^{-1} in reducing soils. The immobilization of S is presumable caused by sulfate reducing bacteria (Pester et al. 2012), during which sulfate is transformed to sulfide minerals (Wu et al. 2016a, Wu et al. 2016b). However, immobilization of S varied in different soils. Up to 85% S was immobilized in WS/BI/

SG, yet only 40% in WX/GZ. This difference might be caused by varying S content/speciation and activity of sulfate reducing bacteria in different soils (Fulda et al. 2013, Pester et al. 2012).

Dissolved Fe, Mn, As and P were almost undetectable in oxidizing, but increased to an average of 474, 26, 1.4 and 0.074 μM L^{-1} respectively in reducing soils (Fig. 4.1). In terms of the release trend of those elements, they all showed a subsurface increase trend, which agree well with previous reports of their typically vertical distributions along SWI (Arsic et al. 2018, Di et al. 2012, Ma et al. 2017, Wu et al. 2016a). In this study, up to 30 times variance was captured in the mobilization of Fe, Mn, As and P among different soils. The reductive mobilization of these elements was supposed to be correlated negatively with Eh and S, yet this was not always true. For instance, the most As was mobilized in GZ with a relatively high Eh and S (~ -15.0 mV, ~ 635 μM L^{-1} S, Fig. 4.1E), while the least As in WX with an extremely low Eh and S (~ -200 mV, ~ 54.8 μM L^{-1} S, Fig. 4.1A). This kind of conflict was frequently reported using different soils (Garnier et al. 2015, Xu et al. 2017), which could be caused by varying physico-chemical properties and biogeochemical reactions in different soils (Bennett et al. 2012a). But, the actual reasons remain not well understood.

In addition to mobilization extent, the discrepant mobilization processes among Fe, Mn, As and P could also be revealed by the high-resolution mapping. For example, As tended to couple more closely with Fe and Mn than P. Dissolved P remained constant in anoxic in all except for SG soil. In contrast, Fe, Mn and As concentrations varied among different soils under anoxic. They remained relatively constant in BI/GZ, but increased slightly or continuously along anoxic zone of WS/WX or SG. The variable mobilization

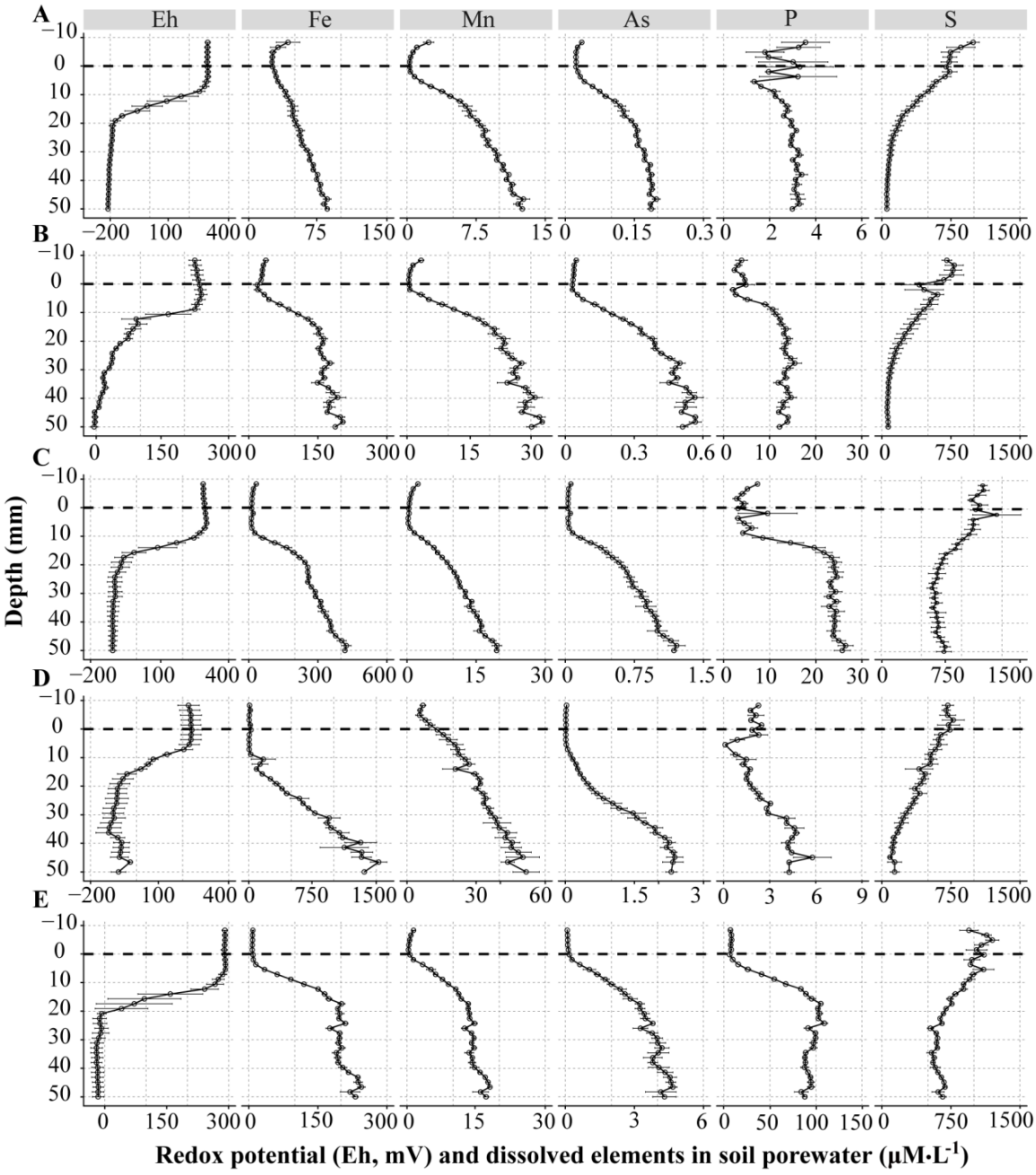

Figure 4.1 Redox potential (Eh, *vs.* Ag/AgCl) and aqueous iron (Fe), manganese (Mn), arsenic (As), phosphorus (P), sulfur (S) ($\mu M \cdot L^{-1}$) across soil-water interface. Soils were collected from Wenshan (WS, A), Bijie (BI, B), Wuxue (WX, C), Shaoguan (SG, D) and Ganzhou (GZ, E) paddies. The black dotted line at depth = 0 represents the soil-water interface. The error bar is standard deviation (SD, n = 3). Note the different axis scales used.

pattern of Fe, Mn and As across SWI may provide an opportunity to *in situ* study the coupling/decoupling processes of those analytes in soils.

4.3.2 Coupling of As with Fe and Mn across SWI

Arsenic showed significant linear correlation with Fe ($R^2 \geq 0.775$, $p < 0.01$) and Mn ($R^2 \geq 0.413$, $p < 0.01$) both in the whole profile (Fig. 4.2) and oxic-anoxic transition zone (Table S3.2). The close positive correlation was yielded in 4/5 soils (including WS, BI, WX and GZ, $R^2 \geq 0.848$, $p < 0.01$), which agrees well with the tightly coupling of As with Fe and Mn in typically natural soils and sediments (Anawar et al. 2004, Arsic et al. 2018, Xu et al. 2017).

By contrast, poor linear pattern was observed in SG (Fig. 4.2), suggesting decoupling of As with Fe and Mn may occur. Along the SWI of SG, the releasing order followed Mn, As and Fe sequentially (Fig. 4.1D), which is consistent with their typical redox ladder (Borch et al. 2010). However, it's hard to distinguish the release order of those elements in other soils. This might be caused by the tiny difference of their release sequence in many soils (Zhang et al. 2018). Due to that, it has been a challenge to distinguish the potential decoupling of As with Fe and Mn in real soils. Fortunately, SG soil provides an opportunity to *in situ* separate the potential decoupling with the dominant coupling process. Further regression residual analysis revealed the potential decoupling process may happen in the oxic-anoxic transition zone (Table S3.2). Much higher residuals were obtained in that zone of SG (residuals ≥ 0.265) than in other soils with a similar regression slope (including WS, BI and WX, residuals ≤ 0.0417). Although decoupling process may also contribute to As release in reducing soils, it's difficult to separate the potential decoupling from the predominant coupling process under that conditions (Bennett et al. 2012a, Xu et al. 2017).

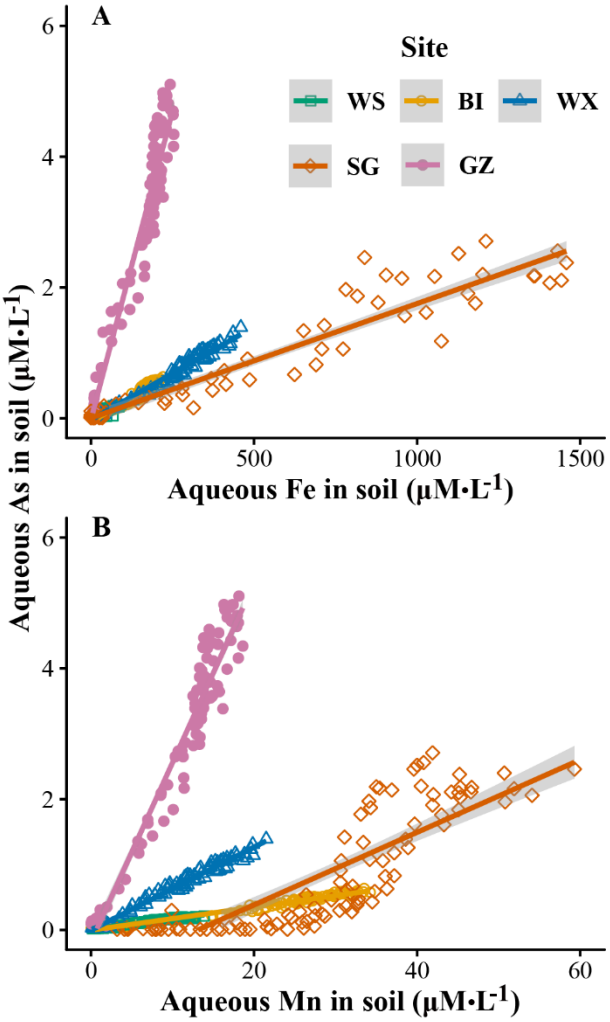

Figure 4.2 The correlation between vertical aqueous As with Fe (A) and Mn (B) (μM L^{-1}) in paddy soils. Soils were collected from Wenshan (WS), Bijie (BI), Wuxue (WX), Shaoguan (SG) and Ganzhou (GZ) paddies.

Visual linear relationships were observed between Fe, Mn and As, but their slopes differed in different soils (Fig. 4.2). Fig. 4.2 showed that those slopes could be clustered into three or four groups. Based on slopes of Fe and As (Fig. 4.2A, Table S3.2), the five soils were divided into three groups: 1) SG (small slope, 0.00157); 2) WS, BI and WX (medium slope, ~0.00286); 3) GZ (high slope, 0.0178). The varying slopes of element regressions were reported in different soils over time or space (Garnier et al. 2015, Xu et al. 2017). Although the actual reasons remain not well understood, these differences may

underline the effect of physico-chemical and biogeochemical conditions on the behaviors of elements.

4.3.3 Decoupling of As with Fe and Mn across SWI

Based on element profiles and linear regression analysis, we identified decoupling of As with Fe and Mn may occur in SG. However, the potential decoupling process remains not well understood. In order to mechanically interpret the potential decoupling of As with Fe and Mn in the soil, we further measured fine-scale As species across the SWI of SG. Profiles of aqueous As species were given in Fig. 4.3.

Two inorganic As species, including As(III) and As(V), were detected in soil porewaters (Fig. 4.3), which is consistent with many reports of As species in porewater or groundwater (Arsic et al. 2018, Hu et al. 2015, Kumar et al. 2016, Xu et al. 2017, Zheng et al. 2003). The concentrations of As(III) and As(V) remained almost undetectable in oxic zone but increased rapidly to as high as 2.2 and 0.75 μM L^{-1} in reducing soils. The subsurface increase trend of As(III) and As(V) is consistent with that of total As in this study (Fig. 4.1) as well as in previous reports using different soils/sediments (Arsic et al. 2018, Bennett et al. 2012a, Yuan et al. 2019b). However, the detailed release process of As species across SWI was rarely reported due to lacking of available method to simultaneously measure different As species in high-resolution. Here, with a powerful method developed in our group (Yuan et al. 2019b), I can depict As(III) proportion profile to vividly show that process. Based on the changing gradient, profile of As(III) proportion was divided into three stages: 1) a rapid decrease from 100 to 80.6% in the first 10 - 20 mm top soil; 2) a slow decrease from 80.6 to 75.5% in 20 - 30 mm soil; 3) a stable value (~ 75%) in deep soils (30 - 50 mm). Surprisingly, the initial release of As

along SWI was mostly composed of As(III) (Stage 1, Fig. 4.3). The similar phenomenon was occasionally mentioned by previous reports by using traditional soil slicing or combined DET and DGT method (Fig. S3.2) (Arsic et al. 2018, Chaillou et al. 2003), yet the detailed process remains unclear. With the fine-scale As specie profiles (Fig. 4.3), we confirmed As(III) excess may occur in the oxic-anoxic transition zone. This could explain the decoupling of As with Fe and Mn in that zone (Fig. 4.1&2, Table S3.2). Although As(III) excess, as a result of solely reduction of As(V) to As(III), is believed to be the main cause of decoupling of As with Fe in simplified water-Fe mineral-bacteria system (Tufano et al. 2008, Yamamura et al. 2003, Zobrist et al. 2000), it remains unresolved in soils.

Obvious As(III) excess (~ 100%, Fig. 4.3) was rarely reported, especially in the oxic-anoxic transition zone beneath SWI. The predominance of As(III) in that zone observed in this study could be caused by several biogeochemical processes. First, As(V) adsorbed on Fe oxides could be biotically reduced and released from the host Fe oxides. And, many facultative microorganisms (e.g. *Shewanella sp.*, *Sulfurospirillum barnesii* and *Bacillus sp.*) has been demonstrated to be able to participate in this process (Tufano et al. 2008, Yamamura et al. 2003, Zobrist et al. 2000). Second, desorption of As(III) could lead to the enrichment of As(III) under certain conditions (Campbell et al. 2006, Williams et al. 2011). However, As(III) only accounts a small proportion of As in non-flooded soils (Takahashi et al. 2004). Arsenite desorption pathway could be negligible in long-flooded soil, because the loosely bound As(III) on Fe oxides tends to release immediately upon flooding (Bennett et al. 2012a, Tufano et al. 2008). Third, As(III) may upward diffuse from reducing soil to the oxic-anoxic transition zone driven by the

concentration gradient (Gorny et al. 2015). Nonetheless, upward diffusion of As(III) could not explain the tremendous varying of As(III) proportion along depth. Although soils in 20 - 30 mm and 30 - 50 mm share the same reducing condition (~ -100 mV, Fig. 4.1D), much higher As(III) proportion was obtained in 20 - 30 mm than in 30 - 50 mm (Fig. 4.3). The extra As(III) in 20 - 30 mm soil could be caused by indigenous biotically reduction of adsorbed As(V) to As(III) or downward diffusion of As(III) from the oxic-anoxic transition zone with an As(III) proportion up to 100%. Therefore, the biotically reduction of adsorbed As(V) to As(III) may play a key role for initial mobilization of As along depth. Future studies, combined *in situ* chemical with microbial profiles, are needed to further confirm this.

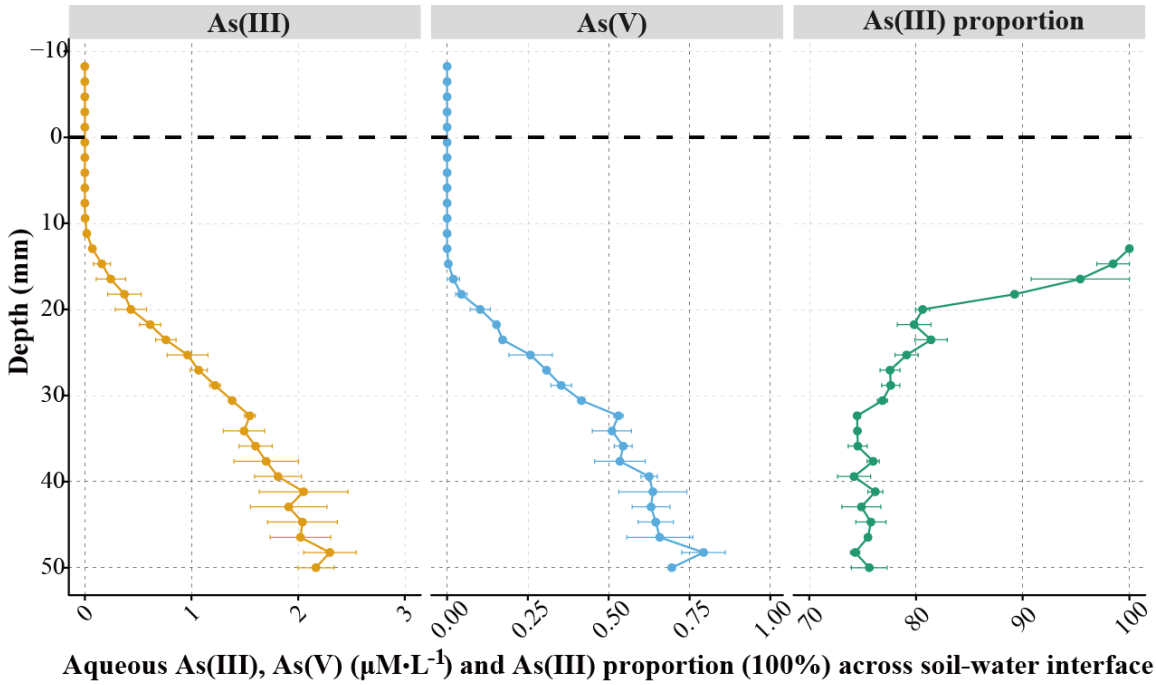

Figure 4.3 Profile of As species (μM L^{-1}) and arsenite [As(III)] proportion across SWI in Shaoguan (SG). Two As species, including As(III) and arsenate [As(V)], were detected in soil porewater.

It is interesting to note that, according to Eh-pH diagram, all the inorganic As in reducing environment should belong to As(III) in circumneutral conditions (Akter et al.

2005). However, a considerable of As(V) (~ 25%), or As(V) excess, was observed in SG soil (Fig. 4.3). To further investigate the mechanisms controlling As speciation in reducing soil, As speciation in our study was compared with previous reports in porewater or groundwater (Table S3.3). The results showed aqueous As under anoxic was usually dominated by As(III) with a As(III) proportion > 80%. However, obvious As(V) excess (~ 20%) was observed in most cases (Arsic et al. 2018, Bondu et al. 2017, Chaillou et al. 2003, Hu et al. 2015, Kazi et al. 2018, Kumar et al. 2016, Lock et al. 2018, Roberts et al. 2010, Shakoor et al. 2015, Somenahally et al. 2011, Wang et al. 2019b, Xu et al. 2017, Zheng et al. 2003). Oxygen contamination could be firstly excluded since As(III) excess (~ 100%) samples were obtained with the identical sampling and measurement both in this study and previous report in porewaters (Chaillou et al. 2003). Hence, the As(V) excess in reducing soils may represent a thermodynamic equilibration of As speciation, which could be impacted by four biogeochemical processes: 1) release of the adsorbed As(V) due to biotically reduction and solubilization of the host Fe oxides (Tufano et al. 2008, Zhang et al. 2018); 2) desorption of As(V) from solid phase due to competition of adsorption sites by analogues (e.g. carbonate, bicarbonate, phosphate, dissolved organic matter) (Anawar et al. 2004, Grafe et al. 2001, Violante and Pigna 2002, Zobrist et al. 2000); 3) abiotically oxidizing of As(III) to As(V) by Mn oxides (Liu 2006, Suda and Makino 2016); 4) a fraction of As(V) adsorbed on dissolved organic could be sampled and measured (Anawar et al. 2003, Chaillou et al. 2003). An improved understanding of the microbial and environmental factors controlling As(V) excess in reducing soil will help better understand biogeochemical cycling of As in the environment.

4.4 Conclusion

This study *in situ* investigated vertical changes of Eh, Fe, Mn, As, P, S as well as As species across SWI in paddy soils. High-resolution (mm) mapping of total aqueous Fe, Mn, As, P and S by SWI profiler visibly showed one-dimensional coupling and decoupling of As with Fe and Mn in different soils. Profile of As species further identified As(III) excess was the main cause of the decoupling of As with Fe and Mn in the oxic-anoxic transition zone. Future studies, combining high-resolution mapping of multi-element with microbial community, are essentially needed to improve the understanding of As behaviors in soils, sediments and other aquatic environments.

5. The cycling of As at paddy rhizosphere

Rice (*Oryza sativa* L.) production is threatened by arsenic (As). The mobile As pool for rice is determined by the dynamic As release in paddy soils (temporal source) and immobilization in oxygenated rhizosphere (spatial barrier). However, the spatiotemporal control of As remains unexplored. Here, high-resolution As and iron (Fe) were monitored across rhizosphere by IPI sampler from days after transplanting 0 to 40, and microbial community in rhizosphere was investigated at the end of the experiment by microbial sequencing techniques. Dissolved Fe and As increased exponentially to a peak at 30 d after flooding, followed by a slow decrease. With growing rice, Fe and As were linearly decreased across 0 - 10 mm distance from root surface, coinciding with the formation of redox zone by radial O_2 loss from root. Surprisingly, the Fe oxides formed in rhizospheric soil can retain most of mobile As (40 - 80%) from bulk soils. The results support Fe oxides formed in rhizosphere soil rather than on rice root are the major barrier for As uptake into rice. In rhizosphere, Fe and As oxidation were stimulated by both abiotic and biotic reactions, resulting in tightly immobilization of arsenate in the newly formed Fe oxides. I present a model of As transport from soil to rice, linking the temporal and spatial dynamic regulation of As in paddy soils. The model provides a comprehensive understanding for As cycling during rice production, and may provide novel insights for managing As risk in rice.

5.1 Introduction

Rice (*Oryza sativa* L.) is the staple food in many regions of the world, but threatened by arsenic (As) in paddy soil (Zhu et al. 2008). Release of As in paddy soil is stimulated by

anaerobic condition induced by periodic flooding during rice production (Bouman et al. 2005, Bouman and Tuong 2001). Along flooding, the release of As changes as a result of the interplay between the mobilization and immobilization of As driven by varying biogeochemical processes (temporal) (Muehe et al. 2019, Xu et al. 2017). In addition, immobilization of As could be promoted in rhizosphere due to the radial O_2 loss (ROL) from rice root, which would significantly affect As release across rhizosphere (spatial) (Chen et al. 2012). However, the spatiotemporal regulation of As is not well resolved in paddy soil.

Temporal release of As in paddy soil is caused by varying biogeochemical processes along flooding. Upon flooding, loosely bound As tends to be immediately released from soil particles or minerals (Bennett et al. 2012a, Tufano et al. 2008). Then anoxia induced by flooding stimulates the reductive dissolution of As-rich Fe oxides, leading to massive release of As into soil porewater (Das et al. 2004, Weber et al. 2010). Many studies have suggested As release could also be enhanced via competition of adsorption sites on solid phase by the potential analogues, such as phosphate, carbonate and bicarbonate etc. (Anawar et al. 2004, Grafe et al. 2001, Violante and Pigna 2002, Zobrist et al. 2000). On the other hand, the dissolved As could also be immobilized via several processes, including transformation of loosely bound arsenite [As(III)] to arsenate [As(V)] (Liu 2006, Suda and Makino 2016), formation of secondary Fe sulfide minerals (e.g. FeS, FeS_2) (Wu et al. 2016a, Wu et al. 2016b), and changes of sorptive capacity of Fe oxides (Smedley and Kinniburgh 2002, Weber et al. 2010). At initial flooding, mobilization usually overpowers immobilization, leading to the increase of As release. Then, immobilization may become comparable or superior to mobilization (Bennett et al.

2012a), thus the increase of As release could be inhibited. In most cases, these processes ultimately result in a firstly increase and then decrease of As release along flooding (Bravin et al. 2008, Muehe et al. 2019, Wang et al. 2019b), indicating the mobile As pool is temporally variable for rice.

Despite the immobilization in bulk soil, As could also be immobilized by ROL. Many studies have documented that ROL drives the formation of Fe plaque on rice root, which could serve as a sink for mobile As (Chen et al. 2012, Chen et al. 2005, Druschel et al. 2008, Emerson et al. 1999, Maisch et al. 2019b, Neubauer et al. 2002). Before uptake by rice roots, lots of mobile As entering the rhizosphere could be strongly adsorbed and immobilized by the newly formed Fe plaque, especially for As(V) (Chen et al. 2005). Thus, Fe plaque has been believed to be the major barrier for uptake of As into rice.

To date, As risk was usually assessed by evaluating the coupled effects of mobile As pool and Fe plaque, yet the effect of ROL diffusion into root surroundings is rarely reported. ROL has been documented to diffuse up to mm or cm distance from root surface, depending on different O_2 saturation, root maturity, plant species and light conditions (Chen et al. 2012, Frederiksen and Glud 2006, Pedersen et al. 1998, Williams et al. 2014). Thereby, ROL could establish a redox zone around root and stimulates Fe oxides formation in that zone (Maisch et al. 2019b). If so, the Fe oxides formed in rhizospheric soil could serve as an important barrier for As uptake into rice due to the high affinity of Fe minerals for As (Hartley and Lepp 2008, Ratering and Schnell 2001, Xu et al. 2017). Recently, Maisch et al., clearly captured the extension of redox zone and the coinciding Fe oxides formation by using planar optode sensors and image analysis

(Maisch et al. 2019b). The newly formed Fe oxides in rhizospheric soil should be far more than that on rice root due to the vast interfacial area of the redox zone with bulk soil. Thus the Fe oxides formed in rhizosphere could serve as the major barrier for As uptake into rice, followed by Fe plaque. However, this has not yet been proved in paddy soils.

To the best of my knowledge, few studies were designed to study the spatiotemporal variance of the redox zone and its impact on As release in rhizosphere. This could be attributed to the lack of an appropriate method to simultaneously measure fine-scale As and other associated elements across rhizosphere (Gorny et al. 2015). For instance, Rhizon sampler is frequently used to sample dissolved As in rhizosphere (Jia et al. 2014, Muehe et al. 2019), but the application of Rhizon sampler in studying fine-scale element behaviors is limited due to its relatively low spatial resolution (cm level) (Bravin et al. 2008, Seeberg‐Elverfeldt et al. 2005). Utilization of diffusive gradients in thin films (DGT) is able to provide fine-scale element profile (Williams et al. 2014), yet it is hard to handle DGT in deep soils. In addition, DGT is not applicable to resolve spatiotemporal element changes because it can only be used once after deployment. I previously demonstrated a technique, called *In-situ* Porewater Iterative (IPI) sampler, to *in situ* measure fine-scale (mm) total aqueous Fe, As and their species repeatedly across soil-water interface (Yuan et al. 2019a, Yuan et al. 2019b). With minor modification, IPI samplers could also serve as a robust and powerful tool to study spatiotemporal dynamics of Fe/As across rhizosphere.

Here with the modified IPI sampler technique, I link temporal and spatial patterns of Fe/As to microbial community in rice rhizosphere. The findings would provide a

comprehensive understanding of As cycling in rhizosphere.

5.2 Materials and methods

5.2.1 Soil and rice properties

The soil sample with high As concentration (146 mg Kg $^{-1}$) was collected from paddy fields in Shaoguan (SG, 25°6'N, 113°38'E), China. The top layer soil (0 - 20 cm) was sampled and soils were wet sieved through a 1.0 mm diameter sieve to remove stones and plant debris. The soil properties are shown in Table S4.1.

Indica rice (*O. sativa* L.) hybrid, Yliangyou-1 (YLY-1), was used. Seeds were sterilized by immersion in 10% H_2O_2 for 15 min, followed by germination in humid perlite (Chen et al. 2012). Before being transplanted into soils, the seedlings were grown in a Hogland culture in a glass greenhouse from 30th, March 2019 to the fourth leaf expanded (1st, May 2019). The room conditions were set at 25/20 ℃ in day (14 h, natural light)/dark (10 h), controlled by an air conditioner.

5.2.2 Porewater sampler preparation and usage

The IPI sampler used in this study shares the same design as reported in previous report (Yuan et al. 2019b). The IPI sampler employs the hollow fiber membrane tube (1.7 mm in diameter) to passively sample porewater in its surroundings (Fig. S4.1A). When the equilibrium state was reached, the solution inside the tube was sampled for downstream instrumental analysis.

Thirteen IPI samplers were assembled side by side in a 3D printed holder to collect a horizontal 0 - 20 mm porewaters every 1.7 mm. This IPI sampler array is also called the Rhizon profiler (Tidu Environment Inc. Suzhou, China). The Rhizon profiler is glued

with a nylon mesh bag (nominal pore size = 37 μm, height × width = 10 × 8 cm^2) by DP-420 epoxy (3M Co., USA) (Fig. S4.1B). Two days before transplanting of rice seedlings, 3000 g well-mixed wet soils (100% moisture) were added into a black plastic bucket (inner diameter × height = 15 - 18 × 18 cm^2) with a soil depth of ~ 15 cm, 600 g of which were enclosed in the root bag. The apparatus, including root bag and Rhizon profiler, was buried in 8 cm depth below soil-water interface (Fig. S4.1C), then ultrapure water was added to maintain an overlying water depth of 3 cm during the experiment.

Before sampling, O_2-free ultrapure water was pumped into IPI sampler with an injection pump (TYD01, Lei Fu, China). After loading of the carrier solution, the IPI sampler was sealed by silicon caps to avoid the possible influence of O_2 and dust in atmosphere (Yuan et al. 2019a, Yuan et al. 2019b). After 24 h equilibration, the sample in the IPI sampler was sampled and preserved in O_2-free HCl or EDTA solution (Gallagher et al. 2001, Yasui et al. 2016, Yuan et al. 2019b). The HCl (20 mM L^{-1}) or EDTA (1 g L^{-1}) was on-line mixed with the porewater sample in IPI sampler at a ratio of 1:1 volume ratio driven by two injection pumps (Fig. S4.2). The sample was collected in a clean 0.6 mL centrifuge tube, and preserved at 4 ℃ fridge before instrumental analysis.

5.2.3 Experiment design

Pot experiment was conducted to study the dynamic changes of As in rhizosphere. The rhizosphere was generated with (treatment) or without (control) growing rice into the root bags. Two seedlings were transplanted into each root bag of the treatment group after three days' soil flooding. A randomized complete block design with three replicates was used in this study. To minimize the potential influence of external environment, positions of pots between treatment and control were switched every other day during the

experiment.

5.2.4 Sampling and elemental analysis

At 0, 3, 8, 15, 24, 30 and 40 days after transplanting (DAT), porewaters were sampled across 0 - 20 mm of rhizosphere by Rhizon profiler, with a resolution of 1.7 mm. Total dissolved Fe and As were measured by inductively coupled plasma-mass spectrometry (ICP-MS, NexION 350X, PerkinElmer, Inc., Shelton, CT USA). The sample in 0.6 mL centrifuge tube (~ 0.2 mL) was self-aspirated into ICM-MS by a PFA-200 Microflow Nebulizer for elemental analysis. The counts of $^{57}Fe^{+}$ and $^{91}AsO^{+}$ were recorded in dynamic reaction cell (DRC) or extended dynamic range (EDR) mode (Yuan et al. 2019b). Spiked standards were measured every 20 samples to enable appropriate correction of signal shift.

At DAT 40, the sample preserved with EDTA was manually injected into the 25 μL sample loop of ion chromatography (IC, Dionex ICS-1100, Thermo Scientific, USA). Arsenic species were measured by IC-ICP-MS with AS23 column and NH_4HCO_3 mobile phase (20 mM, pH = 10) (Suzuki et al. 2009, Yuan et al. 2019b).

5.2.5 Plant sampling and analysis

Plant was harvested and analyzed at jointing stage (DAT 40). After porewater sampling, the apparatus, including the root bag and Rhizon profiler, was retrieved from soils, and rice plants were taken out from the root bag. The rice root was gently cleaned by ultrapure water (Fig. S4.3). Fresh plants were separated into root, stem and leaf. Sub-samples were oven-dried (60℃) and freezing-dried (- 85℃) for the subsequent determination of total elements and As species respectively. Plant dry matter was

weighed, and the plant tissues were grounded before passing them through a 1.0 mm sieve. Then the samples were stored in plastic bags at room temperature until further extraction or digestion.

Samples of 0.5 g oven-dried and grounded biomass were digested using a mixture of HNO_3 and H_2O_2 (Gustave et al. 2019a). The digested samples were filtered through a 0.45 μm pore size filter and diluted with ultrapure water. The total Fe and As were measured by ICP-MS.

Samples of 0.2 g freezing-dried and grounded biomass were extracted with a modified protein extracting solution (Quaghebeur et al. 2003). The extracted samples were filtered through a 0.45 μm pore size filter and diluted with ultrapure water. The As species were measured by IC-ICP-MS.

5.2.6 Soil microbial sampling and analysis

At DAT 40, soils at 0 - 2 mm distance from root surface were sampled from the soil sampling kit on Rhizon profiler (Fig. S4.4). Soil genomic DNA was extracted by using PowerSoil DNA Isolation Kit (MO BIO Laboratories, Inc. Carlsbad, USA) following the manufacturer's instructions.

Extracted DNA was sequenced by the next generation DNA sequencing (Sangon Biotech. Co., Ltd., Shanghai, China). The average length of sequences is 450 bp. The effective sequences were grouped into operational taxonomic units (OTUs) at a similarity of $\geq 97\%$.

The alpha and beta diversity analyses were performed in QIIME1.8.0. Indexes of Chao 1, Shannon, Simpson, Good's coverage were selected for the alpha diversity

analysis. Beta diversity indice, principal coordinates analysis (PCoA), was applied to calculate the differences between samples. Analysis of similarity (ANOSIM) and linear discriminant analysis (LDA) effect size (LEfse) was further utilized to evaluate the changes in microbial community (Gustave et al. 2019a, Segata et al. 2011).

5.2.7 High-throughput quantitative of As genes

High-throughput qPCR reactions were performed using Wafergen SmartChip Real-time reactions (Chen et al. 2016). DNA was diluted to 20 ng $\cdot\mu L^{-1}$ with sterile PCR grade water and stored at - 20℃. Soil DNA was analyzed by high-throughput qPCR AsChip (Zhao et al. 2019). Comprehensive profiling of 19 As genes, including As(III) oxidation (aoxA, aoxB, aoxC, aoxD, aoxR, aoxS, aoxH and aoxA), As(V) reduction (arrA, arrB, arsC and arsR), As methylation and demethylation (arsI and arsM), and As transport (acr3, arsA, arsB, arsD and arsP) genes, were obtained.

5.2.8 Statistical analysis

Statistical program R version 3.5.0 was used to analyze and plot the data in this study. The linear relationships and 95 % confidence limits were used in correlation analysis. Data of different treatments were subjected to one-way analysis of variance (ANOVA, SPSS Inc., Chicago, USA) to determine statistical significance ($p < 0.05$).

5.3 Results and discussion

5.3.1 Release of As in paddy soils

A root bag was used to cultivate rice, where the bag wall represents the root surface of the root system. From DAT 0 to 40, Rhizon profiler was applied to measure the dissolved Fe and As from 0 to 20 mm distance from root surface, with a temporal and spatial

resolution of 3 - 10 d and 1.7 mm respectively. To compare with rough rhizosphere in previous reports (Afroz et al. 2019, Jia et al. 2013, Muehe et al. 2019), I used zones of 0 - 5 and 15 - 20 mm to represent rhizosphere and bulk soil respectively. The dynamic changes of As release in bulk soil and rhizosphere are given in Fig. 5.1.

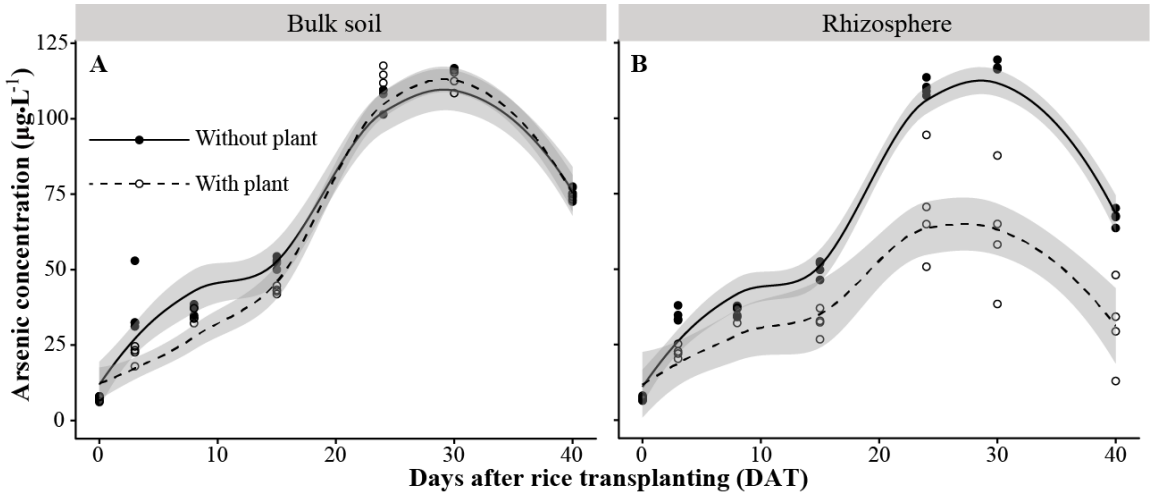

Figure 5.1 Release of arsenic (µg L^{-1}) in bulk soil (A) and rhizosphere (B) from days after rice transplanting (DAT) 0 to 40. Solid line plus closed circle and dashed line plus open circle are without (Control) and with (Treatment) rice plant in root bags respectively.

Release of As in paddy soil is significantly influenced by flooding period and rice planting. Arsenic release can be divided into three stages in bulk soils irrespective of growing rice or not (Fig. 5.1 A): i) exponent increase of As from 7.26 µg L^{-1} at DAT 0 to 112 µg L^{-1} at DAT 24; ii) a release peak at DAT 24 - 30; iii) slow decrease from 117 µg L^{-1} at DAT 30 to 74.9 µg L^{-1} at DAT 40. These results are consistent with previous reports of monitoring As release in bulk soils using Rhizon sampler (Jia et al. 2013, Muehe et al. 2019), which may be generated as a result of an interplay between mobilization and immobilization of As along flooding. It should be noted that initial release of As is very slow after flooding, such as dissolved As was generally < 50 µg L^{-1} within the first 15 days' flooding. The similar phenomenon was also reported in previous

studies using soils with a wide range of As content (Honma et al. 2016, Islam et al. 2004, Muehe et al. 2019). The temporal pattern of As release would be an ideal tool for guiding water management of rice. Many studies demonstrated using of a high-frequency flooding and drainage cycle (e.g. 3 - 5 d) is efficient to reduce As release and subsequent As uptake into rice (Honma et al. 2016). However, the real application of the method is difficult due to the requirement of intensive workload. Based on the temporal pattern of As release (Honma et al. 2016, Islam et al. 2004, Muehe et al. 2019), the cycle frequency of intermittent irrigation could be optimized up to 15 d or more, hence the applicability of intensive water management would be promoted.

Arsenic release in rhizosphere of control treatment showed a similar pattern as in bulk soil (Fig. 5.1B *vs.* 5.1A), while growing rice significantly decreased dissolved As from DAT 15 to 40 by about 50% (Fig. 5.1B). Similar trends were also obtained for Fe release (Fig. S4.4), which is consistent with previous report of Fe release in rhizosphere by using planar optode (Maisch et al. 2019a). The redox changes of As and Fe should be ascribed to ROL (Bravin et al. 2008, Chen et al. 2012, Maisch et al. 2019a), which could generate a redox zone in rhizosphere. Although rough rhizosphere were widely used to reflect the effect of the redox zone on redox, pH, contaminants mobility and microbial colonization (Jia et al. 2013, Martin et al. 2019, Muehe et al. 2019), few information has been provided to resolve a detained understanding of biogeochemical cycling across rhizosphere.

5.3.2 Spatiotemporal changes of As and Fe at rhizosphere

Releases of As and Fe were monitored in rhizosphere (0 - 20 mm) from DAT 0 to 40 in order to track their behaviors at a fine spatiotemporal scale (mm & d). To the best of my

knowledge, this is the first time *in situ* high-resolution spatiotemporal changes of dissolved As and Fe were simultaneously mapped in rhizosphere.

Spatiotemporal changes of As and Fe in the control (without plant) and treatment (with plant) were depicted in heatmaps. In the control group without plant, dissolved As (Fig. S4.5) and Fe (Fig. S4.6) increased from 7.01 μg L^{-1} and 2.59 mg L^{-1} at DAT 0 to a maximum value of 120 μg L^{-1} and 42.3 mg L^{-1} at DAT 30, then decreased to 69.3 μg L^{-1} and 15.9 mg L^{-1} at DAT 40, which share a similar temporal pattern as As and Fe in bulk soils (Fig. 5.1A&S4.4A). Yet, no apparent spatial pattern of As and Fe was observed in the control group. This clearly showed insertion of root bag has no influence on elemental behaviors, supporting root bag is an ideal apparatus for studying biogeochemistry in rhizosphere (Jia et al. 2014, Jia et al. 2013, Wang et al. 2019b).

For the treatment group with plant, the superposed temporal and spatial variation of As and Fe was successfully captured (Fig. 5.2&S4.7). At a relatively far side from root surface (10 - 20 mm), dissolved As and Fe share the same temporal pattern as that in the control group (Fig. 5.2&S4.7 *vs.* S4.5-6), indicating zones ≥ 10 mm would be rarely affected by ROL. These results are consistent with most recent reports of ROL mapping in rhizosphere of seagrasses or rice using planar optodes (Maisch et al. 2019a, Martin et al. 2019). Amazingly, at a narrow zone near root surface (0 - 10 mm), extension of As and Fe gradients was clearly captured (Fig. 5.2/S4.7), indicating ROL could diffuse up to 10 mm into soils and form a redox zone around root. These results demonstrated immobilization of As increased linearly across this zone (Fig. S4.8). Compared with mobile As pool in bulk soil, as much as 40 - 80% mobile As was immobilized in rhizosphere soil. Additionally, massive orange red Fe oxides were observed in that zone

(Fig. S4.9). The presence of the massive newly formed Fe oxides in rhizosphere soil could explain the immobilization of most mobile As entering the rhizosphere, due to the high affinity of which for As (Hartley and Lepp 2008, Herbel and Fendorf 2006, Ratering and Schnell 2001, Xu et al. 2017).

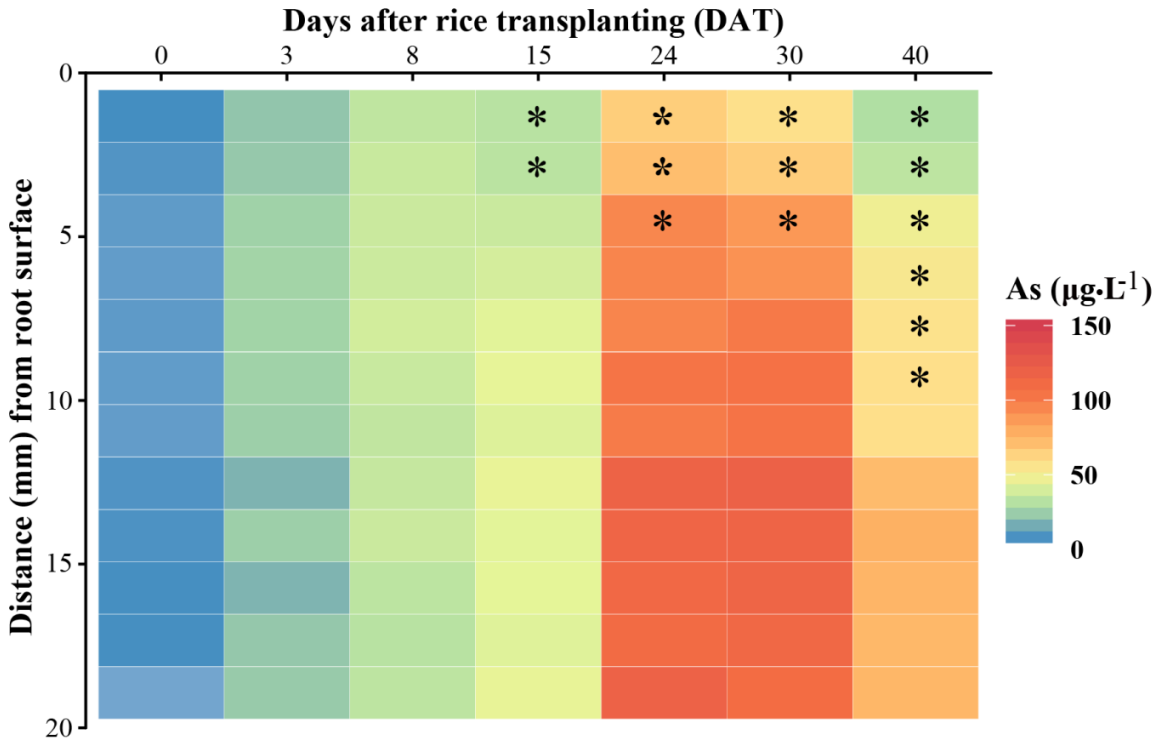

Figure 5.2 Spatiotemporal changes of arsenic (As) across rhizosphere (0 - 20 mm) showed in heatmaps. The cultivation of rice in root bag was from days after transplanting (DAT) 0 - 40. The star represents significance at $p < 0.05$ level.

Although As immobilization is supposed to be induced by ROL and consequent oxidation of Fe, the detailed process regarding As immobilization in rhizosphere is rarely reported. In previous reports, inside and outside of root bags were usually used to represent rhizosphere and bulk soil respectively (Jia et al. 2014, Jia et al. 2013, Wang et al. 2019b), but this strategy is unable to define and reflect the effect of rhizosphere on As immobilization. As a result of this, As immobilization in rhizosphere has long been attributed to the sorption of As by Fe plaque formed on rice root (Chen et al. 2005, Jia et

al. 2018). Although Rhizon sampler array was able to measure the spatial dynamics of As (Frederiksen and Glud 2006), the spatial resolution is too low (cm scale) to reflect the detailed variation of As across rhizosphere (Seeberg‐Elverfeldt et al. 2005). Using Rhizon profiler, we were able to resolve fine-scale spatiotemporal dynamics of As across rhizosphere. The results provided direct evidence to support Fe oxides formed in rhizosphere soil rather than on rice root is the major barrier for As uptake into rice.

5.3.3 Heterogeneous distribution of As species across rhizosphere

Based on spatiotemporal changes of As across rhizosphere, we demonstrated the key role of Fe oxides formed rhizosphere soil to immobilize mobile As pool around root. In order to mechanically interpret the potential biogeochemical processes regulating As redox in rhizosphere, As species variation across rhizosphere was measured (Fig. 5.3).

Two inorganic As species, including As(V) and As(III), were detected in soil porewaters (Fig. 5.3), which is congruent with the previous report using the same soil (Yuan et al. 2019b). I did not observe any organic As in bulk soil or rhizosphere. The lack of organic As in soils could be ascribed to its varying over soil conditions and cultivation time (Chen et al. 2019, Jia et al. 2013, Wang et al. 2019b, Zhao et al. 2013). Although rhizosphere is believed to be a hotspot of As methylation catalyzed by As(III) S-adenosylmethionine methyltransferase (ArsM) (Qin et al. 2006, Zhao et al. 2013), the capture of organic As in rhizosphere is not always successful (Muehe et al. 2019). To date, the cycling of organic As remains cryptic in the environment.

Both As(III) and As(V) were significantly immobilized in the redox zone (Fig. 5.3). For the control group without plant, sum of As(III) and As(V) remained around 90.9

μg L^{-1} across rhizosphere, with an As(III) proportion of 60%. By contrast, sum of As(III) and As(V) decreased linearly from 101 μg L^{-1} at 10 - 20 mm distance from rice root to as low as 23.5 μg L^{-1} at 0 - 2 mm around root, accompanied by an As(III) proportion increasing from 66.0 to 84.3%. The lateral decrease trend of As(III) and As(V) is consistent with that of total As in rhizosphere (Fig. 5.2). However, an opposite trend was observed for As(III) proportion. Fig. 5.3 clearly showed that rhizosphere retained abundant As(III), while As(V) was almost depleted within 0 - 5 mm from root surface. Although it is well documented that As(III) is the predominant As form in the rhizosphere (Jia et al. 2014, Wang et al. 2019b), the spatial As(III) excess or As(V) absence is rarely reported. The As(III) excess could be caused by efflux of As(III) from root or microbes via enzymatic As(V) reduction and subsequent efflux of As(III) from cells (Kumarathilaka et al. 2018a, b, Zhao et al. 2010), while As(V) absence by strong sorption of As(V) by the newly formed Fe oxides (Chen et al. 2005, Tufano et al. 2008). These results strongly support the Fe oxides formed in rhizosphere soil is the key barrier of As uptake into rice, especially for As(V).

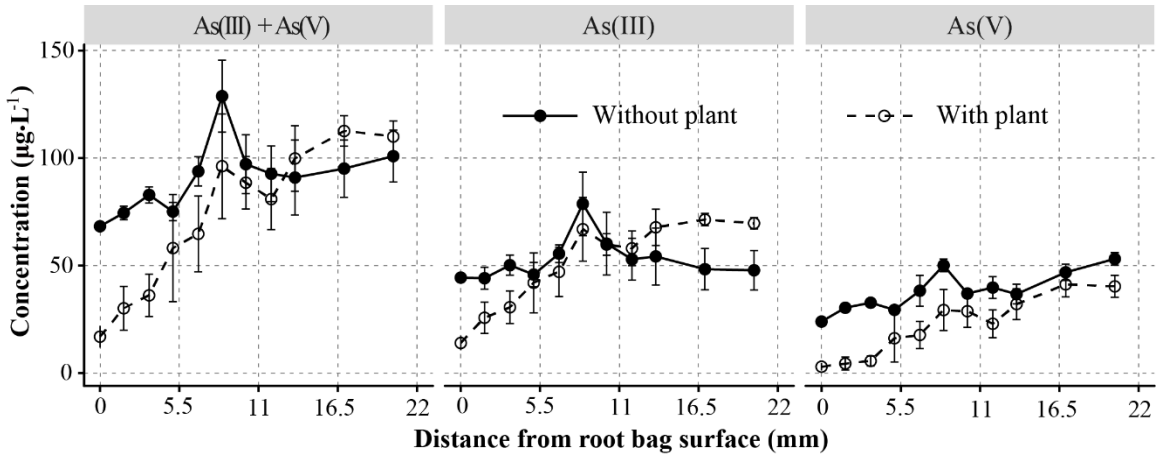

Figure 5.3 Spatial changes of As species across the rhizosphere (0 - 20 mm) at DAT 40. Arsenic species included arsenite [As(III)] and arsenate [As(V)].

5.3.4 Accumulation of As and Fe in rice plant

Total As and Fe, as well as As species, were measured for rice plant after the harvest at DAT 40. Arsenic and Fe were very high in rice root, with a concentration of 0.174 and 33.8 g Kg^{-1} respectively (Fig. S4.10A). By contrast, their concentration was very low in above ground tissues, with an average concentration of 0.00144 and 0.687 g Kg^{-1} respectively (Fig. S4.10B). These results are consistent with previous reports of low As and Fe transportation rate from root to above ground plant tissues (Abedin et al. 2002, Gustave et al. 2019a, Wang et al. 2019a). Interestingly, ratio of Fe to As in root mirrored that in the rhizosphere porewaters, with a value around 300 (Fig. S4.10C/D). However, this value increased up to 500 in stem and leaf, indicating more As was sequestrated than that of Fe during the upward transportation. Due to the predominance of As(III) in rhizosphere and root cells, retention of As(III) may be responsible for the over-sequestration of As during its upward transportation. The over-sequestration of As(III) could be ascribed to the high affinity of As(III) for glutathione and phytochelatins in vacuoles (Kumarathilaka et al. 2018b), which would be of great benefit to migrate As risk in rice grain.

5.3.5 Microbial community shifts across rhizosphere

At 0 - 20 mm distance from root surface, the diversity of the bacterial community was assessed by high-throughput sequencing of the 16S rRNA gene. For alpha diversity, indexes of Chao1, Shannon and Good's coverage were calculated. The high values of Good's coverage (> 0.96, Table S4.2) indicate the sequencing was deep enough to cover the bacterial communities. Chao 1, Shannon and observed OUTs showed no obvious difference between the treatment (with plant) and control (without plant). However, this

is not consistent with previous reports of rhizospheric effect on microbial richness (Jia et al. 2014, Wang et al. 2019b), in which bacterial diversity tends to be greatly promoted by the aerobic conditions in rhizosphere. I thought the close similarity of bacterial richness should be ascribed to the activity of soil animals, which are supposed to be attracted by the aerobic condition in the rhizosphere (Neori and Agami 2017). If so, soil animals could "pollute" rhizospheric microbial composition by their burrowing between bulk soil and rhizosphere. This is supported by our observation of rapid retreat of soil animals from root surface to bulk soils when sampling the soils.

Following alpha analyses, beta diversity, ANOSIM and LEfse analyses were further used to identify the possible microbial shift and the most variable microbe in rhizosphere. These results showed that growing rice altered the bacterial community across the rhizosphere (Fig. 5.4A). Principal coordinates analysis PCoA1 *vs.* PCoA2 (explaining 72.0%) showed bacterial community were different between control and treatment, yet the difference was not significantly different as shown in ANOSIM analysis (Fig. S4.11). This could be also ascribed to the interference of soil animals. Interestingly, LEfse analysis identified many bacteria were enriched in the oxygenated rhizosphere (Fig. S4.12), including *Bacteroidetes*, *Betaproteobacteria*, *Acidobacteria*, *Thiobacillus*, *Gammaprotebacteria*, *Nitrospira*, *Sideroxydans*, *Gallionellaceae* etc. These bacteria include typically Fe and As oxidizing (*Acidobacteria*, *Thiobacillus*) (Ratering and Schnell 2001, Wang et al. 2019b, Ward et al. 2009) and reducing (*Bacteroidetes*, *Betaproteobacteria*) bacteria (Wang et al. 2009), indicating rhizosphere is a hotspot of Fe and As cycling in soils. Stimulation of Fe and As oxidation bacteria could be ascribed to the microoxic conditions generated by ROL diffusion into soils (Druschel et al. 2008,

Emerson et al. 1999, Maisch et al. 2019a). Both the biotic and abiotic process will contribute to Fe oxides formation and subsequent As immobilization in rhizosphere, which in turn could provide rich "food" for those Fe and As reducing bacteria (Campbell et al. 2006, Zobrist et al. 2000). This might be the reason why those bacteria were enriched in the relative oxic zone around root. These results indicate, despite abiotic process, biotic processes are also involved in regulating As release in rhizosphere.

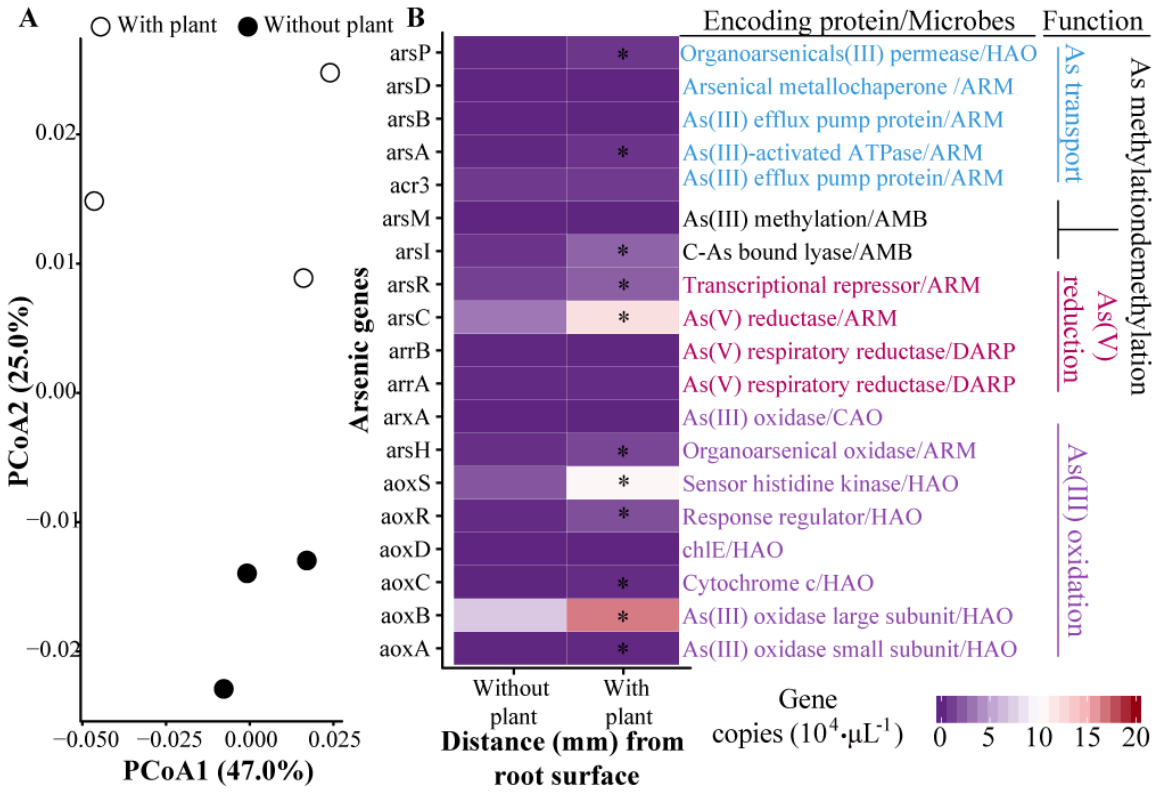

Figure 5.4 Principal coordinates analysis (PcoA) of microbial community (A) and abundance of 19 As genes (B) around root bag at DAT 40. Abbreviation used: HAO, heterotrophic As(III) oxidizers; ARM, As resistant microorganisms; CAO, chemoautotrophic As(III) oxidizers; DARP, dissimilatory As(V) reducing prokaryotes. The star represents significance $p < 0.05$ level.

5.3.6 Shift of As genes across rhizosphere

In order to further assess the role of biotic regulation of As, 19 As genes were investigated in rhizosphere by AsChip analysis. The abundance of As genes (copies per

μL) ranged from 0 to 7.34×10^4 (average 1.68×10^4), which was comparable to precious reports by using the same method (Zhao et al. 2019). The profiling of As genes was showed in a heatmap (Fig. 5.4B).

Biotic transformation appears to play an important role for As cycling in rhizosphere. In control group without growing rice, aoxB and arsC were the most abundant genes in soils (Fig. 5.4B), while aoxD and arsD are undetectable. These results are consistent with previous reports of sequencing As genes in different paddy soils (Wang et al. 2019b, Zhao et al. 2019). AoxB and arsC genes are involved in As oxidation and reduction, hence both reactions may represent the dominant As metabolic pathway in soils. Amazingly, growing rice significantly increased the abundance of all As(III) oxidation genes, suggesting biotic As oxidation is greatly stimulated by oxygenation of rhizosphere. Biotic oxidation of As(III) to As(V) could enhance As immobilization due to the much higher affinity of Fe oxides for As(V) than that of As(III) (Tufano et al. 2008). In addition, As(III) oxidation could also be enhanced by dissolved O_2 via catalyst of ferrous Fe on Fe and manganese minerals (Dong et al. 2014, Ona-Nguema et al. 2010). Thus, intensive immobilizing of As in rhizosphere could be partially ascribed to both abiotic and biotic oxidation of As(III) to As(V).

For As reduction, methylation and transport, part of their genes were promoted in the rhizosphere, including arsACIPR. The promotion of demethylation gene (arsI) may indicate a rapid transformation of any organic As synthesized in rhizosphere. This may be the reason why organic As was usually missing in rhizosphere (Wang et al. 2019b). The genes of As reduction (arsRC) and transport (arsAP) were reported to participate in intracellular As reduction and subsequent efflux of the reaction product [As(III)] to the

external environment (Kumarathilaka et al. 2018b). Hence, overexpression of those genes provides evidence to support that microbes may contribute to As(III) excess observed in rhizosphere (Fig. 5.3).

5.3.7 Regulation of As release at rhizosphere

Based on pot experiment, I present a conceptual model explaining the spatiotemporal regulation of As uptake into rice (Fig. 5.5). Along flooding, Eh decreases in soils due to lack of O_2. Initially, adsorption and desorption are the main processes involving in mobilization of As into porewater. Then, massive As mobilization is triggered by reductive dissolution of Fe oxides and subsequent reduction of As(V) to As(III). Immobilization of As can occur in long-flooded soils due to diagenesis process. With the development of rice root, ROL would be promoted, resulting in formation of a redox transition zone around root. This zone is a trap for mobile As from bulk soil because of massive Fe oxides formed by chemical and biological processes. Soil animals can disturb those processes in rhizosphere. Before uptake of As into rice root, Fe plaque can act as another barrier.

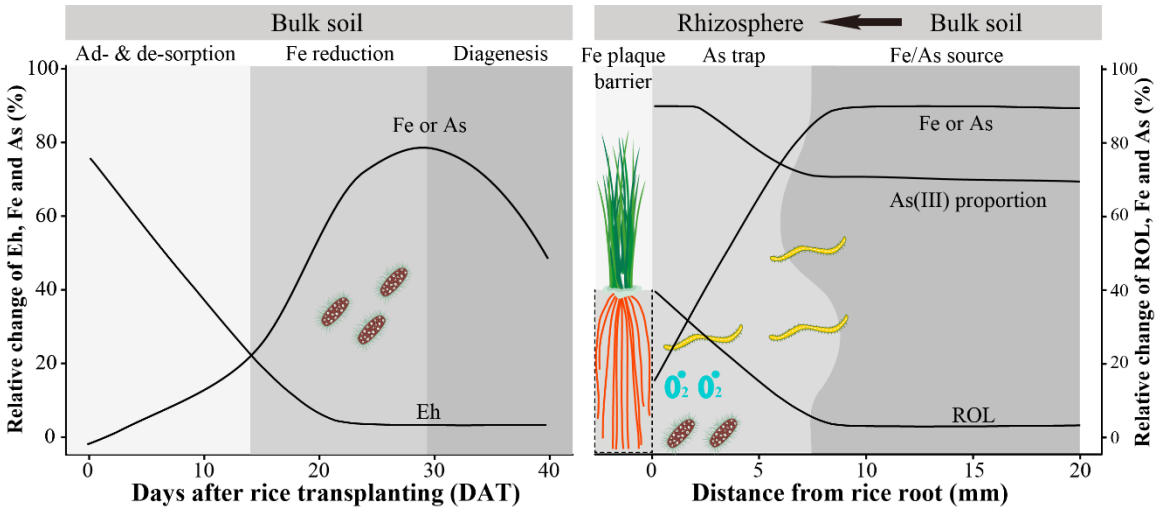

Figure 5.5 A conceptual model explaining the spatiotemporal regulation of As uptake from soil

to rice. Microbes and radical oxygen are involved in biotransformation of Fe and As in rhizosphere, which could be interfered by soil animals.

5.4 Conclusion

This work investigated dynamic profiles of dissolved As and Fe in rhizosphere. *In situ* measuring of total aqueous As and Fe by Rhizon profiler visibly showed spatiotemporal control of As by Fe. When growing rice, mobile As was immobilized in 0 - 10 mm distance from root surface, coinciding with the formation of redox zone by ROL from root. Iron oxides formed in rhizosphere soil can retain most of mobile As (40 - 80%) from bulk soils. Microbial analysis revealed As(V) formation was greatly enhanced, which was further depleted by newly formed Fe oxides in rhizosphere. Future studies, combining spatiotemporal change of multi-element with plant physiology, are essentially needed to improve the understanding of the journey of As from soil to plant.

6. General conclusions and perspectives

6.1 General conclusions

Micro interfaces, including soil-water interface (SWI) and rhizosphere, are key zones controlling As transformation and migration in paddy water-soil-rice system. However, effect of SWI and rhizosphere varies at the mm to cm scale (spatially), and is easily shifted when the external environment changes (temporally) (e.g., pH, Eh etc.). Hence, illustration of the associated mechanisms responsible for regulating As behavior at micro interfaces is hindered to date by techniques available to capture those spatiotemporal changes.

To monitor spatiotemporal dynamics of As and associated elements across SWI in high-resolution, a novel technique, called the *In-situ* Porewater Iterative (IPI) sampler, was initially developed.

To increase measurement throughput of elements in volume limited samples (μL level). ICP-MS and IC-ICP-MS were optimized to measure As, iron (Fe), manganese (Mn), phosphorus (P,) sulfur (S) and speciation of P, S, As in μL level samples collected by high-resolution porewater samplers (e.g. IPI sampler) in a single run.

The cycling of As across SWI and rhizosphere was studied with the updated IPI sampler and state-of-art analytical technique. Mobilization of As is mainly coupled with Fe, while direct evidence was obtained to support decoupling processes could happen in the oxic-anoxic transition zone of SWI. Spatiotemporally mapping of As and Fe across rhizosphere vividly showed Fe oxides formed in rhizosphere, rather than on rice root, is

the key migrator of As risk for rice. Moreover, spatiotemporally modelling of As behavior in rhizosphere offers a better understanding of As cycling in paddy soils.

6.2 Perspectives

In this work, spatiotemporal control of As was investigated in SWI and rhizosphere with novel techniques. To better understand the mechanism involved in As cycling in SWI and rhizosphere, detailed biogeochemical processes may address:

- Biogeochemical processes responsible for arsenate excess in anoxic porewaters.
- Biogeochemical processes responsible for arsenite excess in oxic-anoxic transition zone of SWI.
- Biogeochemical processes responsible for Fe and As oxidation in rhizosphere.

Moreover, the novel techniques could be further optimized to improve their performance. In these contexts, the following points can be considered:

- Develop a user-friendly system to enable sample porewater from the sampler automatically.
- Optimize analysis method to simultaneously measure main anions (e.g. fluoride, chloride, sulfate, sulfide, phosphate, nitrate, nitrite, ammonium etc.) in limited porewaters collected from the sampler.
- Optimize analysis method to measure dissolved gases (e.g. methane) in limited porewaters collected from the sampler.

Finally, other micro interfaces and the related biogeochemical processes can be investigated with the techniques and research system developed in this study:

- After applying fertilizer (e.g. organic or inorganic ones), a fertilizer-soil micro

interface is formed, and elucidation of fertilizer effect should consider this interface.

- After applying amendments for remediating heavy metals or organic pollutants contaminated paddy soils, an amendment-soil micro interface is formed, and elucidation of amendment effect should consider this interface.

Appendix 1

Table S1.1 The selected characteristics of two paddy soils used in this study

Location	Soil type	pH	Ni (mg Kg^{-1})	As (mg Kg^{-1})	Cd (mg Kg^{-1})	Sb (mg Kg^{-1})	Pb (mg Kg^{-1})
GZ	sandy	6.71	27.5	36.1	0.5	2.5	39.3
QY	loamy	6.52	35.7	50.7	0.2	3.5	7.2

Note: Location is Ganzhou (GZ) and Qingyuan (QY); elements, including nickel (Ni), arsenic (As), cadmium (Cd), antimony (Sb) and lead (Pb), were tested.

Table S1.2 The sensitivity of elements when using IPI samplers under acidic (pH 1) and near neutral (pH 6) conditions with different carrier solutions

Carrier solution	**pH**	**Sensitivity (counts/(μg·L^{-1}))**				
		Ni	As	Cd	Sb	Pb
Ultrapure water	1	1296	316	650	1967	1729
	6	928	331	298	2075	0
10 mM $NaNO_3$	1	1295	322	661	1852	1703
	6	1205	306	477	1733	0
10 mM NaCl	1	1248	369	643	2006	2123
	6	1260	389	746	1889	2251

Table S1.3 Comparison of Rhizon sampler and IPI sampler for measuring Ni, As, Cd, Sb and Pb in Ganzhou (GZ) and Qingyuan (QY) paddy soil pore water (n = 3)

Elements (μg Ł$^{-1}$)	**GZ soil**		***p* value**	**QY soil**		***p* value**
	Rhizon	IPI		Rhizon	IPI	
Ni	15.4 ± 1.04	4.88 ± 0.916	<0.05	20.3 ± 0.448	8.09 ± 0.762	<0.05
As	223 ± 19.5	195 ± 14.7	0.181	80.3 ± 12.3	78.7 ± 13.2	0.906
Cd	0.455 ± 0.025	0.979 ± 0.924	0.468	0.394 ± 0.023	0.610 ± 0.017	<0.05
Sb	0.452 ± 0.073	0.418 ± 0.070	0.655	0.882 ± 0.023	0.793 ± 0.143	0.433
Pb	4.32 ± 0.231	3.26 ± 1.08	0.245	4.31 ± 0.678	2.50 ± 0.232	<0.05

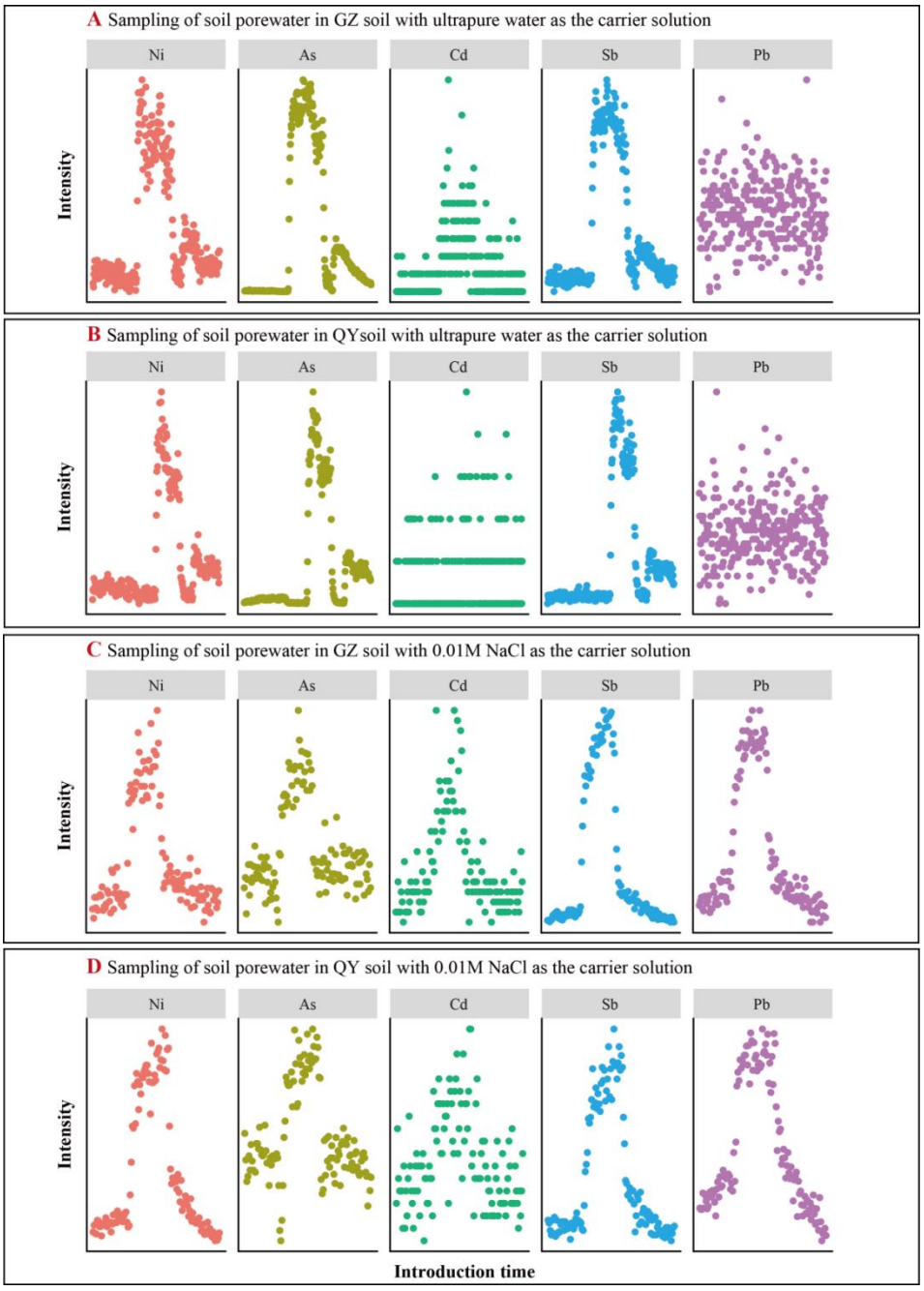

Figure S1.1 Comparison of two carrier solution in soil porewater. (A, B) use ultrapure water as the carrier solution for IPI samplers in GZ, QY soils; (C, D) use 10 mM NaCl as the carrier solution for IPI samplers in GZ, QY soils. Note: obvious peaks were observed for Ni and Sb with ultrapure water or 10 mM NaCl as the carrier solution, thus I called their signals are strong; strong signals of As were observed with ultrapure water as the carrier solution, but became moderate with 10 mM NaCl as the carrier solution; extremely weak signal was observed for Pb with ultrapure water as the carrier solution, but became strong with 10 mM NaCl as the carrier solution; for Cd, weak signals were observed in GZ and QY soils.

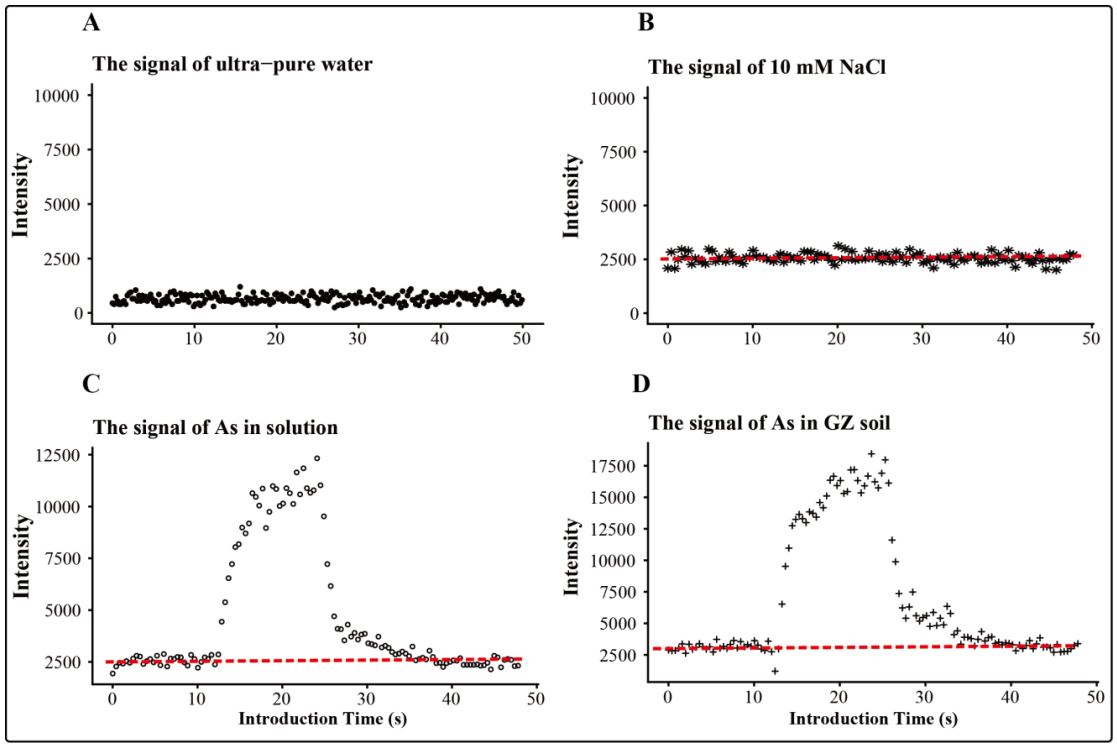

Figure S1.2 The signal of arsenic (As) in ultrapure water (A), 10 mM NaCl (B), and in standard solution (10 μg·L^{-1}, C) and Ganzhou (GZ) soil (D) with 10 mM NaCl as the carrier solution. The red dash line points the baseline of As is around 2500.

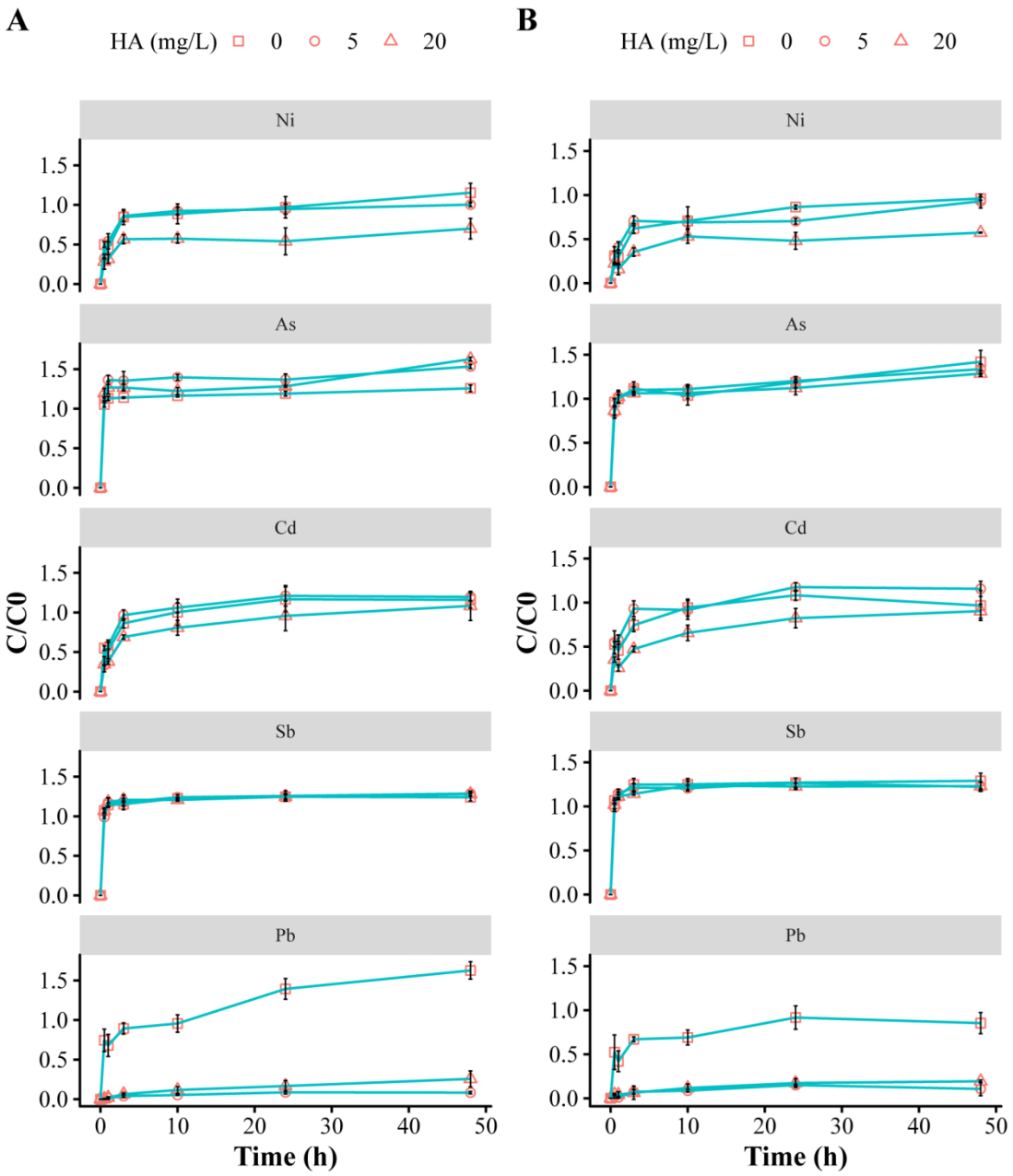

Figure S1.3 The dynamic equilibration process of different elements under different humic acid (HA) concentrations. A) 20 μg·L^{-1} Ni, As, Cd, Sb and Pb; B) 100 μg·L^{-1} Ni, As, Cd, Sb and Pb. The error bars are standard deviations (SD, *n* = *3*).

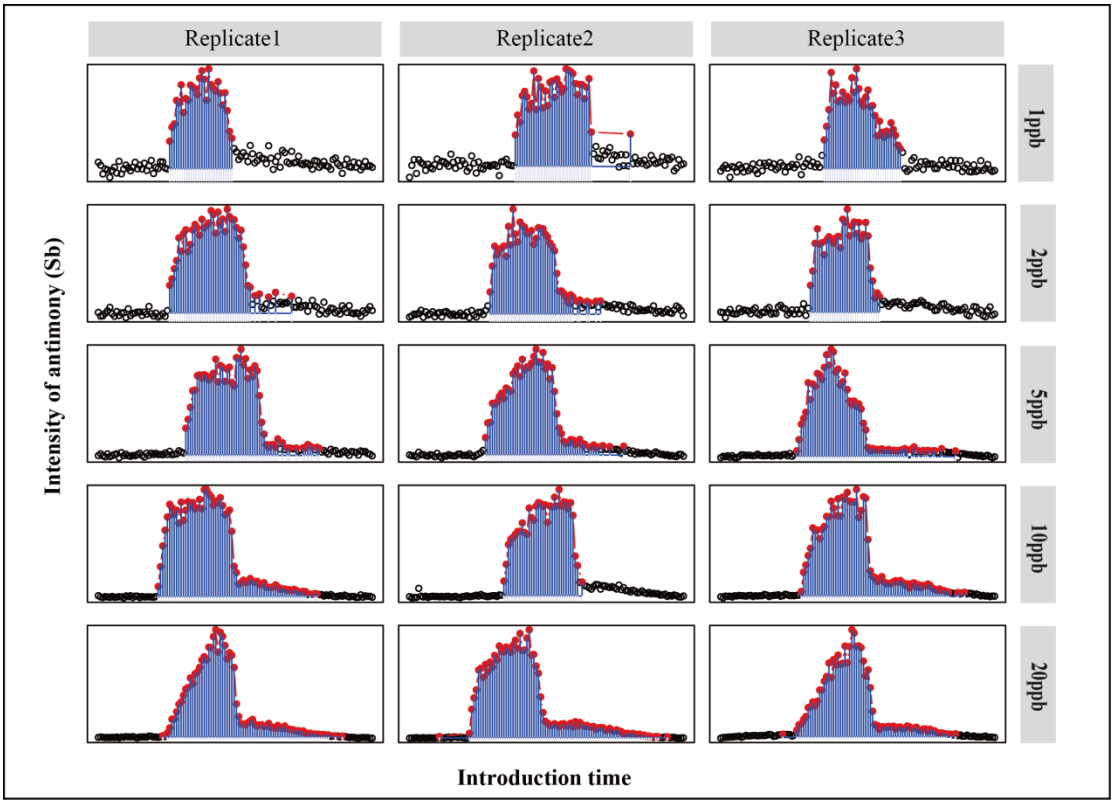

Figure S1.4 Peak areas of antimony (Sb) calculated at a series of concentration (1.0, 2.0, 5.0, 10, 20 $\mu g \cdot L^{-1}$). The areas are integrated of the space under the points (red points) higher than baseline+5SD.

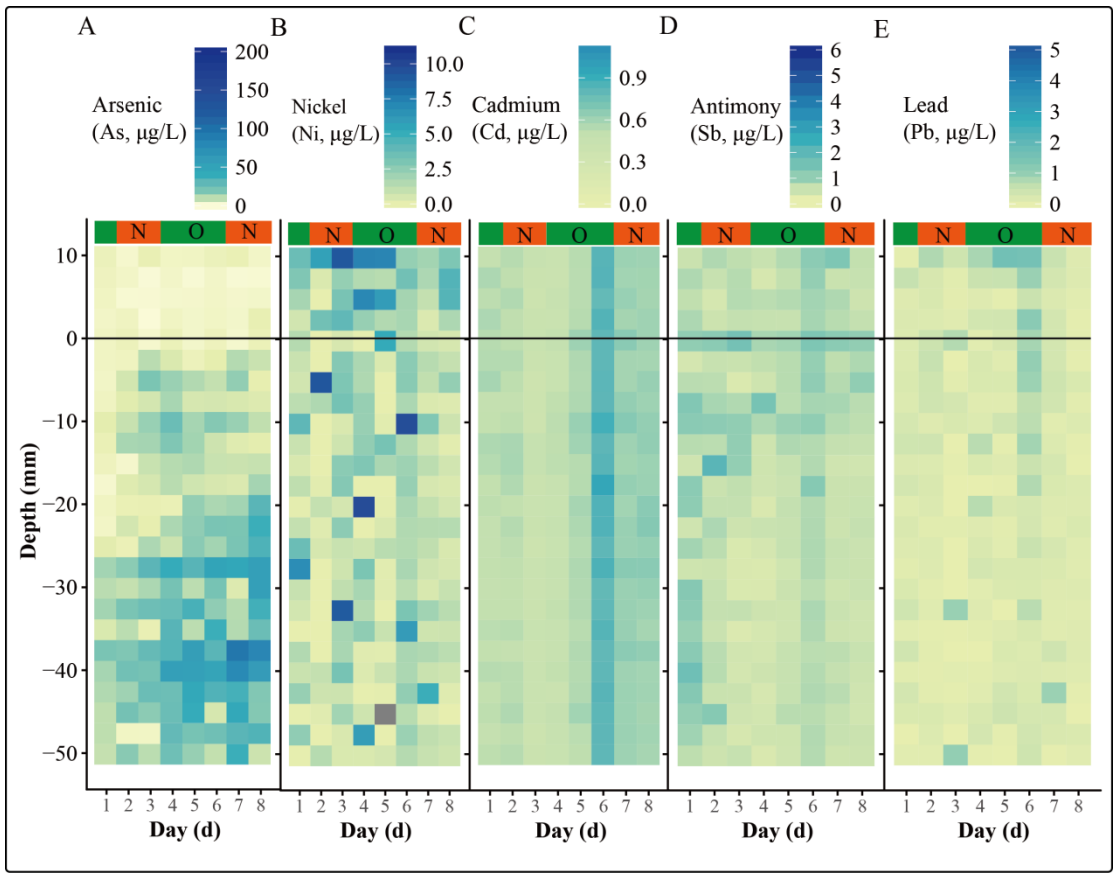

Figure S1.5 The dynamic vertical SD profile changes of As (A), Ni (B), Cd (C), Sb (D), and Pb (E) in GZ soil showed in heatmaps.

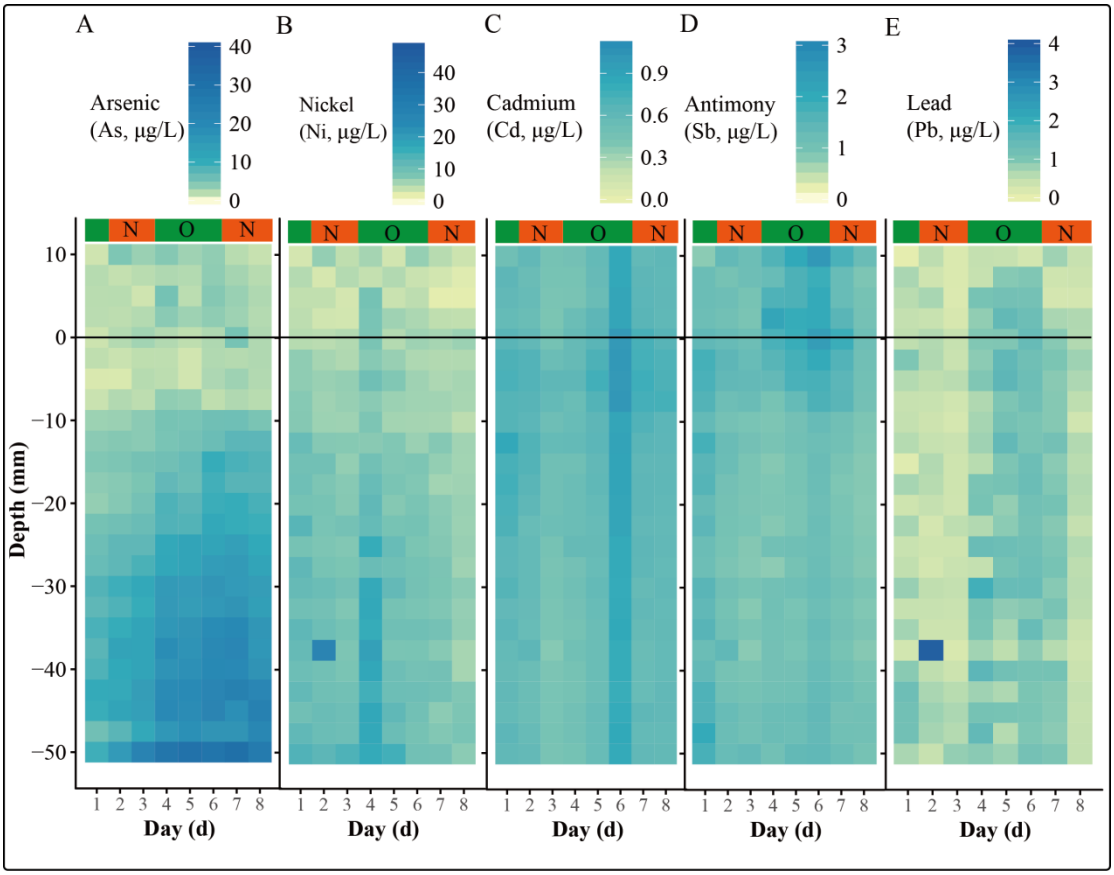

Figure S1.6 The dynamic vertical profile changes of As (A), Ni (B), Cd (C), Sb (D), and Pb (E) in QY soils showed in heatmaps.

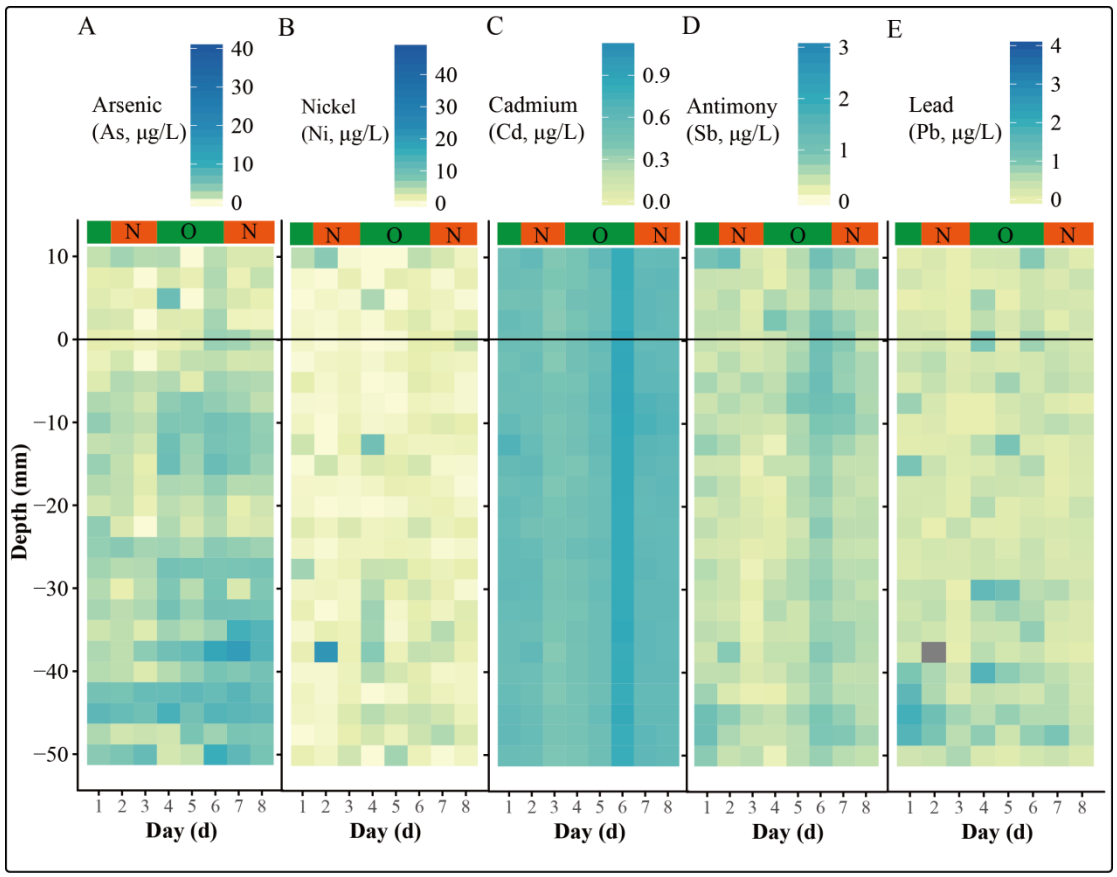

Figure S1.7 The dynamic vertical SD profile changes of As (A), Ni (B), Cd (C), Sb (D), and Pb (E) in QY soil showed in heatmaps.

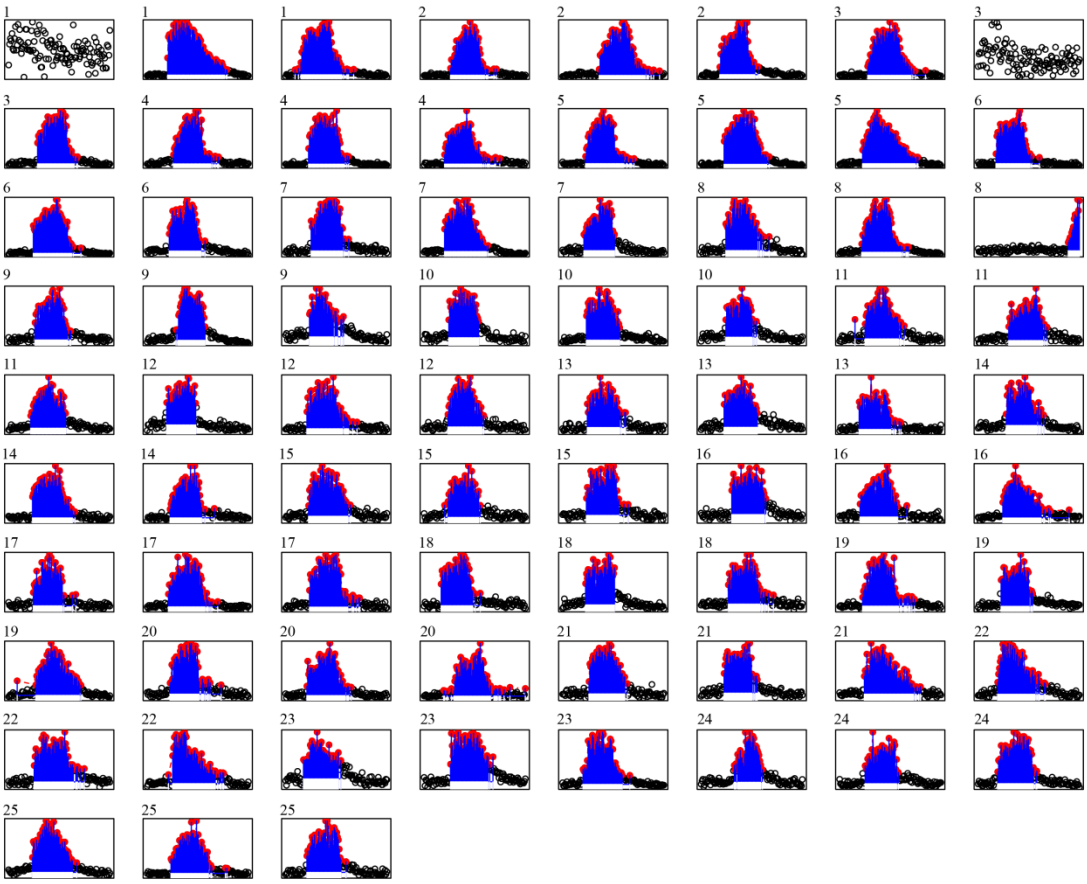

Figure S1.8 The preview of peak selection for antimony (Sb). The number 1 - 25 means the 25 samplers of IPI arrays; I used three arrays for each soil.

Appendix 2

Table S2.1 The selected characteristics of Shaoguan (SG) paddy soils used in this study

Location	Soil type	As (mg ⱠKg^{-1})	Fe (g ⱠKg^{-1})	P (mg ⱠKg^{-1})	S (%)	Mn (g ⱠKg^{-1})
SG	loamy	146	227	40.0	0.40	1.50

Note: Elements, including arsenic (As), iron (Fe), phosphorus (P), sulfur (S) and manganese (Mn), were tested.

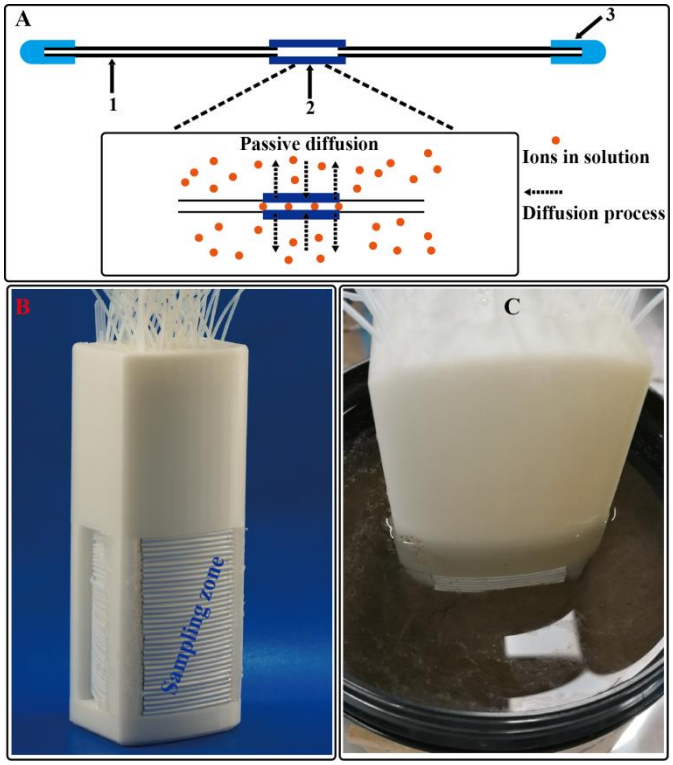

Figure S2.1 Schematic diagram of Integrated Porewater Injection (IPI) sampler. (A) the design and work mechanism of IPI sampler; (B) photo of SWI profiler; (C) photo of SWI profiler deployed in soils. Note (A): 1. pipe; 2. hollow fiber membrane tube; 3. silicon cap.

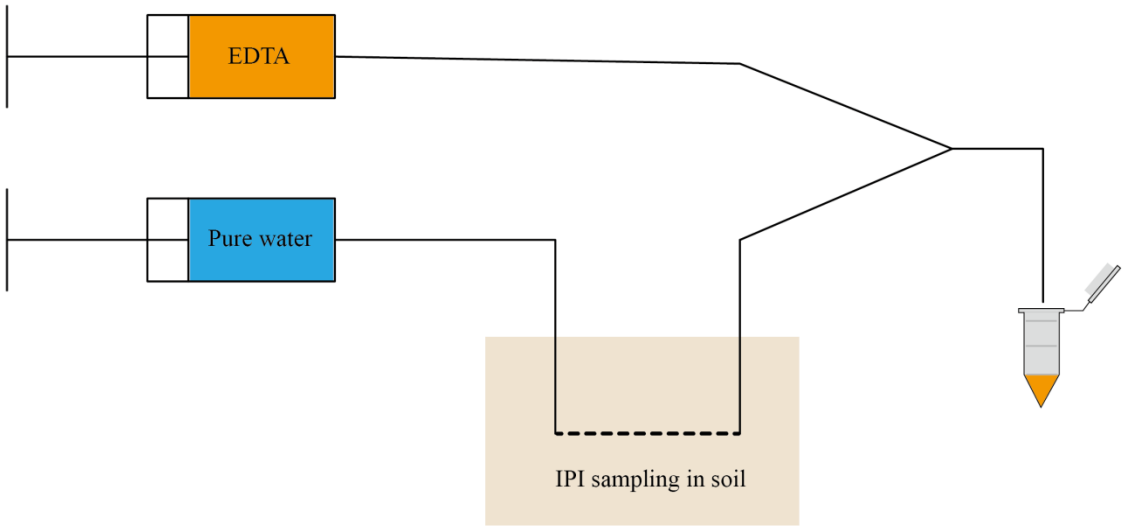

Figure S2.2 The sampling process of IPI sampler in saturated soils.

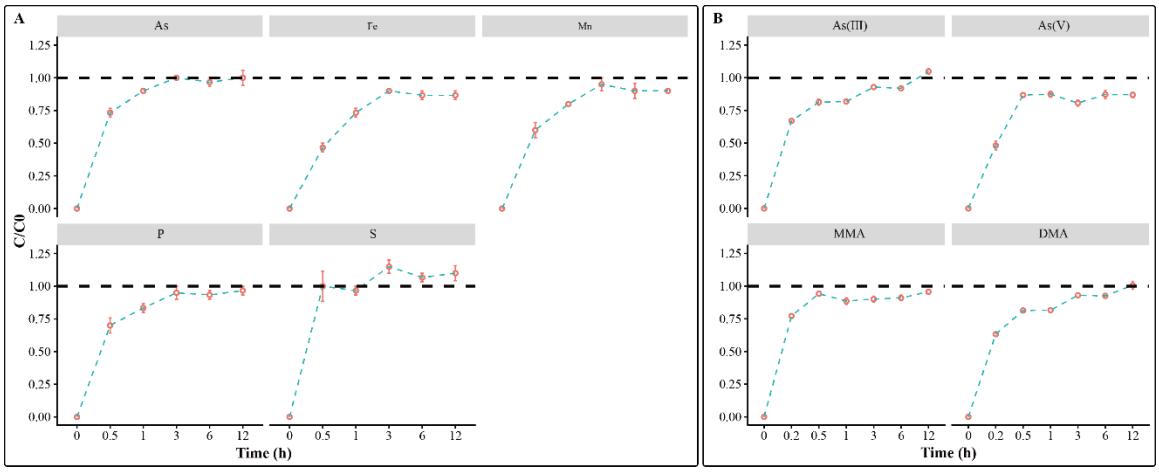

Figure S2.3 The dynamic response of total elements (A) and redox species (B) in IPI sampler (normalized element concentration in solutions). A) Total elements include arsenic (As), iron (Fe), manganese (Mn), phosphorus (P) and sulfur (S) measured by ICP-MS. B) Four As species, including arsenite [As(III)], arsenate [As(V)], monomethylarsonic (MMA) and dimethylarsinic (DMA) acid, were tested by IC-ICP-MS. The error bar is standard deviation (SD, n = 3).

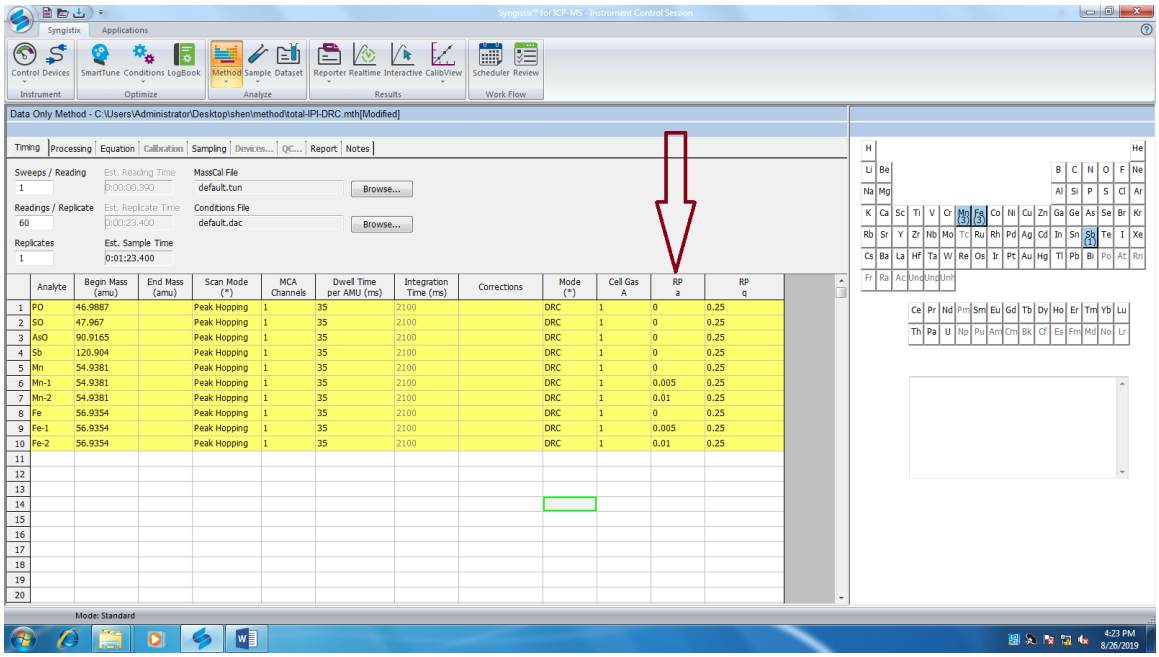

Figure S2.4 Multi-element analysis with extended dynamic range (EDR) and data only analysis in ICP-MS. Red arrow points the parameter (Rpa value) of EDR mode.

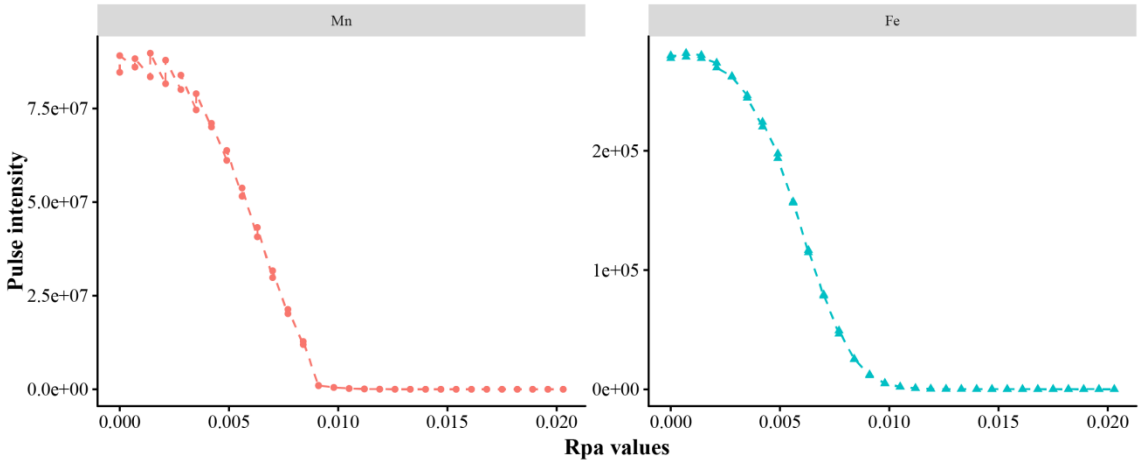

Figure S2.5 Response of iron (Fe) and manganese (Mn) to different Rpa values.

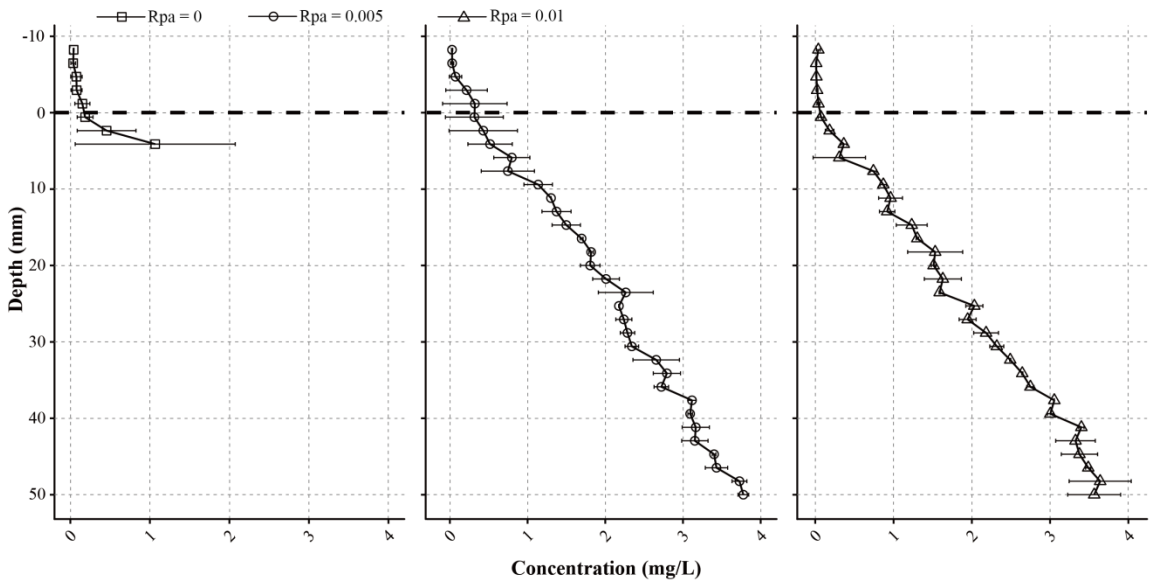

Figure S2.6 Manganese (Mn) profile measured by EDR method with different Rpa values in Shaoguan (SG) paddy. Rpa values were set at 0, 0.005 and 0.01 respectively. The error bar is standard deviation (SD, n = 2).

Appendix 2

Appendix 3

Table S3.1 The selected characteristics of five paddy soils used in this study

Location	Soil type	pH	Fe (g ⱠKg^{-1})	Mn (g ⱠKg^{-1})	P (g ⱠKg^{-1})	S (g ⱠKg^{-1})	As (mg ⱠKg^{-1})
WS	Sandy	6.19	21.9	6.32	1.30	1.74	52.1
BI	Loamy	6.57	84.6	1.52	0.722	1.56	29.4
WX	Loamy	5.52	93.1	0.932	0.712	0.469	25.6
SG	Loamy	5.68	227	1.50	1.237	0.694	146
GZ	sandy	5.92	71.9	1.12	0.859	0.631	36.1

Note: Locations are Wenshan (WS), Bijie (BI), Wuxue (WX), Shaoguan (SG) and Ganzhou (GZ). Elements, including iron (Fe), manganese (Mn), phosphoros (P), sufur (S) and arsenic (As), were tested.

Table S3.2 Linear relationship between arsenic (As) with iron (Fe) and manganese (Mn) across paddy soil-water interface

Site	**Fe *vs.* As**						**Mn *vs.* As**					
	Whole profile			Oxic-anoxic transition zone §			Whole profile			Oxic-anoxic transition zone		
	Slope	R^2	Residual	Slope	R^2	Residual	Slope	R^2	Residual	Slope	R^2	Residual
Wenshan	0.00297	0.848**	0.0253	0.00376	0.775**	0.0179	0.0150	0.974**	0.0105	0.0166	0.980**	0.00541
Bijie	0.00309	0.948**	0.0461	0.00245	0.974**	0.0193	0.0175	0.979**	0.0293	0.0161	0.984**	0.0151
Wuxue	0.00285	0.978**	0.0632	0.00236	0.980**	0.0336	0.0635	0.983**	0.0559	0.0674	0.969**	0.0417
Shaoguan	0.00168	0.965**	0.294	0.00157	0.899**	0.265	0.0541	0.711**	0.496	0.0535	0.413**	0.390
Ganzhou	0.0188	0.937**	0.411	0.0178	0.775**	0.401	0.274	0.950**	0.366	0.313	0.860**	0.302

§: Oxic-anoxic transition zone indicates the 0 - 3 cm zone beneath soil-water interface.

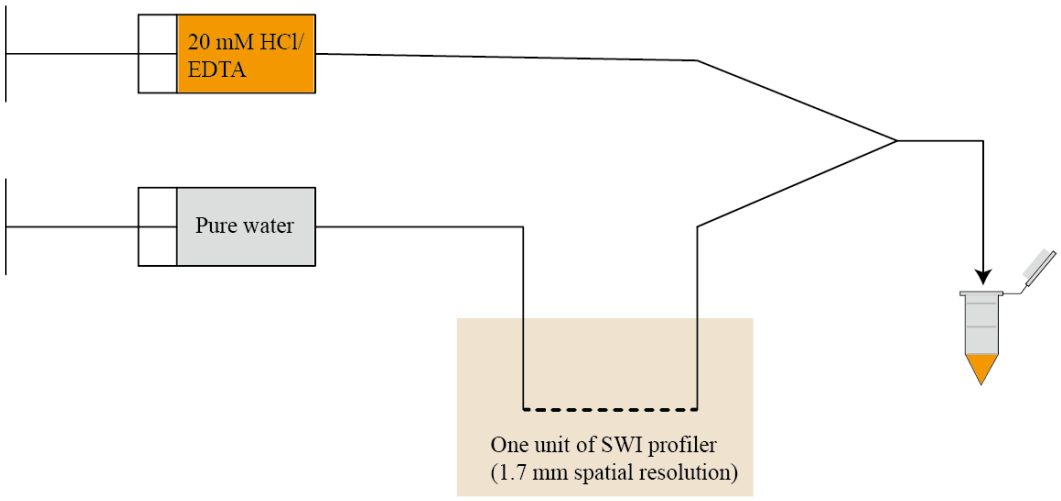

Figure S3.1 The sampling process of IPI sampler in saturated soils.

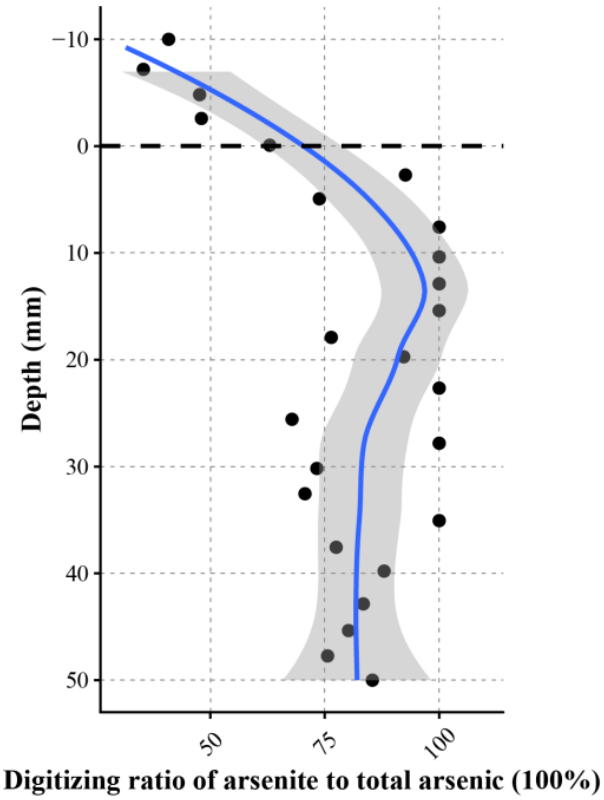

Figure S3.2 Ratio of As (III) to total As digitized from Arsic et al. (2018). The black dotted line at depth = 0 represents soil-water interface.

Appendix 4

Table S4.1 The selected characteristics of Shaoguan (SG) paddy soils used in this study

Location	Soil type	As (mg Ƙg^{-1})	Fe (g Ƙg^{-1})
SG	loamy	146	227

Note: elements, including arsenic (As) and iron (Fe), were tested.

Table S4.2 Richness of microbial community in soils

Treatment	Index	Mean ±SD
Without plant	Observed OTUs	5897 ±541
	Chao1	10173 ±811
	Shannon	6.71 ±0.023
	Good's coverage	0.963 ±0.0047
With plant	Observed OTUs	5958 ±104
	Chao1	10333 ±160
	Shannon	6.74 ±0.022
	Good's coverage	0.965 ±0.0042

Note: SD is standard deviation; OUT means operational taxonomic unit.

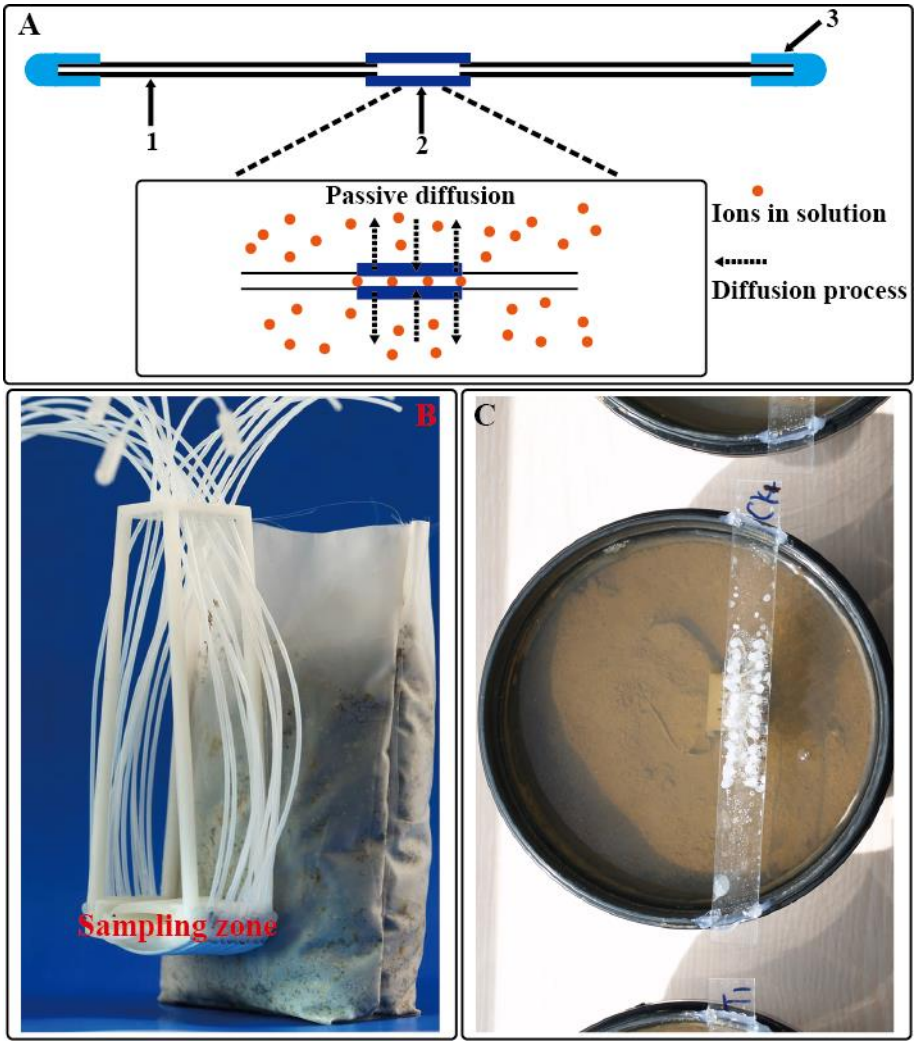

Figure S4.1 Schematic diagram of IPI sampler. (A) The design and work mechanism of IPI sampler; (B) photo of Rhizon profiler; (C) photo of Rhizon profiler deployed in soils. Note (A): 1. pipe; 2. hollow fiber membrane tube; 3. silicon cap.

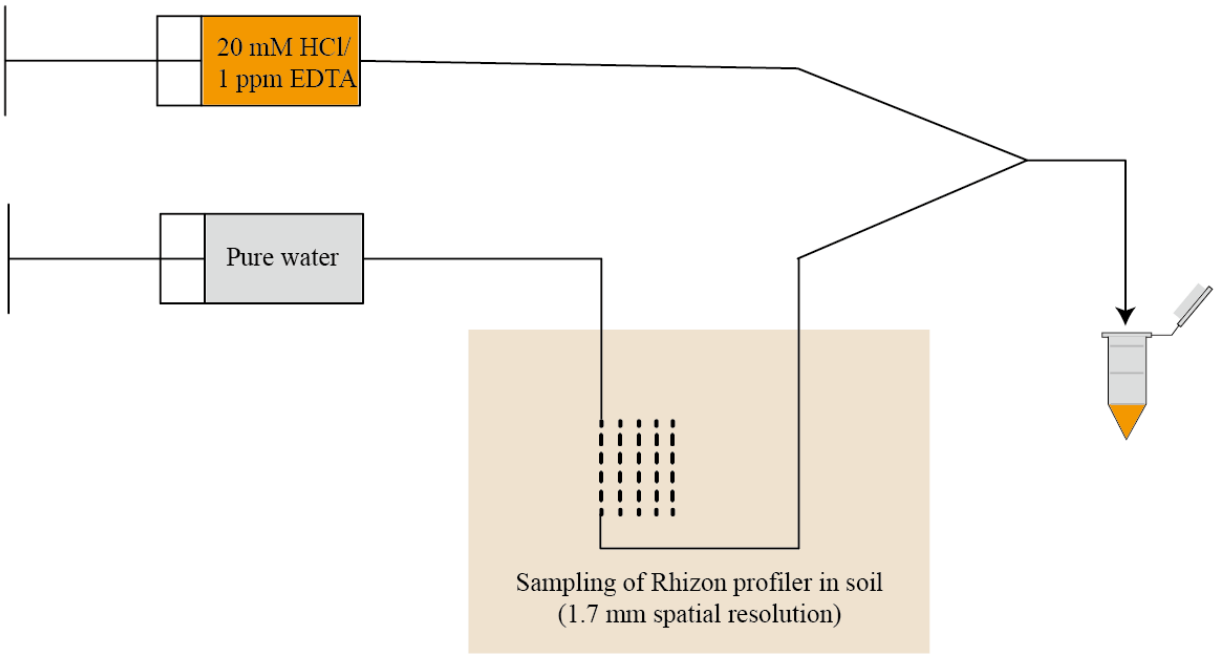

Figure S4.2 The sampling process of IPI sampler in rhizosphere of rice

Figure S4.3 The original (A) and washed (B) rice root grown in root bag.

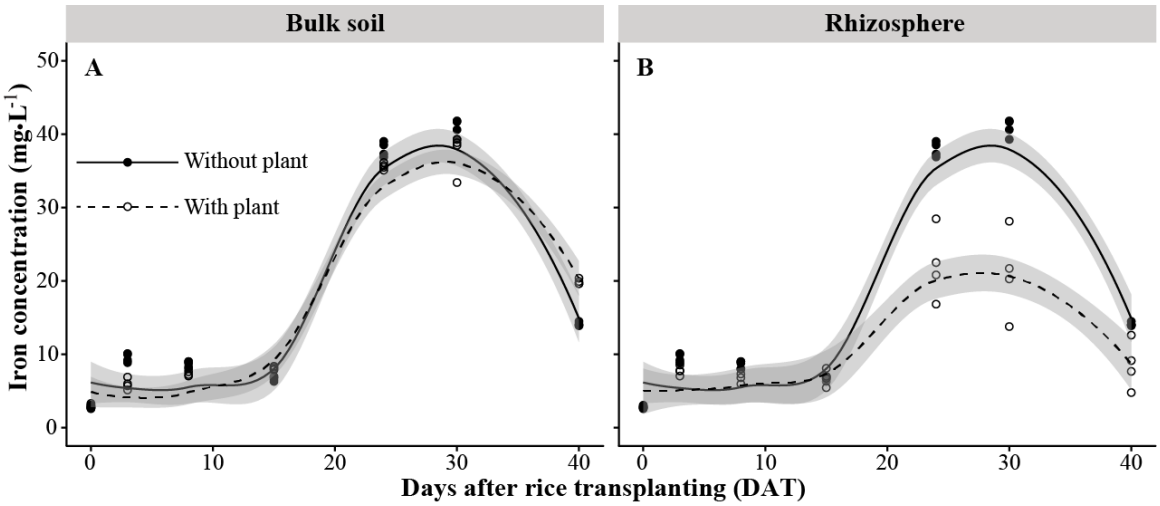

Figure S4.4 Mobilization of iron (mg L^{-1}) in rhizosphere (A) and bulk soil (B) from days after rice transplanting (DAT) 0 to 40 d. Solid line plus closed circle and dashed line plus open circle represent without (Control) and with (Treatment) rice plant in root bag.

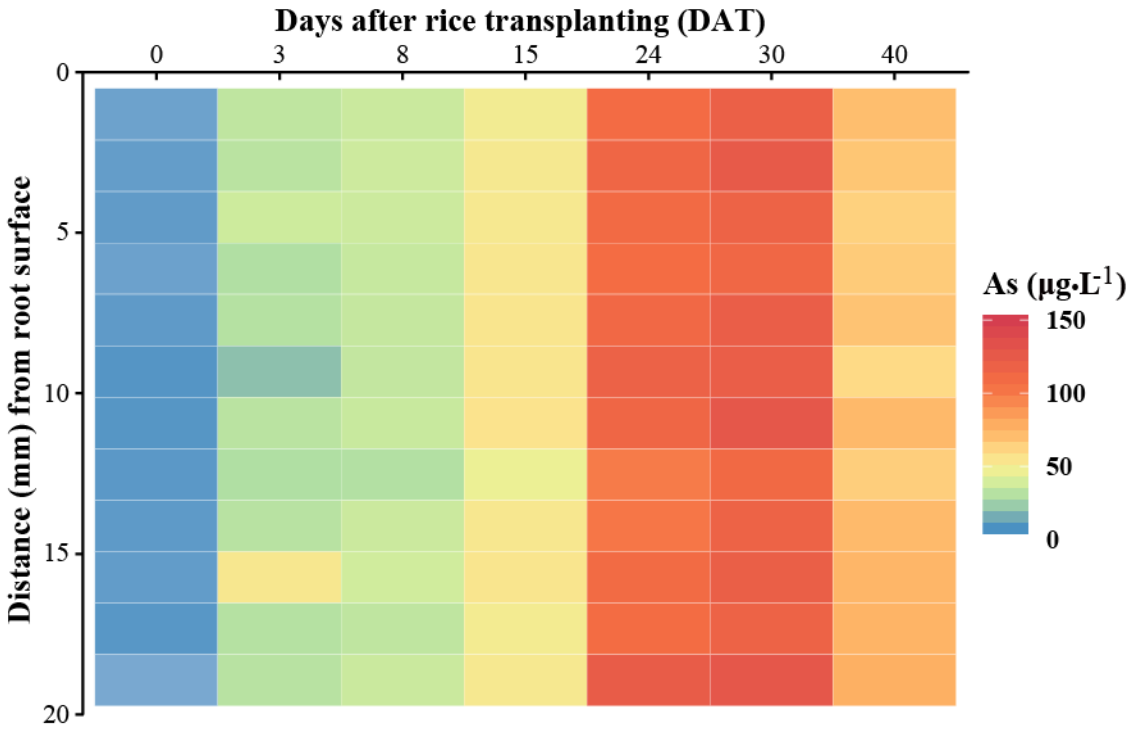

Figure S4.5 Spatiotemporal changes of arsenic (As, µg L^{-1}) across rhizosphere (0 - 20 mm) showed in heatmaps. No rice was grown in root bag from days after rice transplanting (DAT) 0 - 40.

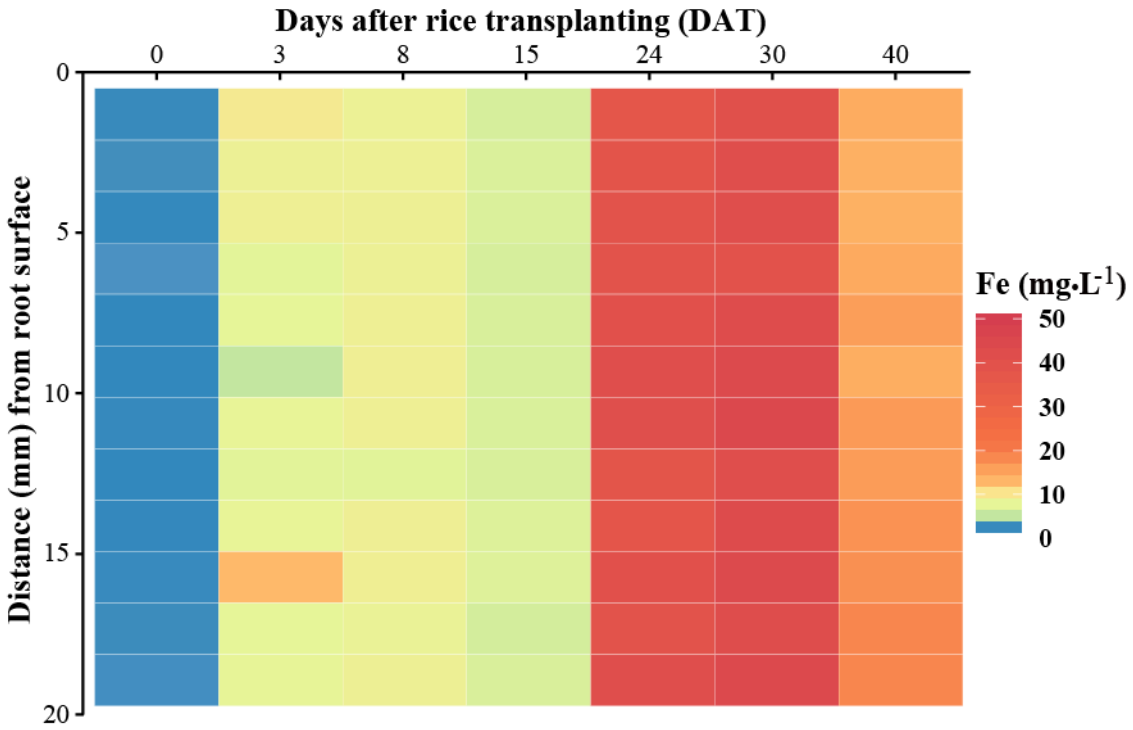

Figure S4.6 Spatiotemporal changes of iron (Fe, mg L^{-1}) across rhizosphere (0 - 20 mm) showed in heatmaps. No rice was grown in root bag from days after rice transplanting (DAT) 0 - 40.

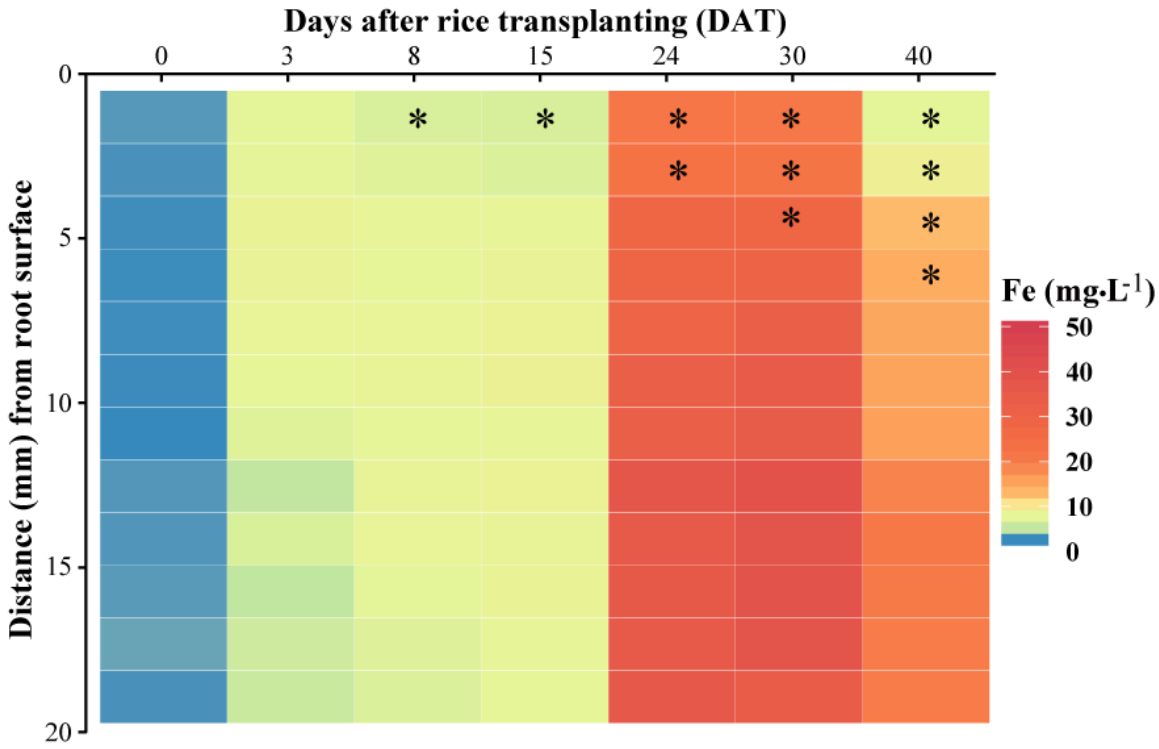

Figure S4.7 Spatiotemporal changes of iron (Fe, mg L^{-1}) across rhizosphere (0 - 20 mm) showed in heatmaps. The cultivation of rice in root bag was from days after rice transplanting (DAT) 0 - 40. The star represents significance at $p < 0.05$ level.

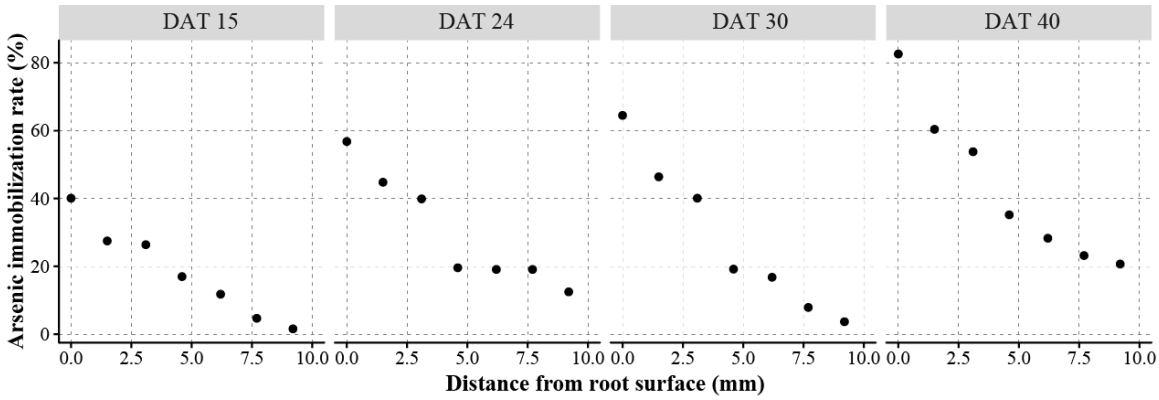

Figure S4.8 The rate of arsenic immobilization across rhizosphere at DAT 15, 24, 30 and 40.

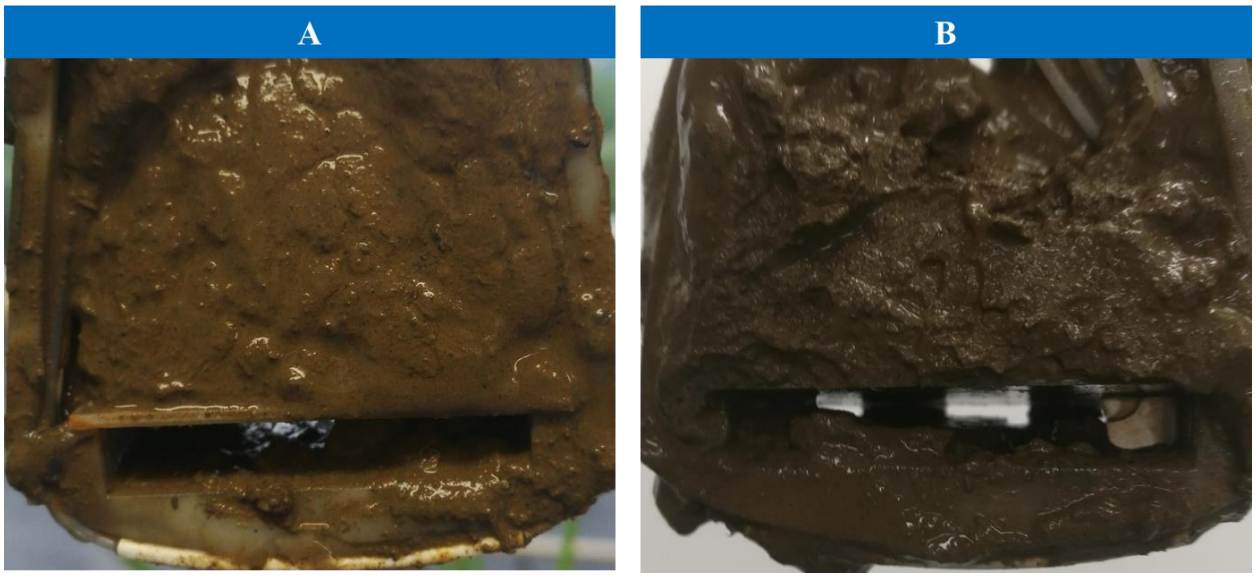

Figure S4.9 The front (A) and back (B) side of Rhizon profiler after taking out from soil at DAT 40. Orange red Fe oxides were observed in soils near rice root.

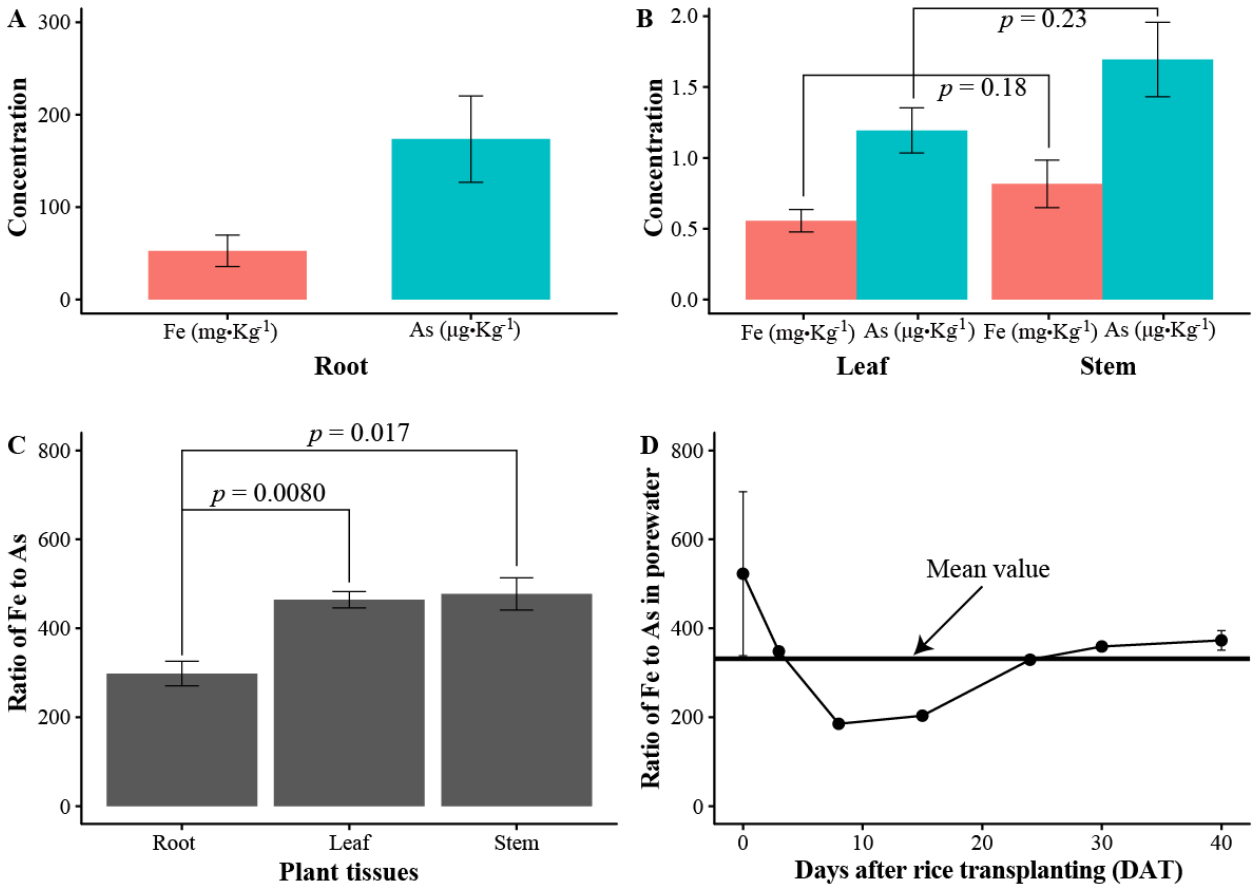

Figure S4.10 The distribution of iron (Fe) and arsenic (As) in rice plant tissues and rhizosphere. A) concentration of Fe and As in dried root; B) concentration of Fe and As in dried leaf and stem; C) ratio of Fe to As in plant tissues (root, leaf, stem); D) ratio of Fe to As in rhizosphere (0 - 2 mm distance from root surface) from days after rice transplanting (DAT) 0 - 40. The error bar represents standard error (SE, n = 3).

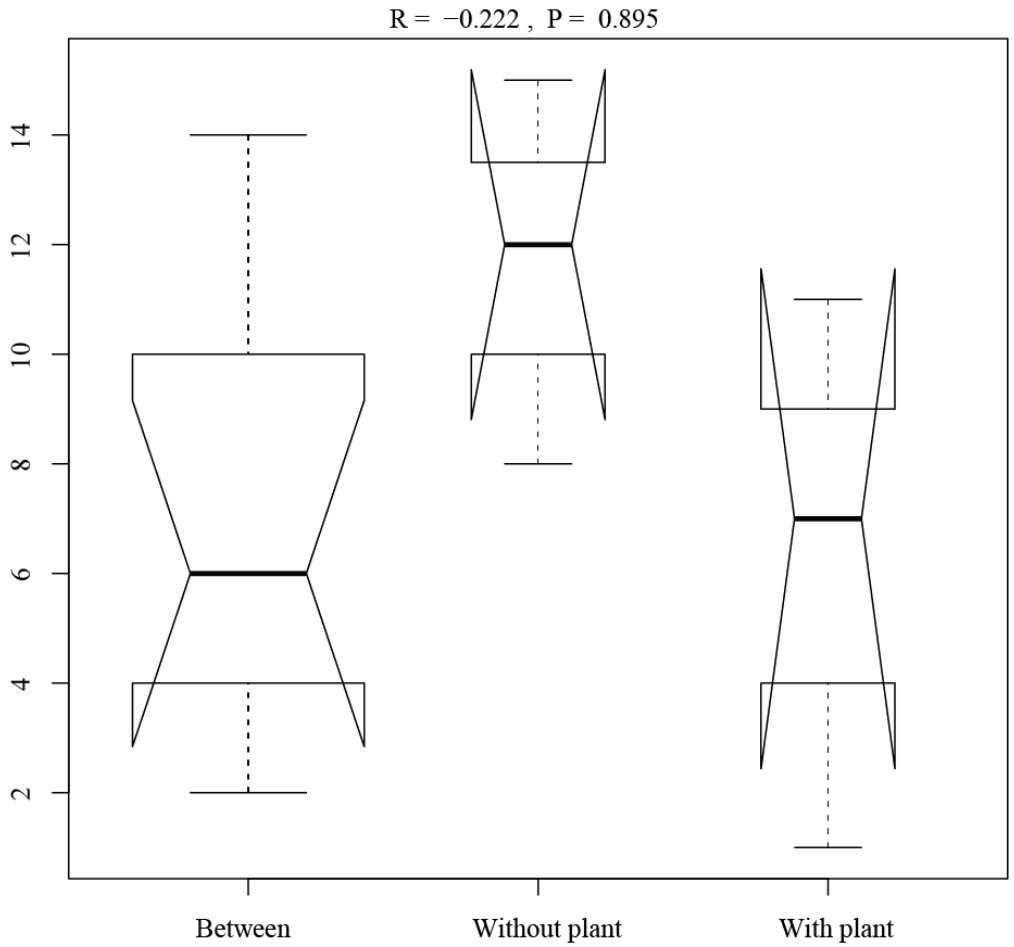

Figure S4.11 Anosim analysis between control (without plant) and treatment (with plant) at 1 mm distance from root surface.

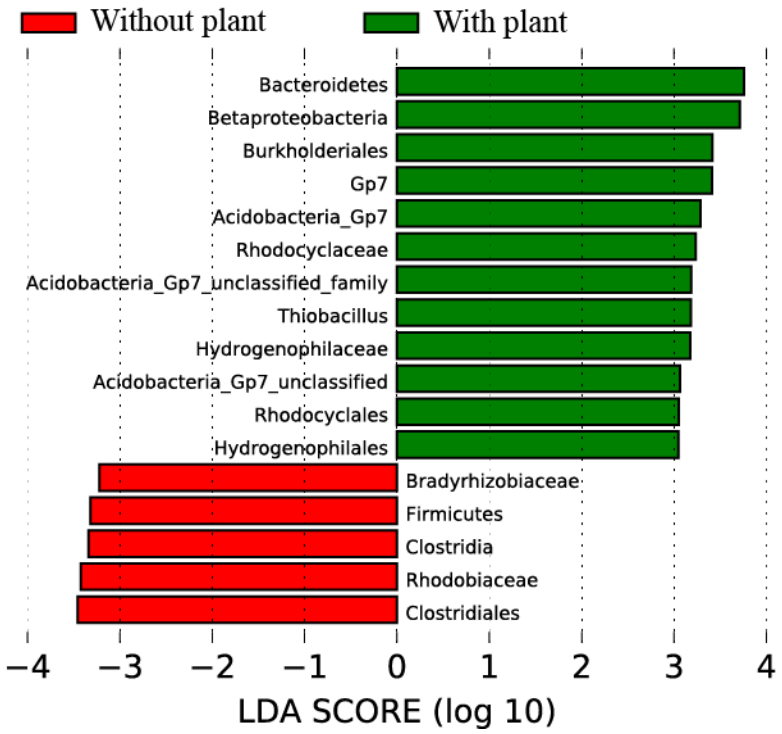

Figure S4.12 Linear discriminant analysis (LDA) effect size (LEfse) between control (without plant) and treatment (with plant) at 1 mm distance from root surface. *Hydrogenophilaceae* belongs to *Thiobacillus*.

References

Abedin, M.J., Cresser, M.S., Meharg, A.A., Feldmann, J. and Cotter-Howells, J. (2002) Arsenic accumulation and metabolism in rice (*Oryza sativa* L.). *Environ. Sci. Technol.* 36(5), 962-968.

Afroz, H., Su, S., Carey, M.P., Meharg, A.A. and Meharg, C. (2019) Inhibition of microbial methylation via arsM in the rhizosphere: arsenic speciation in the soil to plant continuum. *Environ. Sci. Technol.* 53(7), 3451-3463.

Akter, K.F., Owens, G., Davey, D.E. and Naidu, R. (2005) Reviews of environmental contamination and toxicology, pp. 97-149, Springer.

Almkvist, G., Hocker, E., Sahlstedt, M. and Museums, S.M. (2013) Iron removal from waterlogged wood. *Swedish University of Agricultural Sciences. SLU Repro, Uppsala*.

Anawar, H.M., Akai, J., Komaki, K., Terao, H., Yoshioka, T., Ishizuka, T., Safiullah, S. and Kato, K. (2003) Geochemical occurrence of arsenic in groundwater of Bangladesh: sources and mobilization processes. *J. Geochem. Explor.* 77(2-3), 109-131.

Anawar, H.M., Akai, J. and Sakugawa, H. (2004) Mobilization of arsenic from subsurface sediments by effect of bicarbonate ions in groundwater. *Chemosphere* 54(6), 753-762.

Anderson, R.K., Thompson, M. and Culbard, E. (1986) Selective reduction of arsenic species by continuous hydride generation. Part I. Reaction media. *Analyst* 111(10),

1143-1152.

Arsic, M., Teasdale, P.R., Welsh, D.T., Johnston, S.G., Burton, E.D., Hockmann, K. and Bennett, W.W. (2018) Diffusive gradients in thin films (DGT) reveals antimony and arsenic mobility differs in a contaminated wetland sediment during an oxic-anoxic transition. *Environ. Sci. Technol.* 52(3), 1118-1127.

Awasthi, S., Chauhan, R., Srivastava, S. and Tripathi, R.D. (2017) The journey of arsenic from soil to grain in rice. *Front. Plant Sci.* 8, 1007.

Beauchemin, D., Siu, K., McLaren, J.W. and Berman, S.S. (1989) Determination of arsenic species by high-performance liquid chromatography-inductively coupled plasma mass spectrometry. *J. Anal. Atom. Spectrom.* 4(3), 285-289.

Beesley, L., Moreno-Jimenez, E., Clemente, R., Lepp, N. and Dickinson, N. (2010) Mobility of arsenic, cadmium and zinc in a multi-element contaminated soil profile assessed by in-situ soil pore water sampling, column leaching and sequential extraction. *Environ. Pollut.* 158(1), 155-160.

Bennett, W.W., Teasdale, P.R., Panther, J.G., Welsh, D.T., Zhao, H. and Jolley, D.F. (2012a) Investigating arsenic speciation and mobilization in sediments with DGT and DET: a mesocosm evaluation of oxic-anoxic transitions. *Environ. Sci. Technol.* 46(7), 3981-3989.

Bennett, W.W., Teasdale, P.R., Welsh, D.T., Panther, J.G. and Jolley, D.F. (2012b) Optimization of colorimetric DET technique for the in situ, two-dimensional measurement of iron (II) distributions in sediment porewaters. *Talanta* 88, 490-495.

Bittig, H.C., Körtzinger, A., Neill, C., van Ooijen, E., Plant, J.N., Hahn, J., Johnson, K.S., Yang, B. and Emerson, S.R. (2018) Oxygen optode sensors: Principle,

characterization, calibration, and application in the ocean. *Front. Mar. Sci.* 4, 429.

Bondu, R., Cloutier, V., Rosa, E. and Benzaazoua, M. (2017) Mobility and speciation of geogenic arsenic in bedrock groundwater from the Canadian Shield in western Quebec, Canada. *Sci. Total Environ.* 574, 509-519.

Borch, T., Kretzschmar, R., Kappler, A., Cappellen, P.V., Gindervogel, M., Voegelin, A. and Campbell, K. (2010) Biogeochemical redox processes and their impact on contaminant dynamics. *Environ. Sci. Technol.* 44(1), 15-23.

Bottrell, S.H., Mortimer, R.J., Spence, M., Krom, M.D., Clark, J.M. and Chapman, P.J. (2007) Insights into redox cycling of sulfur and iron in peatlands using high-resolution diffusive equilibrium thin film (DET) gel probe sampling. *Chem. Geol.* 244(3-4), 409-420.

Bouman, B., Peng, S., Castaneda, A. and Visperas, R. (2005) Yield and water use of irrigated tropical aerobic rice systems. *Agr. Water Manage.* 74(2), 87-105.

Bouman, B. and Tuong, T.P. (2001) Field water management to save water and increase its productivity in irrigated lowland rice. *Agr. Water Manage.* 49(1), 11-30.

Brannon, J., Gunnison, D., Smart, R. and Chen, R. (1984) Effects of added organic matter on iron and manganese redox systems in sediment. *Geomicrobiol. J.* 3(4), 319-341.

Bravin, M.N., Travassac, F., Le Floch, M., Hinsinger, P. and Garnier, J.-M. (2008) Oxygen input controls the spatial and temporal dynamics of arsenic at the surface of a flooded paddy soil and in the rhizosphere of lowland rice (*Oryza sativa* L.): a microcosm study. *Plant Soil* 312(1-2), 207-218.

Brendel, P.J. and Luther, G.W.I. (1995) Development of a gold amalgam voltammetric

microelectrode for the determination of dissolved Fe, Mn, O_2, and S (-II) in porewaters of marine and freshwater sediments. *Environ. Sci. Technol.* 29(3), 751-761.

Bryan, G. and Langston, W. (1992) Bioavailability, accumulation and effects of heavy metals in sediments with special reference to United Kingdom estuaries: a review. *Environ. Pollut.* 76(2), 89-131.

Burns, R.G. and Burns, V.M. (1975) Mechanism for nucleation and growth of manganese nodules. *Nature* 255(5504), 130-131.

Buschmann, J. and Berg, M. (2009) Impact of sulfate reduction on the scale of arsenic contamination in groundwater of the Mekong, Bengal and Red River deltas. *Appl. Geochem.* 24(7), 1278-1286.

Campbell, K.M., Malasarn, D., Saltikov, C.W., Newman, D.K. and Hering, J.G. (2006) Simultaneous microbial reduction of iron (III) and arsenic (V) in suspensions of hydrous ferric oxide. *Environ. Sci. Technol.* 40(19), 5950-5955.

Chaillou, G., Schäfer, J., Anschutz, P., Lavaux, G. and Blanc, G. (2003) The behaviour of arsenic in muddy sediments of the Bay of Biscay (France). *Geochim. Cosmochim. Ac.* 67(16), 2993-3003.

Chen, C., Li, L., Huang, K., Zhang, J., Xie, W.Y., Lu, Y., Dong, X. and Zhao, F.J. (2019) Sulfate-reducing bacteria and methanogens are involved in arsenic methylation and demethylation in paddy soils. *ISME J.* 13, 2523-2535.

Chen, H., Tang, Z., Wang, P. and Zhao, F.J. (2018) Geographical variations of cadmium and arsenic concentrations and arsenic speciation in Chinese rice. *Environ. Pollut.* 238, 482-490.

Chen, M., Ding, S., Liu, L., Xu, D., Han, C. and Zhang, C. (2015a) Iron-coupled inactivation of phosphorus in sediments by macrozoobenthos (chironomid larvae) bioturbation: evidences from high-resolution dynamic measurements. *Environ. Pollut.* 204, 241-247.

Chen, M., Tang, H., Ma, H., Holland, T.C., Ng, K.S. and Salley, S.O. (2011) Effect of nutrients on growth and lipid accumulation in the green algae Dunaliella tertiolecta. *Bioresource Technol.* 102(2), 1649-1655.

Chen, Q., An, X., Li, H., Su, J., Ma, Y. and Zhu, Y. (2016) Long-term field application of sewage sludge increases the abundance of antibiotic resistance genes in soil. *Environ. Int.* 92, 1-10.

Chen, T.H., Wang, J.Z., Wang, J., Xie, J.J., Zhu, C.Z. and Zhan, X.M. (2015b) Phosphorus removal from aqueous solutions containing low concentration of phosphate using pyrite calcinate sorbent. *Int. J. Environ. Sci. Technol.* 12(3), 885-892.

Chen, Z., Huang, Y.C., Liang, J.H., Zhao, F. and Zhu, Y.G. (2012) A novel sediment microbial fuel cell with a biocathode in the rice rhizosphere. *Bioresource Technol.* 108, 55-59.

Chen, Z., Kim, K.W., Zhu, Y.G., McLaren, R., Liu, F. and He, J.Z. (2006) Adsorption (AsIII, V) and oxidation (AsIII) of arsenic by pedogenic Fe–Mn nodules. *Geoderma* 136(3-4), 566-572.

Chen, Z., Zhu, Y.G., Liu, W.J. and Meharg, A.A. (2005) Direct evidence showing the effect of root surface iron plaque on arsenite and arsenate uptake into rice (*Oryza sativa*) roots. *New Phytol.* 165(1), 91-97.

Chou, W.L., Yu, D.G. and Yang, M.C. (2005) The preparation and characterization of silver‐loading cellulose acetate hollow fiber membrane for water treatment. *Polym. Advan. Technol.* 16(8), 600-607.

Cotta, A.J.B. and Enzweiler, J. (2009) Quantification of major and trace elements in water samples by ICP-MS and collision cell to attenuate Ar and Cl-based polyatomic ions. *J. Anal. Atom. Spectrom.* 24(10), 1406-1413.

da Rosa, F.C., Nunes, M.A.G., Duarte, F.A., de Moraes Flores, É.M., Hanzel, F.B., Vaz, A.S., Pozebon, D. and Dressler, V.L. (2019) Arsenic speciation analysis in rice milk using LC-ICP-MS. *Food Chem.* 2, 100028.

Damgaard, L.R., Risgaard‐Petersen, N. and Nielsen, L.P. (2014) Electric potential microelectrode for studies of electrobiogeophysics. *J. Geophys. Res-Biogeo.* 119(9), 1906-1917.

Das, H., Mitra, A.K., Sengupta, P., Hossain, A., Islam, F. and Rabbani, G. (2004) Arsenic concentrations in rice, vegetables, and fish in Bangladesh: a preliminary study. *Environ. Int.* 30(3), 383-387.

Das, T.K. (2012) Protein particulate detection issues in biotherapeutics development--current status. *Aaps Pharmscitech* 13(2), 732-746.

Davison, W. (2016) Diffusive gradients in thin-films for environmental measurements, Cambridge University Press.

Davison, W. and Zhang, H. (1994) *In situ* speciation measurements of trace components in natural waters using thin-film gels. *Nature* 367(6463), 546.

Davlson, W. and Zhang, H. (1994) *In situ* speciation measurements of trace components in natural waters using thin-film gels. *Nature* 367(6463), 546.

De Lange, G., Cranston, R., Hydes, D. and Boust, D. (1992) Extraction of pore water from marine sediments: a review of possible artifacts with pertinent examples from the North Atlantic. *Mar. Geol.* 109(1-2), 53-76.

Di, X., Wei, W., Shiming, D., Qin, S. and Chaosheng, Z. (2012) A high-resolution dialysis technique for rapid determination of dissolved reactive phosphate and ferrous iron in pore water of sediments. *Sci. Total Environ.* 421-422(4), 245-252.

Ding, S., Wang, Y., Wang, D., Li, Y.Y., Gong, M. and Zhang, C. (2016) *In situ*, high-resolution evidence for iron-coupled mobilization of phosphorus in sediments. *Sci. Rep.* 6, 24341.

Divjak, B. and Goessler, W. (1999) Ion chromatographic separation of sulfur-containing inorganic anions with an ICP–MS as element-specific detector. *J. Chromatography A* 844(1-2), 161-169.

Dočekalová, H., Clarisse, O., Salomon, S. and Wartel, M. (2002) Use of constrained DET probe for a high-resolution determination of metals and anions distribution in the sediment pore water. *Talanta* 57(1), 145-155.

Dong, D.T., Yamaguchi, N., Makino, T. and Amachi, S. (2014) Effect of soil microorganisms on arsenite oxidation in paddy soils under oxic conditions. *Soil Sci. Plant Nutr.* 60(3), 377-383.

Druschel, G.K., Emerson, D., Sutka, R., Suchecki, P. and Luther III, G.W. (2008) Low-oxygen and chemical kinetic constraints on the geochemical niche of neutrophilic iron (II) oxidizing microorganisms. *Geochim. Cosmochim. Ac.* 72(14), 3358-3370.

Duan, Y., Hou, M., Du, Z. and Jin, Q. (1993) Evaluation of the performance of microwave-induced plasma atomic absorption spectrometry (MIP-AAS). *Appl.*

Spectrosc. 47(11), 1871-1879.

Emerson, D., Weiss, J.V. and Megonigal, J.P. (1999) Iron-oxidizing bacteria are associated with ferric hydroxide precipitates (Fe-plaque) on the roots of wetland plants. *Appl. Environ. Microbiol.* 65(6), 2758-2761.

Fang, W., Williams, P.N., Fang, X., Amoah-Antwi, C., Yin, D., Li, G., Ma, L.Q. and Luo, J. (2018) Field-scale heterogeneity and geochemical regulation of arsenic, iron, lead, and sulphur bioavailability in paddy soil. *Environ. Sci. Technol.* 52(21), 12098–12107.

Fawcett, S.E., Jamieson, H.E., Nordstrom, D.K. and McCleskey, R.B. (2015) Arsenic and antimony geochemistry of mine wastes, associated waters and sediments at the Giant Mine, Yellowknife, Northwest Territories, Canada. *Appl. Geochem.* 62, 3-17.

Fitzgerald, M.A., McCouch, S.R. and Hall, R.D. (2009) Not just a grain of rice: the quest for quality. *Trends Plant Sci.* 14(3), 133-139.

Franz, E.D., Wiramanaden, C.I., Gallego‐Gallegos, M., Tse, J.J., Phibbs, J., Janz, D.M., Pickering, I.J. and Liber, K. (2013) An *in situ* assessment of selenium bioaccumulation from water‐, sediment‐, and dietary‐exposure pathways using caged chironomus dilutus larvae. *Environ. Toxicol. Chem.* 32(12), 2836-2848.

Frederiksen, M.S. and Glud, R.N. (2006) Oxygen dynamics in the rhizosphere of Zostera marina: a two‐dimensional planar optode study. *Limnol. Oceanogr.* 51(2), 1072-1083.

Frenzel, P., Rothfuss, F. and Conrad, R. (1992) Oxygen profiles and methane turnover in a flooded rice microcosm. *Biol. Fert. Soils* 14(2), 84-89.

Fulda, B., Voegelin, A. and Kretzschmar, R. (2013) Redox-controlled changes in cadmium solubility and solid-phase speciation in a paddy soil as affected by reducible sulfate and copper. *Environ. Sci. Technol.* 47(22), 12775-12783.

Gaillardet, J., Viers, J. and Dupré, B. (2003) Trace elements in river waters.

Gallagher, P.A., Schwegel, C.A., Wei, X. and Creed, J.T. (2001) Speciation and preservation of inorganic arsenic in drinking water sources using EDTA with IC separation and ICP-MS detection. *J. Environ. Monitor.* 3(4), 371-376.

Ganesh, S., Khan, F., Ahmed, M., Velavendan, P., Pandey, N. and Kamachi Mudali, U. (2012) Spectrophotometric determination of trace amounts of phosphate in water and soil. *Water Sci. Technol.* 66(12), 2653-2658.

Gao, L., Gao, B., Zhou, H., Xu, D., Wang, Q. and Yin, S. (2016) Assessing the remobilization of antimony in sediments by DGT: a case study in a tributary of the Three Gorges Reservoir. *Environ. Pollut.* 214, 600-607.

Gao, Y., Leermakers, M., Elskens, M., Billon, G., Ouddane, B., Fischer, J.-C. and Baeyens, W. (2007) High resolution profiles of thallium, manganese and iron assessed by DET and DGT techniques in riverine sediment pore waters. *Sci. Total Environ.* 373(2-3), 526-533.

Gao, Y., Leermakers, M., Gabelle, C., Divis, P., Billon, G., Ouddane, B., Fischer, J.C., Wartel, M. and Baeyens, W. (2006) High-resolution profiles of trace metals in the pore waters of riverine sediment assessed by DET and DGT. *Sci. Total Environ.* 362(1-3), 266-277.

Garnier, J.M., Garnier, J., Jézéquel, D. and Angeletti, B. (2015) Using DET and DGT probes (ferrihydrite and titanium dioxide) to investigate arsenic concentrations in

soil porewater of an arsenic-contaminated paddy field in Bangladesh. *Sci. Total Environ.* 536, 306-315.

Giles, C.D., Cade-Menun, B.J., Liu, C.W. and Hill, J.E. (2015) The short-term transport and transformation of phosphorus species in a saturated soil following poultry manure amendment and leaching. *Geoderma* 257, 134-141.

Gorny, J., Billon, G., Lesven, L., Dumoulin, D., Madé, B. and Noiriel, C. (2015) Arsenic behavior in river sediments under redox gradient: a review. *Sci. Total Environ.* 505, 423-434.

Grafe, M., Eick, M. and Grossl, P. (2001) Adsorption of arsenate (V) and arsenite (III) on goethite in the presence and absence of dissolved organic carbon. *Soil Sci. Soc. Am. J.* 65(6), 1680-1687.

Guan, D.X. (2019) An effective and simple tool for assessing contaminant bioavailability in waters, soils and sediments. *Springer*.

Guan, D.X., Williams, P.N., Luo, J., Zheng, J.L., Xu, H.C., Cai, C. and Ma, L.Q. (2015) Novel precipitated zirconia-based DGT technique for high-resolution imaging of oxyanions in waters and sediments. *Environ. Sci. Technol.* 49(6), 3653-3661.

Gustave, W., Yuan, Z.F., Ren, Y.X., Sekar, R. and Chen, Z. (2019a) Arsenic alleviation in rice by using paddy soil microbial fuel cells. *Plant Soil* 441(1-2), 111-127.

Gustave, W., Yuan, Z.F., Sekar, R., Chang, H.C., Zhang, J., Wells, M., Ren, Y.X. and Chen, Z. (2018a) Arsenic mitigation in paddy soils by using microbial fuel cells. *Environ. Pollut.* 238, 647-655.

Gustave, W., Yuan, Z.F., Sekar, R., Ren, Y.X., Chang, H.C., Liu, J.Y. and Chen, Z. (2018b) The change in biotic and abiotic soil components influenced by paddy soil

microbial fuel cells loaded with various resistances. *J. Soils Sediments* 19(1), 106-115.

Gustave, W., Yuan, Z.F., Sekar, R., Ren, Y.X., Liu, J.Y., Zhang, J. and Chen, Z. (2019b) Soil organic matter amount determines the behavior of iron and arsenic in paddy soil with microbial fuel cells. *Chemosphere*, 124459.

Han, C., Williams, P.N., Ren, J., Wang, Z., Fang, X., Xu, D., Xie, X., Geng, J., Ma, L.Q. and Luo, J. (2018) *In situ* sampling and speciation method for measuring dissolved phosphite at ultratrace concentrations in the natural environment. *Water Res.* 137, 281-289.

Harper, M.P., Davison, W. and Tych, W. (1997) Temporal, spatial, and resolution constraints for *in situ* sampling devices using diffusional equilibration: dialysis and DET. *Environ. Sci. Technol.* 31(11), 3110-3119.

Harper, M.P., Davison, W., Zhang, H. and Tych, W. (1998) Kinetics of metal exchange between solids and solutions in sediments and soils interpreted from DGT measured fluxes. *Geochim. Cosmochim. Ac.* 62(16), 2757-2770.

Hartley, W. and Lepp, N.W. (2008) Remediation of arsenic contaminated soils by iron-oxide application, evaluated in terms of plant productivity, arsenic and phytotoxic metal uptake. *Sci. Total Environ.* 390(1), 35-44.

Hatat-Fraile, M. and Barbeau, B. (2019) Performance of colorimetric methods for the analysis of low levels of manganese in water. *Talanta* 194, 786-794.

Heitkemper, D.T., Vela, N.P., Stewart, K.R. and Westphal, C.S. (2001) Determination of total and speciated arsenic in rice by ion chromatography and inductively coupled plasma mass spectrometry. *J. Anal. Atom. Spectrom.* 16(4), 299-306.

Herbel, M. and Fendorf, S. (2006) Biogeochemical processes controlling the speciation and transport of arsenic within iron coated sands. *Chem. Geol.* 228(1-3), 16-32.

Hesslein, R.H. (1976) An in situ sampler for close interval pore water studies 1. *Limnol. Oceanogr.* 21(6), 912-914.

Hilbig, H., Huber, M., Gmell, A. and Heinz, D. (2017) Determination of heavy metals in a highly porous sorptive filter material of road runoff treatment systems with LA-ICP-MS. *Water Air Soil Poll.* 228(9), 331.

Hirata, S. and Toshimitsu, H. (2005) Determination of arsenic species and arsenosugars in marine samples by HPLC–ICP–MS. *Anal. Bioanal. Chem.* 383(3), 454-460.

Hirata, S., Toshimitsu, H. and Aihara, M. (2006) Determination of arsenic species in marine samples by HPLC-ICP-MS. *Anal. Sci.* 22(1), 39-43.

Honma, T., Ohba, H., Kaneko-Kadokura, A., Makino, T., Nakamura, K. and Katou, H. (2016) Optimal soil Eh, pH, and water management for simultaneously minimizing arsenic and cadmium concentrations in rice grains. *Environ. Sci. Technol.* 50(8), 4178-4185.

Hu, B., Chen, B., He, M., Nan, K., Xu, Y. and Xu, C. (2019) Separation methods applied to arsenic speciation. *Compr. Ana. Chem.* 85, 89-144.

Hu, P., Ouyang, Y., Wu, L., Shen, L., Luo, Y. and Christie, P. (2015) Effects of water management on arsenic and cadmium speciation and accumulation in an upland rice cultivar. *J. Environ. Sci.* 27, 225-231.

Islam, F.S., Gault, A.G., Boothman, C., Polya, D.A., Charnock, J.M., Chatterjee, D. and Lloyd, J.R. (2004) Role of metal-reducing bacteria in arsenic release from Bengal delta sediments. *Nature* 430(6995), 68.

Jackson, B.P. and Bertsch, P.M. (2001) Determination of arsenic speciation in poultry wastes by IC-ICP-MS. *Environ. Sci. Technol.* 35(24), 4868-4873.

Jacob, D.L. and Otte, M.L. (2003) Conflicting processes in the wetland plant rhizosphere: metal retention or mobilization? *Water Air Soil Pollut.* 3(1), 91-104.

Jain, C. and Ali, I. (2000) Arsenic: occurrence, toxicity and speciation techniques. *Water Res.* 34(17), 4304-4312.

Jajda, H., Patel, K., Patel, S., Solanki, V., Patel, K. and Singh, S. (2015) Comparative efficacy of two standard methods for determination of iron and zinc in fruits, pulses and cereals. *J. Food Sci. Technol.* 52(2), 1096-1102.

Jia, X., Otte, M., Liu, Y., Qin, L., Tian, X., Lu, X., Jiang, M. and Zou, Y. (2018) Performance of iron plaque of wetland plants for regulating iron, manganese, and phosphorus from agricultural drainage water. *Water* 10(1), 42.

Jia, Y., Huang, H., Chen, Z. and Zhu, Y.G. (2014) Arsenic uptake by rice is influenced by microbe-mediated arsenic redox changes in the rhizosphere. *Environ. Sci. Technol.* 48(2), 1001-1007.

Jia, Y., Huang, H., Zhong, M., Wang, F.H., Zhang, L.M. and Zhu, Y.G. (2013) Microbial arsenic methylation in soil and rice rhizosphere. *Environ. Sci. Technol.* 47(7), 3141-3148.

Kalbitz, K. and Wennrich, R. (1998a) Mobilization of heavy metals and arsenic in polluted wetland soils and its dependence on dissolved organic matter. *Sci. Total Environ.* 209(1), 27-39.

Kalbitz, K. and Wennrich, R. (1998b) Mobilization of heavy metals and arsenic in polluted wetland soils and its dependence on dissolved organic matter. *Science of the*

Total Environment 209(1), 27-39.

Kärger, J. and Ruthven, D.M. (2016) Diffusion in nanoporous materials: fundamental principles, insights and challenges. *New J. Chem.* 40(5), 4027-4048.

Kazi, T.G., Brahman, K.D., Baig, J.A. and Afridi, H.I. (2018) A new efficient indigenous material for simultaneous removal of fluoride and inorganic arsenic species from groundwater. *J. Hazard. Mater.* 357, 159-167.

Keller-Lehmann, B., Corrie, S., Ravn, R., Yuan, Z. and Keller, J. (2006) Preservation and simultaneous analysis of relevant soluble sulfur species in sewage samples, p. 28.

Klinkhammer, G.P. (1980a) Early diagenesis in sediments from the eastern equatorial Pacific, II. Pore water metal results. *Earth Planet. Sci. Lett.* 49(1), 81-101.

Klinkhammer, G.P. (1980b) Early diagenesis in sediments from the eastern equatorial Pacific, II. Pore water metal results. *Earth and Planetary Science Letters* 49(1), 81-101.

Koningsberger, D. and Prins, R. (1988) X-ray absorption: principles, applications, techniques of EXAFS, SEXAFS, and XANES, New York.

Kumar, M., Ramanathan, A., Rahman, M.M. and Naidu, R. (2016) Concentrations of inorganic arsenic in groundwater, agricultural soils and subsurface sediments from the middle Gangetic plain of Bihar, India. *Sci. Total Environ.* 573, 1103-1114.

Kumarathilaka, P., Seneweera, S., Meharg, A. and Bundschuh, J. (2018a) Arsenic accumulation in rice (*Oryza sativa* L.) is influenced by environment and genetic factors. *Sci. Total Environ.* 642, 485-496.

Kumarathilaka, P., Seneweera, S., Meharg, A. and Bundschuh, J. (2018b) Arsenic speciation dynamics in paddy rice soil-water environment: sources, physico-

chemical, and biological factors-a review. *Water Res.* 140, 403-414.

Leermakers, M., Gao, Y., Gabelle, C., Lojen, S., Ouddane, B., Wartel, M. and Baeyens, W. (2005) Determination of high resolution pore water profiles of trace metals in sediments of the Rupel River (Belgium) using DET (diffusive equilibrium in thin films) and DGT (diffusive gradients in thin films) techniques. *Water, Air, Soil Pollut.* 166(1-4), 265-286.

Li, C., Ding, S., Yang, L., Wang, Y., Ren, M., Chen, M., Fan, X. and Lichtfouse, E. (2019) Diffusive gradients in thin films: devices, materials and applications. *Environ. Chem. Lett.* 17(2), 801-831.

Li, X., Chen, Y., Ye, J., Fu, F., Pokhrel, G.R., Zhang, H., Zhu, Y. and Yang, G. (2017) Determination of different arsenic species in food‐grade spirulina powder by ion chromatography combined with inductively coupled plasma mass spectrometry. *J. Sep. Sci.* 40(18), 3655-3661.

Liu, F. (2006) Arsenite oxidation by three types of manganese oxides. *J. Environ. Sci.* 18(2), 292-298.

Liu, G.M., An, Q., Wang, L.J., Jia, X., Feng, S.H., Xia, S.M., Wu, Y.N. and Qi, H. (2018) Release and kinetics of arsenic and plumbum in the Songhua River surficial sediments. *Environ. Sci. Pollut. R.* 25(1), 541-551.

Liu, Z.G. and Huang, X.J. (2014) Voltammetric determination of inorganic arsenic. *TrAC-Trends Anal. Chem.* 60, 25-35.

Lock, A., Wallschläger, D., Belzile, N., Spiers, G. and Gueguen, C. (2018) Rates and processes affecting As speciation and mobility in lake sediments during aging. *J. Environ. Sci.* 66, 338-347.

Long, G.L. and Winefordner, J.D. (1983) Limit of detection. A closer look at the IUPAC definition. *Anal. Chem.* 55(7), 712A-724A.

Luo, J., Zhang, H., Santner, J. and Davison, W. (2010) Performance characteristics of diffusive gradients in thin films equipped with a binding gel layer containing precipitated ferrihydrite for measuring arsenic (V), selenium (VI), vanadium (V), and antimony (V). *Anal. Chem.* 82(21), 8903-8909.

Ma, W.W., Zhu, M.X., Yang, G.P. and Li, T. (2017) *In situ*, high-resolution DGT measurements of dissolved sulfide, iron and phosphorus in sediments of the East China Sea: Insights into phosphorus mobilization and microbial iron reduction. *Mar. Pollut. Bull.* 124(1), 400-410.

Maisch, M., Lueder, U., Kappler, A. and Schmidt, C. (2019a) Iron lung: how rice roots induce iron redox changes in the rhizosphere and create niches for microaerophilic Fe (II)-oxidizing bacteria. *Environ. Sci. Technol. Lett.* 6(10), 600-605.

Maisch, M., Lueder, U., Laufer, K., Scholze, C., Kappler, A. and Schmidt, C. (2019b) Contribution of microaerophilic iron (II)-oxidizers to iron (III) mineral formation. *Environ. Sci. Technol.* 53(14), 8197-8204.

Malkin, S.Y., Rao, A.M., Seitaj, D., Vasquezcardenas, D., Zetsche, E.M., Hidalgomartinez, S., Boschker, H.T. and Meysman, F.J. (2014) Natural occurrence of microbial sulphur oxidation by long-range electron transport in the seafloor. *ISME J.* 8(9), 1843-1854.

Martin, B.C., Bougoure, J., Ryan, M.H., Bennett, W.W., Colmer, T.D., Joyce, N.K., Olsen, Y.S. and Kendrick, G.A. (2019) Oxygen loss from seagrass roots coincides with colonisation of sulphide-oxidising cable bacteria and reduces sulphide stress.

ISME J. 13(3), 707.

Martin, J.B., Hartl, K.M., Corbett, D.R., Swarzenski, P.W. and Cable, J.E. (2003) A multi-level pore-water sampler for permeable sediments. *J. Sediment. Res.* 73(1), 128-132.

Masscheleyn, P.H., Delaune, R.D. and Patrick Jr, W.H. (1991) Effect of redox potential and pH on arsenic speciation and solubility in a contaminated soil. *Environ. Sci. Technol.* 25(8), 1414-1419.

Mattusch, J. and Wennrich, R. (1998) Determination of anionic, neutral, and cationic species of arsenic by ion chromatography with ICPMS detection in environmental samples. *Anal. Chem.* 70(17), 3649-3655.

Mayer, L.M. (1976) Chemical water sampling in lakes and sediments with dialysis bags 1. *Limnol. Oceanogr.* 21(6), 909-912.

Mcadams, B.C., Adams, R.M., Arnold, W.A. and Chin, Y.P. (2016) Novel insights into the distribution of reduced sulfur species in prairie pothole wetland pore waters provided by bismuth film electrodes. *Environ. Sci. Technol. Lett.* 3(3), 104-109.

Meharg, A.A. (2004) Arsenic in rice–understanding a new disaster for South-East Asia. *Trends Plant Sci.* 9(9), 415-417.

Meijboom, F. and van Noordwijk, M. (1991) Rhizon soil solution samplers as artificial roots, pp. 793-795.

Meijer, L.E. and Avnimelech, Y. (1999) On the use of micro-electrodes in fish pond sediments. *Aquacult. Eng.* 21(2), 71-83.

Miranda, J.L., Mesquita, R.B., Nunes, A., Rangel, M. and Rangel, A.O. (2016) Iron speciation in natural waters by sequential injection analysis with a hexadentate 3-

hydroxy-4-pyridinone chelator as chromogenic agent. *Talanta* 148, 633-640.

Monbet, P., McKelvie, I.D. and Worsfold, P.J. (2008) Combined gel probes for the *in situ* determination of dissolved reactive phosphorus in porewaters and characterization of sediment reactivity. *Environ. Sci. Technol.* 42(14), 5112-5117.

Motelica-Heino, M., Naylor, C., Zhang, H. and Davison, W. (2003) Simultaneous release of metals and sulfide in lacustrine sediment. *Environ. Sci. Technol.* 37(19), 4374-4381.

Mucci, A., Richard, L.F., Lucotte, M. and Guignard, C. (2000) The differential geochemical behavior of arsenic and phosphorus in the water column and sediments of the Saguenay Fjord estuary, Canada. *Aquat. Geochem.* 6(3), 293-324.

Muehe, E.M., Wang, T., Kerl, C.F., Planer-Friedrich, B. and Fendorf, S. (2019) Rice production threatened by coupled stresses of climate and soil arsenic. *Nat. Commun.* 10(1), 1-10.

Neori, A. and Agami, M. (2017) The functioning of rhizosphere biota in wetlands–a review. *Wetlands* 37(4), 615-633.

Neubauer, S.C., Emerson, D. and Megonigal, J.P. (2002) Life at the energetic edge: kinetics of circumneutral iron oxidation by lithotrophic iron-oxidizing bacteria isolated from the wetland-plant rhizosphere. *Appl. Environ. Microbiol.* 68(8), 3988-3995.

Ng, K.C. and Garner, T.J. (1993) Microwave-induced plasma atomic absorption spectrometry with solution nebulization and desolvation-condensation. *Appl. Spectrosc.* 47(2), 241-243.

Nielsen, L.P., Risgaardpetersen, N., Fossing, H., Christensen, P.B. and Sayama, M.

(2010) Electric currents couple spatially separated biogeochemical processes in marine sediment. *Nature* 463(7284), 1071-1074.

Olesik, J.W. (1991) Elemental analysis using ICP-OES and ICP/MS. *Anal. Chem.* 63(1), 12A-21A.

Ona-Nguema, G., Morin, G., Wang, Y., Foster, A.L., Juillot, F., Calas, G. and Brown Jr, G.E. (2010) XANES evidence for rapid arsenic (III) oxidation at magnetite and ferrihydrite surfaces by dissolved O_2 via Fe^{2+}-mediated reactions. *Environ. Sci. Technol.* 44(14), 5416-5422.

Pedersen, O., Borum, J., Duarte, C.M. and Fortes, M.D. (1998) Oxygen dynamics in the rhizosphere of Cymodocea rotundata. *Mar. Ecol. Prog. Ser.* 169, 283-288.

Peng, C., Bryce, C., Sundman, A. and Kappler, A. (2019) Cryptic cycling of complexes containing Fe (III) and organic matter by phototrophic Fe (II)-oxidizing bacteria. *Appl. Environ. Microbiol.* 85(8), e02826-02818.

Persson, D.P., Hansen, T.H., Laursen, K.H., Schjoerring, J.K. and Husted, S. (2009) Simultaneous iron, zinc, sulfur and phosphorus speciation analysis of barley grain tissues using SEC-ICP-MS and IP-ICP-MS. *Metallomics* 1(5), 418-426.

Pester, M., Knorr, K.H., Friedrich, M.W., Wagner, M. and Loy, A. (2012) Sulfate-reducing microorganisms in wetlands–fameless actors in carbon cycling and climate change. *Front. Microbiol.* 3, 72.

Pi, K., Wang, Y., Postma, D., Teng, M., Su, C. and Xie, X. (2018) Vertical variability of arsenic concentrations under the control of iron-sulfur-arsenic interactions in reducing aquifer systems. *J. Hydrol.* 561, 200-210.

Pongratz, R. (1998) Arsenic speciation in environmental samples of contaminated soil.

Sci.Total Environ. 224(1-3), 133-141.

Pyle, S.M., Nocerino, J.M., Deming, S.N., Palasota, J.A., Palasota, J.M., Miller, E.L., Hillman, D.C., Kuharic, C.A., Cole, W.H. and Fitzpatrick, P.M. (1995) Comparison of AAS, ICP-AES, PSA, and XRF in determining lead and cadmium in soil. *Environ. Sci. Technol.* 30(1), 204-213.

Qin, J., Rosen, B.P., Zhang, Y., Wang, G., Franke, S. and Rensing, C. (2006) Arsenic detoxification and evolution of trimethylarsine gas by a microbial arsenite S-adenosylmethionine methyltransferase. *P. Natl. Acad. Sci. USA* 103(7), 2075-2080.

Quaghebeur, M., Rengel, Z. and Smirk, M. (2003) Arsenic speciation in terrestrial plant material using microwave-assisted extraction, ion chromatography and inductively coupled plasma mass spectrometry. *J. Anal. Atom. Spectrom.* 18, 128-134.

Ratering, S. and Schnell, S. (2000) Localization of iron-reducing activity in paddy soilby profile studies. *Biogeochemistry* 48(3), 341-365.

Ratering, S. and Schnell, S. (2001) Nitrate‐dependent iron (II) oxidation in paddy soil. *Environ. Microbiol.* 3(2), 100-109.

Rathnayake, K.N., Bennett, W.W., Teasdale, P.R., Huang, J. and Welsh, D.T. (2017) Comparing *in situ* colorimetric DET and DGT techniques with ex situ core slicing and centrifugation for measuring ferrous iron and dissolved sulfide in coastal sediment pore waters. *Chemosphere* 188, 119.

Reynolds, B., Stevens, P., Hughes, S. and Brittain, S. (2004) Comparison of field techniques for sampling soil solution in an upland peatland. *Soil Use Manage.* 20(4), 454-456.

Rietra, R.P.J.J., Hiemstra, T. and Van Riemsdijk, W.H. (2001) Interaction between

calcium and phosphate adsorption on goethite. *Environ. Sci. Technol.* 35(16), 3369-3374.

Ritsema, R., Dukan, L., van Leeuwen, W., Oliveira, N., Wolfs, P. and Lebret, E. (1998) Speciation of arsenic compounds in urine by LC–ICP MS. *Appl. Organomet. Chem.* 12(8‐9), 591-599.

Roberts, L.C., Hug, S.J., Voegelin, A., Dittmar, J., Kretzschmar, R., Wehrli, B., Saha, G.C., Badruzzaman, A.B.M. and Ali, M.A. (2010) Arsenic dynamics in porewater of an intermittently irrigated paddy field in Bangladesh. *Environ. Sci. Technol.* 45(3), 971-976.

Robertson, D., Teasdale, P.R. and Welsh, D.T. (2008) A novel gel‐based technique for the high resolution, two‐dimensional determination of iron (II) and sulfide in sediment. *Limnol. Oceanogr-Meth.* 6(10), 502-512.

Samanta, G. and Clifford, D.A. (2006) Preservation and field speciation of inorganic arsenic species in groundwater. *Water Qual. Res. J. Can.* 41(2), 107-116.

Santner, J., Prohaska, T., Luo, J. and Zhang, H. (2010) Ferrihydrite containing gel for chemical imaging of labile phosphate species in sediments and soils using diffusive gradients in thin films. *Anal. Chem.* 82(18), 7668-7674.

Seeberg‐Elverfeldt, J., Schlüter, M., Feseker, T. and Kölling, M. (2005) Rhizon sampling of porewaters near the sediment‐water interface of aquatic systems. *Limnol. Oceanogr-Meth.* 3(8), 361-371.

Segata, N., Izard, J., Waldron, L., Gevers, D., Miropolsky, L., Garrett, W.S. and Huttenhower, C. (2011) Metagenomic biomarker discovery and explanation.

Genome Biol. 12(6), R60.

Serrat, F.B. (1998) 3, 3′, 5, 5′-Tetramethylbenzidme for the colorimetric determination of manganese in water. *Microchim. Acta* 129(1-2), 77-80.

Seward, T.M. (1984) The formation of lead(II) chloride complexes to 300℃: A spectrophotometric study. *Geochim. Cosmochim. Ac.* 48(1), 121-134.

Shaheen, S.M., Tsadilas, C.D. and Rinklebe, J. (2013) A review of the distribution coefficients of trace elements in soils: Influence of sorption system, element characteristics, and soil colloidal properties. *Adv. Colloid Interface* 201, 43-56.

Shakoor, M., Niazi, N., Bibi, I., Rahman, M., Naidu, R., Dong, Z., Shahid, M. and Arshad, M. (2015) Unraveling health risk and speciation of arsenic from groundwater in rural areas of Punjab, Pakistan. *Int. J. Environ. Res. Pub. He.* 12(10), 12371-12390.

Shotbolt, L. (2010) Pore water sampling from lake and estuary sediments using Rhizon samplers. *J. Paleolimnol.* 44(2), 695-700.

Shuttleworth, S.M., Davison, W. and Hamilton-Taylor, J. (1999) Two-dimensional and fine structure in the concentrations of iron and manganese in sediment pore-waters. *Environ. Sci. Technol.* 33(23), 4169-4175.

Smedley, P.L. and Kinniburgh, D.G. (2002) A review of the source, behaviour and distribution of arsenic in natural waters. *Appl. Geochem.* 17(5), 517-568.

Somenahally, A.C., Hollister, E.B., Yan, W., Gentry, T.J. and Loeppert, R.H. (2011) Water management impacts on arsenic speciation and iron-reducing bacteria in contrasting rice-rhizosphere compartments. *Environ. Sci. Technol.* 45(19), 8328-8335.

Stürup, S., Bendahl, L. and Gammelgaard, B. (2006) Optimization of LC-DRC-ICP-MS for the speciation of selenotrisulfides with simultaneous detection of sulfur and selenium as oxides combined with determination of elemental and isotope ratios. *J. Anal. Atom. Spectrom.* 21(2), 201-203.

Su, J.Y., Syu, C.H. and Lee, D.Y. (2018) Growth inhibition of rice (*Oryza sativa* L.) seedlings in Ga-and In-contaminated acidic soils is respectively caused by Al and Al^{+} In toxicity. *J. Hazard. Mater.* 344, 274-282.

Suda, A. and Makino, T. (2016) Functional effects of manganese and iron oxides on the dynamics of trace elements in soils with a special focus on arsenic and cadmium: a review. *Geoderma* 270, 68-75.

Suzuki, Y., Shimoda, Y., Endo, Y., Hata, A., Yamanaka, K. and Endo, G. (2009) Rapid and effective speciation analysis of arsenic compounds in human urine using anion-exchange columns in HPLC-ICP-MS. *J. Occup. Health* 51(4), 380-385.

Takahashi, Y., Minamikawa, R., Hattori, K.H., Kurishima, K., Kihou, N. and Yuita, K. (2004) Arsenic behavior in paddy fields during the cycle of flooded and non-flooded periods. *Environ. Sci. Technol.* 38(4), 1038-1044.

Teasdale, P.R., Batley, G.E., Apte, S.C. and Webster, I.T. (1995) Pore water sampling with sediment peepers. *TrAC-Trends Anal. Chem.* 14(6), 250-256.

Tesfaldet, Z.O., van Staden, J.F. and Stefan, R.I. (2004) Sequential injection spectrophotometric determination of iron as Fe (II) in multi-vitamin preparations using 1, 10-phenanthroline as complexing agent. *Talanta* 64(5), 1189-1195.

Tufano, K.J., Reyes, C., Saltikov, C.W. and Fendorf, S. (2008) Reductive processes controlling arsenic retention: revealing the relative importance of iron and arsenic

reduction. *Environ. Sci. Technol.* 42(22), 8283-8289.

Tufano, K.J. and Scott, F. (2008) Confounding impacts of iron reduction on arsenic retention. *Environ. Sci. Technol.* 42(13), 4777-4783.

Urbansky, E.T. and Schock, M.R. (2000) Can fluoridation affect lead (II) in potable water? Hexafluorosilicate and fluoride equilibria in aqueous solution. *Int. J. Environ. Stud.* 57(5), 597-637.

Violante, A., Cozzolino, V., Perelomov, L., Caporale, A. and Pigna, M. (2010) Mobility and bioavailability of heavy metals and metalloids in soil environments. *J. Soil Sci. Pant nut.* 10(3), 268-292.

Violante, A. and Pigna, M. (2002) Competitive sorption of arsenate and phosphate on different clay minerals and soils. *Soil Sci. Soc. Am. J.* 66(6), 1788-1796.

Wallschläger, D. and Stadey, C.J. (2007) Determination of (oxy) thioarsenates in sulfidic waters. *Anal. Chem.* 79(10), 3873-3880.

Wang, H.Y., Chen, P., Zhu, Y.G., Cen, K. and Sun, G.X. (2019a) Simultaneous adsorption and immobilization of As and Cd by birnessite-loaded biochar in water and soil. *Environ. Sci. Pollut. R.* 26(9), 8575–8584.

Wang, M., Tang, Z., Chen, X.P., Wang, X., Zhou, W.X., Tang, Z., Zhang, J. and Zhao, F.J. (2019b) Water management impacts the soil microbial communities and total arsenic and methylated arsenicals in rice grains. *Environ. Pollut.* 247, 736-744.

Wang, X.J., Yang, J., Chen, X.P., Sun, G.X. and Zhu, Y.G. (2009) Phylogenetic diversity of dissimilatory ferric iron reducers in paddy soil of Hunan, South China. *J. Soils Sediments* 9(6), 568-577.

Ward, N.L., Challacombe, J.F., Janssen, P.H., Henrissat, B., Coutinho, P.M., Wu, M.,

Xie, G., Haft, D.H., Sait, M. and Badger, J. (2009) Three genomes from the phylum Acidobacteria provide insight into the lifestyles of these microorganisms in soils. *Appl. Environ. Microbiol.* 75(7), 2046-2056.

Weber, F.A., Hofacker, A.F., Voegelin, A. and Kretzschmar, R. (2010) Temperature dependence and coupling of iron and arsenic reduction and release during flooding of a contaminated soil. *Environ. Sci. Technol.* 44(1), 116-122.

Welter, E., Calmano, W., Mangold, S. and Tröger, L. (1999) Chemical speciation of heavy metals in soils by use of XAFS spectroscopy and electron microscopical techniques. *Fresenius J. Anal. Chem.* 364(3), 238-244.

Widerlund, A. and Davison, W. (2007) Size and density distribution of sulfide-producing microniches in lake sediments. *Environ. Sci. Technol.* 41(23), 8044-8049.

Williams, P.N., Santner, J., Larsen, M., Lehto, N.J., Oburger, E., Wenzel, W., Glud, R.N., Davison, W. and Zhang, H. (2014) Localized flux maxima of arsenic, lead, and iron around root apices in flooded lowland rice. *Environ. Sci. Technol.* 48(15), 8498-8506.

Williams, P.N., Zhang, H., Davison, W., Meharg, A.A., Hossain, M., Norton, G.J., Brammer, H. and Islam, M.R. (2011) Organic matter-solid phase interactions are critical for predicting arsenic release and plant uptake in Bangladesh paddy soils. *Environ. Sci. Technol.* 45(14), 6080-6087.

Wu, Z., Jiao, L., Wang, S. and Xu, Y. (2016a) Multi-metals measured at sediment–water interface (SWI) by diffusive gradients in thin films (DGT) technique for geochemical research. *Arch. Environ. Con. Tox.* 70(2), 429-437.

Wu, Z., Ren, D., Zhou, H., Hang, G. and Li, J. (2016b) Sulfate reduction and formation

of iron sulfide minerals in nearshore sediments from Qi'ao Island, Pearl River Estuary, Southern China. *Quatern. Int.* 452, 137-147.

Xie, R., Johnson, W., Spayd, S., Hall, G.S. and Buckley, B. (2006) Arsenic speciation analysis of human urine using ion exchange chromatography coupled to inductively coupled plasma mass spectrometry. *Anal. Chim. Acta* 578(2), 186-194.

Xu, X., Chen, C., Wang, P., Kretzschmar, R. and Zhao, F.J. (2017) Control of arsenic mobilization in paddy soils by manganese and iron oxides. *Environ. Pollut.* 231(Pt 1), 37-47.

Yamamoto, M., Nishida, A., Otsuka, K., Komai, T. and Fukushima, M. (2010) Evaluation of the binding of iron (II) to humic substances derived from a compost sample by a colorimetric method using ferrozine. *Bioresource Technol.* 101(12), 4456-4460.

Yamamura, S., Ike, M. and Fujita, M. (2003) Dissimilatory arsenate reduction by a facultative anaerobe, *Bacillus sp.* strain SF-1. *J. Biosci. Bioeng.* 96(5), 454-460.

Yasui, S., Kanda, J., Usui, T. and Ogawa, H. (2016) Seasonal variations of dissolved organic matter and nutrients in sediment pore water in the inner part of Tokyo Bay. *J. Oceanogr.* 72(6), 851-866.

Yi, X.Y., Yang, Y.P., Yuan, H.Y., Chen, Z., Duan, G.L. and Zhu, Y.G. (2019) Coupling metabolisms of arsenic and iron with humic substances through microorganisms in paddy soil. *J. Hazard. Mater.* 373, 591-599.

Yola, M.L. and Özaltin, N. (2011) Adsorptive stripping voltammetric methods for determination of ezetimibe in tablets. *Rev. Anal. Chem.* 30(1), 29-36.

Yuan, Z.F., Ata-Ul-Karim, S.T., Cao, Q., Lu, Z., Cao, W., Zhu, Y. and Liu, X. (2016)

Indicators for diagnosing nitrogen status of rice based on chlorophyll meter readings. *Field Crops Res.* 185(185), 12-20.

Yuan, Z.F., Gustave, W., Bridge, J., Liang, Y., Sekar, R., Boyle, J., Jin, C.Y., Pu, T.Y., Ren, Y.X. and Chen, Z. (2019a) Tracing the dynamic changes of element profiles by novel soil porewater samplers with ultralow disturbance to soil–water interface. *Environ. Sci. Technol.* 53(9), 5124-5132.

Yuan, Z.F., Gustave, W., Sekar, R., Bridge, J., Wang, J.Y., Feng, W.J., Guo, B. and Chen, Z. (2019b) Simultaneous measurement of aqueous redox sensitive elements and their species across soil-water interface. *EarthArXiv* (November 20).

Zhai, H., Wang, L., Hövelmann, J., Qin, L., Zhang, W. and Putnis, C.V. (2018) Humic acids limit the precipitation of cadmium and arsenate at the Brushite− Fluid interface. *Environ. Sci. Technol.* 53(1), 194-202.

Zhang, G., Bai, J., Zhao, Q., Jia, J. and Wen, X. (2017a) Heavy metals pollution in soil profiles from seasonal-flooding riparian wetlands in a Chinese delta: Levels, distributions and toxic risks. *Phys. Chem. Earth Pt A/B/C* 97, 54-61.

Zhang, H. and Davison, W. (1999) Diffusional characteristics of hydrogels used in DGT and DET techniques. *Anal. Chim. Acta* 398(2-3), 329-340.

Zhang, J., Ma, T., Yan, Y., Xie, X., Abass, O.K., Liu, C., Zhao, Z. and Wang, Z. (2018) Effects of Fe-S-As coupled redox processes on arsenic mobilization in shallow aquifers of Datong Basin, northern China. *Environ. Pollut.* 237, 28-38.

Zhang, J., Zhao, S., Xu, Y., Zhou, W., Huang, K., Tang, Z. and Zhao, F.-J. (2017b) Nitrate stimulates anaerobic microbial arsenite oxidation in paddy soils. *Environ. Sci. Technol.* 51(8), 4377-4386.

Zhao, F.J., Ago, Y., Mitani, N., Li, R.Y., Su, Y.H., Yamaji, N., McGrath, S.P. and Ma, J.F. (2010) The role of the rice aquaporin Lsi1 in arsenite efflux from roots. *New Phytol.* 186(2), 392-399.

Zhao, F.J., Harris, E., Yan, J., Ma, J., Wu, L., Liu, W., McGrath, S.P., Zhou, J. and Zhu, Y.G. (2013) Arsenic methylation in soils and its relationship with microbial arsM abundance and diversity, and As speciation in rice. *Environ. Sci. Technol.* 47(13), 7147-7154.

Zhao, Y., Su, J., Ye, J., Rensing, C., Tardif, S., Zhu, Y. and Brandt, K.K. (2019) AsChip: a high-throughput qPCR chip for comprehensive profiling of genes linked to microbial cycling of arsenic. *Environ. Sci. Technol.* 53(2), 798-807.

Zheng, J., Hintelmann, H., Dimock, B. and Dzurko, M.S. (2003) Speciation of arsenic in water, sediment, and plants of the Moira watershed, Canada, using HPLC coupled to high resolution ICP–MS. *Anal. Bioanal. Chem.* 377(1), 14-24.

Zhu, Y.G., Williams, P.N. and Meharg, A.A. (2008) Exposure to inorganic arsenic from rice: a global health issue? *Environ. Pollut.* 154(2), 169-171.

Zobrist, J., Dowdle, P.R., Davis, J.A. and Oremland, R.S. (2000) Mobilization of arsenite by dissimilatory reduction of adsorbed arsenate. *Environ. Sci. Technol.* 34(22), 4747-4753.